BRILLOUIN SPECTROSCOPY:
Measurements of elastic and photoelastic constants of some alkali halide crystals

by

Hans Bräul, B.Sc. (Hons.)

A thesis
submitted to the Department of Physics
in partial fulfilment of the requirements
for the degree of
Master of Science

December 1979

Brock University
St. Catharines, Ontario

To my wife, Kathy

ACKNOWLEDGEMENTS

I would like to express my sincere thanks to Dr. C. A. Plint for his kind support and encouragement during the course of this work.

Special thanks are also due to Dr. R. C. Shukla with whom many valuable discussions took place, and whose energy never failed to be an inspiration.

I would also like to thank Dr. F. P. Koffyberg for the lending of his experimental expertise.

I am very grateful to the staff of the electronics and instruments shops for their excellent work.

I thank Miss J. M. Hastie for her careful and patient typing of this thesis.

I would like to express my very special appreciation to my wife, Kathy, to whom this work is dedicated, and without whose faith and loving support this thesis would not have been completed.

Thanks are due to the Natural Sciences and Engineering Research Council of Canada and to the Department of Physics, Brock University for their financial assistance.

ABSTRACT

The assembly and testing of apparatus for the measurement of elastic and photoelastic constants by Brillouin scattering, using a Fabry-Perot interferometer and with argon ion laser excitation is described. Such measurements are performed on NaCl, KBr and LiF using the λ = 488.0 nm laser line. The elastic constants obtained here are in very good agreement with the ultrasonic data for all three materials. The discrepancy between ultrasonic and hypersonic sound velocities which was reported by some authors for KBr and LiF is not confirmed, and the elastic constants obtained for LiF are the most accurate to date. Also, the present photoelastic constants are in good agreement with the data obtained by ultrasonic techniques for all three crystals. The results for the KBr and LiF crystals constitute the first set of photoelastic constants obtained for these materials by Brillouin spectroscopy. Our results for LiF are the best available to date.

TABLE OF CONTENTS

LIST OF FIGURES

(Continued) LIST OF FIGURES

LIST OF TABLES

I. INTRODUCTION

Brillouin spectroscopy is the observation of light scattered from thermal fluctuations in liquids and solids (Einstein (1910), Brillouin (1922)). It has long been recognized (Gross (1930), Krishnan (1947)) that the measurement of the frequencies and intensities of the components of the Brillouin spectrum could lead directly to the determination of the elastic and photoelastic constants at hypersonic frequencies ($\sim 10^{10}$ Hz). It is only with the relatively recent developments of lasers and high resolution Fabry-Perot interferometers that accuracies comparable to ultrasonic techniques have been achieved (Benckert and Bäckström (1973, 1974), Grimsditch and Ramdas (1974), Sandercock (1970)).

Brillouin spectroscopy has the advantage that the light is used only to probe already existing fluctuations and therefore is not subject to uncertainties arising in the ultrasonic method from sample dimensions or experimentally produced stresses. Particular advantage is gained in the study of small samples or crystals which would be shattered by the production of ultrasonic waves and in fact, Brillouin spectroscopy is the only known tool for the measurement of the elastic and photoelastic constants of the rare-gas single crystals (Gornall and Stoicheff (1971), McLaren et al. (1975), Kato and Stoicheff (1975)).

This thesis describes the establishment of a Brillouin spectroscopy laboratory and the subsequent determination of the elastic and photoelastic constants of three alkali halides, namely NaCl, KBr and LiF at room temperature.

The first Brillouin study of the alkali halides was reported by Benedek and Fritsch (1966) for KCl, RbCl and KI, using a 2 mW He-Ne laser and a grating spectrometer. Although the resolution (~3 GHz) of their instrument was below that of modern Fabry-Perot interferometers, the elastic constants obtained are generally in good agreement with ultrasonic results. More recent experiments on NaCl, NaF, KCl and KI by Benckert and Bäckström (1973, 1974) using a 8 mW He-Ne laser and a Fabry-Perot interferometer (resolution ~1.5 GHz) have produced results which are generally in good agreement with ultrasonic data.

To our knowledge, the only significant departures at room temperature from ultrasonic data are the elastic constants reported by a group at Hebrew University in Israel, namely Kaplan, Shaham and Low (1970) in the case of KBr, and Shaham, Kaplan, Low and Foguel (1970) in the case of LiF. These authors attribute the 3%-30% discrepancies to dispersion effects between the ultrasonic and hypersonic frequency regions.

The study to determine the elastic constants of NaCl was undertaken for comparison with the abundance of available ultrasonic data (Landolt-Börnstein

(1979)) and with the above mentioned works of Benckert and Bäckström. The measurements of the elastic constants of KBr and LiF were made to investigate the discrepancies reported by Kaplan et al. (1970) and Shaham et al. (1970).

The measurements of the photoelastic constants in NaCl were carried out for comparison with well established ultrasonic results and with the Brillouin study by Benckert and Bäckström (1973). The photoelastic constants of KBr and LiF were measured by Brillouin spectroscopy for the first time.

This thesis consists of six chapters (including the present) and two appendices. Chapter II contains a discussion of the theory of the scattering process, as well as an explanation of the experimental geometries appropriate to the determination of the elastic and photoelastic constants of crystals with NaCl-type structures. The equipment and experimental method are described in Chapter III. The fourth chapter contains the presentation of the results and estimates of experimental error. In Chapter V, the results are discussed and compared with other works in the literature, and an assessment of the validity of this work is attempted. The conclusions drawn from this work are given in Chapter VI. Appendix A gives a summary of the equations governing the performance of the Fabry-Perot interferometer. Appendix B outlines some important, yet generally overlooked, data handling considerations for spectra taken with a triple-pass Fabry-Perot interferometer.

II. THEORY

Brillouin scattering is the result of an inelastic exchange of energy between a beam of light and the collective thermal vibrations of atoms in a liquid or a solid (Cowley (1964)). Since the energies of both the light and the collective vibrations are quantized, a complete theory of the scattering process must involve the calculation of the quantum mechanical scattering cross section (see Schiff (1968), p. 285). This requires the evaluation of matrix elements of the type

$$\langle m|H'|n\rangle \qquad \text{(II-1)}$$

where H' is the interaction Hamiltonian of light and matter, and m and n are the two quantum states involved in the scattering process.

The interaction Hamiltonian H' consists of terms of the type $(e/c)\vec{A}\cdot\vec{p}_i$ (Birman (1974), sect. 120), where e is the electronic charge, c is the velocity of light, $\vec{A}$ is the vector potential of the incident radiation and $\vec{p}_i$ is the momentum operator for the electrons and the ions. Equivalently, from the approximation of the plane wave representation of $\vec{A}$, we can write

$$H' \propto \hat{e}\cdot\vec{\mu}_i \qquad \text{(II-2)}$$

where $\hat{e}$ is the polarization of the incident radiation, and $\vec{\mu}_i$ is the dipole moment operator.

At this point, one is confronted with the choice between a phenomenological and a first-principles approach. The latter route requires, in the case of a solid, the evaluation of the matrix elements of the dipole moment operator

$$\vec{\mu}_i = c_i(a_i + a_i^+) \ , \qquad \text{(II-3)}$$

where a_i and a_i^+ are the usual phonon annihilation and creation operators and c_i is an unknown coefficient. A serious difficulty arises in the determination of the c_i and although such attempts are presently being made for Raman scattering (for a review of these, see Birman (1974), sections 121, 124), we are not aware of any first-principles approach in Brillouin scattering.

Therefore, rather than calculating the Brillouin scattering cross-section from first principles for comparison with the experimental results, it is customary to adopt a phenomenological treatment. That is, the interaction Hamiltonian is expressed in terms of measurable parameters, such as the elastic and photo-elastic constants which are determined from the frequencies and the intensities of the Brillouin components.

The essential results of such a parameterization of H' and an explanation of how the parameters are extracted from

experimental data are given below. The reader is referred to Born and Huang (1954) for details.

(1) ELASTIC CONSTANTS

Two essential conditions implicit in the above theory permit the calculation of elastic constants from the Brillouin spectrum. The first condition is imposed on the wavevectors of the incident light $\vec{k}_0$, the scattered light $\vec{k}$, and the scattering phonon $\vec{K}$, viz.,

$$\vec{K} = \vec{k} - \vec{k}_0 \qquad \text{(II-4)}$$

The second condition provides a relationship between the frequencies of the photons and the phonons, viz.,

$$\nu_0 - \nu_s = \pm\nu\begin{pmatrix}\vec{K}\\ j\end{pmatrix} \qquad \text{(II-5)}$$

where ν_0 is the incident light frequency, ν_s is the scattered light frequency, and $\nu\begin{pmatrix}\vec{K}\\ j\end{pmatrix}$ is the frequency of the phonon $(\vec{K}, j)$, where j is the branch index.

The wavevector conservation condition (II-4) allows us to draw the following wavevector diagram (Fig. II-1).

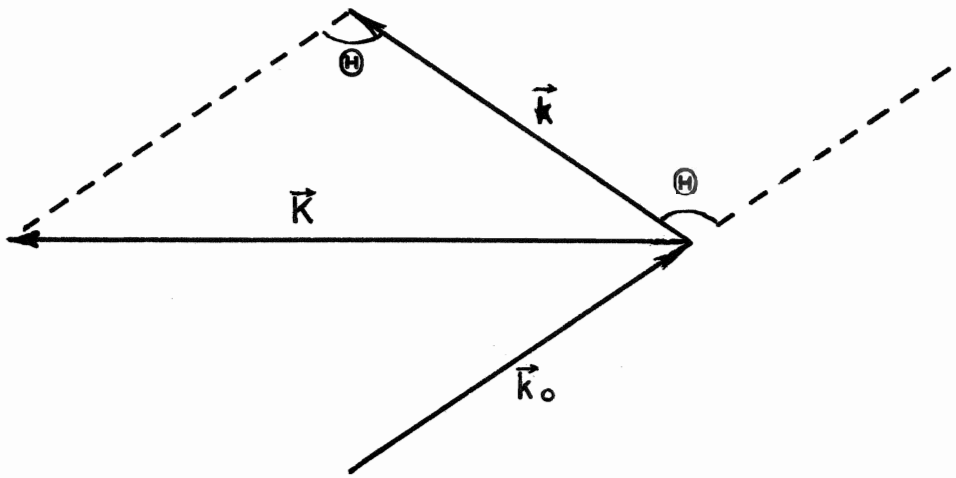

Figure II-1

Since acoustic phonon frequencies are much lower than optical frequencies (5×10^{10} Hz compared with 5×10^{14} Hz), we can write

$$k_0 = \frac{2\pi\nu_0}{c_m} \simeq \frac{2\pi}{c_m}\left(\nu_0 \pm \nu\left(\vec{K}_j\right)\right) = k \qquad \text{(II-6)}$$

where c_m is the speed of light in the medium. Hence, it becomes evident from Figure II-1 that

$$K = 2k_0 \sin(\theta/2) \ . \qquad \text{(II-7)}$$

Using the first equality in (II-6) along with

$$K = \frac{2\pi\nu\left(\vec{K}_j\right)}{v\left(\vec{K}_j\right)} \qquad \text{(II-8)}$$

where $v\begin{pmatrix}\vec{K}\\ j\end{pmatrix}$ is the phonon velocity, we obtain

$$\nu\begin{pmatrix}\vec{K}\\ j\end{pmatrix} = 2\frac{\nu_0}{c_m} v\begin{pmatrix}\vec{K}\\ j\end{pmatrix}\sin(\theta/2) \quad . \qquad \text{(II-9)}$$

By solving the equations of motion in the long wavelength limit for the desired crystal orientation, it is possible to write the phonon velocities in terms of the elastic constants (de Launay (1956)). Thus, the measurement of the Brillouin frequencies provides a means of measuring the elastic constants of transparent crystals at hypersonic frequencies.

APPLICATION TO CUBIC CRYSTALS

In this thesis, we are concerned with crystals possessing cubic symmetry. In all experiments, crystal orientation was varied with $\vec{K}$ confined to either the [100]-plane, or the [110]-plane. If the angle ϕ is defined to be the angle between the phonon wavevector $\vec{K}$ and the cube axis <100> the phonon velocities can be expressed in terms of the elastic constants and the angle ϕ. This is done below.

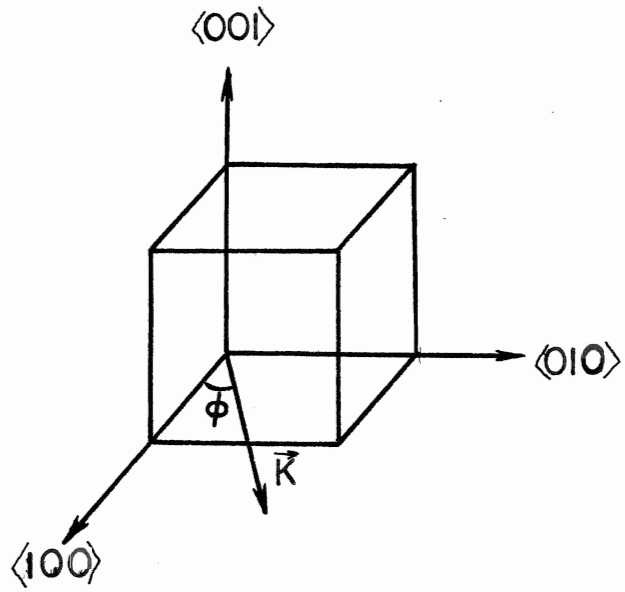

Figure II-2

[100]-PLANE:

Wavevectors in the [100]-plane can be written in the form

$$\vec{K} = K\langle \cos\phi,\ \sin\phi,\ 0\rangle \quad . \tag{II-10}$$

Then by solving the equations of motion for this $\vec{K}$, we obtain three simultaneous equations in the components of the polarization $\hat{e}\begin{pmatrix}\phi\\ j\end{pmatrix}$

$$\begin{pmatrix} a & c & 0 \\ c & b & 0 \\ 0 & 0 & d \end{pmatrix} \cdot \hat{e}\begin{pmatrix}\phi\\ j\end{pmatrix} = 0 \ , \tag{II-11}$$

where $a = (c_{11} - c_{44})\cos^2\phi + c_{44} - \rho v^2\begin{pmatrix}\phi\\ j\end{pmatrix}$,

$b = (c_{11} - c_{44})\sin^2\phi + c_{44} - \rho v^2\begin{pmatrix}\phi\\ j\end{pmatrix}$

$$c = (c_{12} + c_{44})\cos\phi\sin\phi \quad ,$$

and $$d = c_{44} - \rho v^2 \left(\begin{matrix}\phi \\ j\end{matrix}\right) \quad .$$

The solutions are

$$\rho v^2 \left(\begin{matrix}\phi \\ 1\end{matrix}\right) = c_{44}$$

$$\rho v^2 \left(\begin{matrix}\phi \\ 2,3\end{matrix}\right) = \frac{1}{2}\Big[(c_{11} + c_{44}) \pm \Big\{(c_{11} + c_{44})^2 - 4\big[((c_{11} - c_{44})^2 - (c_{12} + c_{44})^2) \cdot \sin^2\phi\cos^2\phi + c_{11}c_{44}\big]\Big\}^{\frac{1}{2}}\Big] \quad . \qquad \text{(II-12)}$$

The polarization vectors are then:

$$\hat{e}\left(\begin{matrix}\phi \\ j\end{matrix}\right) = \langle 1, e\left(\begin{matrix}\phi \\ j\end{matrix}|2\right), 0\rangle \left[1 + e\left(\begin{matrix}\phi \\ j\end{matrix}|2\right)^2\right]^{-\frac{1}{2}} \quad , \qquad \text{(II-13)}$$

where

$$e\left(\begin{matrix}\phi \\ j\end{matrix}|2\right) = - \frac{(c_{11} - c_{44})\cos^2\phi + c_{44} - \rho v^2 \left(\begin{matrix}\phi \\ j\end{matrix}\right)}{((c_{12} + c_{44})\sin\phi\cos\phi} \quad , \ \phi \neq 0.$$

[110]-PLANE:

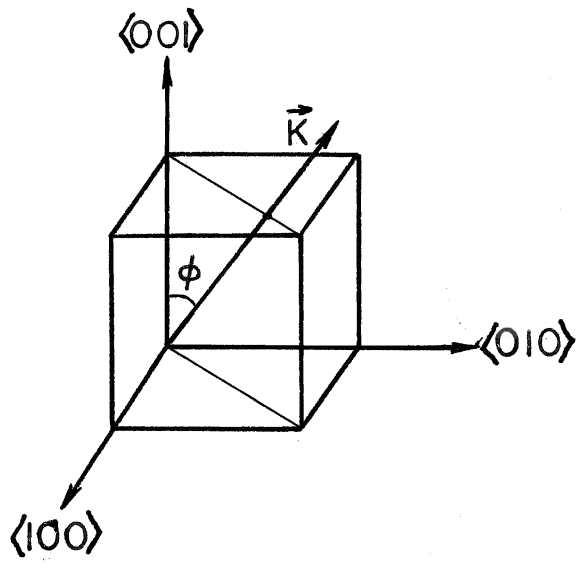

Figure II-3

Wavevectors in the [110]-plane can be written as

$$\vec{K} = K\left\langle \frac{\sin\phi}{\sqrt{2}}, \frac{\sin\phi}{\sqrt{2}}, \cos\phi \right\rangle . \qquad \text{(II-14)}$$

The equations of motion can be solved for this K to give:

$$\begin{pmatrix} a & b & c \\ b & a & c \\ c & c & d \end{pmatrix} \cdot \hat{e}\begin{pmatrix} \phi \\ j \end{pmatrix} = 0 \quad , \qquad \text{(II-15)}$$

where $a = (c_{11} - c_{44})\,\frac{\sin^2\phi}{2} + c_{44} - \rho v^2\begin{pmatrix} \phi \\ j \end{pmatrix}$

$$b = (c_{12} + c_{44})\,\frac{\sin^2\phi}{2}$$

$$c = (c_{12} + c_{44})\,\frac{\sin\phi\cos\phi}{\sqrt{2}}$$

and $\quad d = (c_{11} + c_{44})\cos^2\phi + c_{44} - \rho v^2\left(\begin{matrix}\phi\\ j\end{matrix}\right)$.

By solving (II-15), we arrive at the following:

$$\rho v^2\left(\begin{matrix}\phi\\ 1\end{matrix}\right) = \frac{1}{2}[(c_{11} - c_{12}) + (2c_{44} + c_{12} - c_{11})\cos^2\phi]$$

$$\rho v^2\left(\begin{matrix}\phi\\ 2,3\end{matrix}\right) = \frac{1}{4}\Big[(c_{11} + c_{12} + 4c_{44}) - \cos^2\phi(2c_{44} + c_{12} - c_{11})$$

$$\pm \Big\{(c_{11} + c_{12})^2 + (2c_{44} + c_{12} - c_{11})$$

$$\cdot[(8c_{44} + 14c_{12} + 6c_{11})\cos^2\phi$$

$$- (6c_{44} + 15c_{12} + 9c_{11})\cos^4\phi]\Big\}^{\frac{1}{2}}\Big] \qquad \text{(II-16)}$$

with the polarization vectors

$$\hat{e}\left(\begin{matrix}\phi\\ j\end{matrix}\right) = \langle 1,1,e\left(\begin{matrix}\phi\\ j\end{matrix}|3\right)\rangle\cdot\left[2 + e\left(\begin{matrix}\phi\\ j\end{matrix}|3\right)\right]^{-\frac{1}{2}} \qquad \text{(II-17)}$$

where

$$e\left(\begin{matrix}\phi\\ j\end{matrix}|3\right) = -\frac{(c_{11} + c_{12})\sin^2\phi + 2c_{44} - 2\rho v^2\left(\begin{matrix}\phi\\ j\end{matrix}\right)}{\sqrt{2}(c_{12} + c_{44})\sin\phi\cos\phi}, \phi \neq 0°, 90°.$$

The elastic constants can be obtained most directly by measuring the sound velocities for $\hat{K} = \langle 100\rangle$ and $\hat{K} = \frac{1}{\sqrt{2}}\langle 110\rangle$. The elastic constants are given in terms of the phonon velocities in these two orientations in the form of Table II-1.

Table II-1

$\hat{K}$	$\hat{e}(j)$	Mode designation	$\rho v^2(j)$
<100>	<100>	longitudinal	c_{11}
	<010>	transverse (1)	c_{44}
	<001>	transverse (2)	c_{44}
$\frac{1}{\sqrt{2}}$<110>	$\frac{1}{\sqrt{2}}$<110>	longitudinal	$\frac{1}{2}(c_{11} + c_{12} + 2c_{44})$
	$\frac{1}{\sqrt{2}}$<1,-1,0>	transverse (1)	$\frac{1}{2}(c_{11} - c_{12})$
	$\frac{1}{\sqrt{2}}$<001>	transverse (2)	c_{44}

(2) PHOTOELASTIC CONSTANTS

The Brillouin scattering intensity from the phonon $(\vec{K}, j)$ per unit solid angle (see Born and Huang (1956), p. 379) is

$$I\left(\begin{matrix}\vec{K}\\ j\end{matrix}\right) = 2\pi I_0 \left(\frac{V}{\rho}\right) \frac{k_B T \nu_0^4}{c_0^3 v^2\left(\begin{matrix}\vec{K}\\ j\end{matrix}\right)} \left(\hat{n} \cdot \underline{T}\left(\begin{matrix}\vec{K}\\ j\end{matrix}\right) \cdot \hat{E}\right)^2 \qquad \text{(II-18)}$$

where I_0 = incident intenisty

V = illuminated volume

ρ = density of material

k_B = Boltzmann's constant

T = temperature (K)

ν_0 = incident light frequency

c_0 = speed of light in vacuum

$v\left(\begin{matrix}\vec{K}\\ j\end{matrix}\right)$ = velocity of phonon $(\vec{K}, j)$

$\hat{n}$ = unit vector specifying the polarization of the incident beam

$\hat{E}$ = unit vector specifying the polarization of the scattered beam

$\underline{T}\begin{pmatrix}\vec{K}\\ j\end{pmatrix}$ = Brillouin scattering tensor

The Brillouin scattering tensor, $\underline{T}\begin{pmatrix}\vec{K}\\ j\end{pmatrix}$ completely determines the intensity of the scattering from the phonon $(\vec{K}, j)$, once the scattering geometry and the sound velocities $v\begin{pmatrix}\vec{K}\\ j\end{pmatrix}$ (or the elastic constants) are known. It is defined for cubic symmetry as follows:

$$\underline{T}\begin{pmatrix}\vec{K}\\ j\end{pmatrix} = \varepsilon_0^2 \hat{K}\cdot\underline{p}\cdot\hat{e}\begin{pmatrix}\vec{K}\\ j\end{pmatrix} \qquad \text{(II-19)}$$

where $\underline{p}$ is the fourth-rank photo-elastic tensor and ε_0 is the dielectric constant. For cubic symmetry, the only non-zero elements of $\underline{p}$ in Voigt's notation are p_{11}, p_{12} and p_{44}.

We are now in a position to write down the Brillouin intensities, for a given crystal and scattering geometry, in terms of the photo-elastic and elastic constants. If the crystal symmetry and the phonon propagation direction and polarization are known, the scattering tensor can be determined from equations (II-18) and (II-19) and the measured intensity ratios $I\begin{pmatrix}\vec{K}\\ j\end{pmatrix}/I_0$.

For the crystal class m3m, relevant to the NaCl structure, the scattering tensors for the three polarizations are given below, for the orientations $\hat{K} = \langle 100\rangle$ and $\hat{K} = \frac{1}{\sqrt{2}}\langle 110\rangle$.

These tensors, as well as those for the high symmetry directions in all other crystal classes are tabulated by Cummins and Schoen (1972).

$\hat{K} = \langle 100 \rangle$:

$$L: \quad \underline{T} = \varepsilon_0^2 \begin{pmatrix} p_{11} & 0 & 0 \\ 0 & p_{12} & 0 \\ 0 & 0 & p_{12} \end{pmatrix}$$

$$T_1: \quad \underline{T} = \varepsilon_0^2 \begin{pmatrix} 0 & p_{44} & 0 \\ p_{44} & 0 & 0 \\ 0 & 0 & 0 \end{pmatrix}$$

$$T_2: \quad \underline{T} = \varepsilon_0^2 \begin{pmatrix} 0 & 0 & p_{44} \\ 0 & 0 & 0 \\ p_{44} & 0 & 0 \end{pmatrix}$$

$\hat{K} = \frac{1}{\sqrt{2}}\langle 110 \rangle$:

$$L: \quad \underline{T} = \frac{1}{2}\varepsilon_0^2 \begin{pmatrix} p_{11}+p_{12} & 2p_{44} & 0 \\ 2p_{44} & p_{11}+p_{12} & 0 \\ 0 & 0 & 2p_{12} \end{pmatrix}$$

$$T_1: \quad \underline{T} = \frac{1}{2}\varepsilon_0^2 \begin{pmatrix} p_{11}-p_{12} & 0 & 0 \\ 0 & p_{12}-p_{11} & 0 \\ 0 & 0 & 0 \end{pmatrix}$$

$$T_2: \quad \underline{T} = \frac{1}{\sqrt{2}}\varepsilon_0^2 \begin{pmatrix} 0 & 0 & p_{44} \\ 0 & 0 & p_{44} \\ p_{44} & p_{44} & 0 \end{pmatrix}$$

From this and the previous section, we see that it is possible, for a cubic crystal, to obtain all the elastic and photoelastic constants by studying the Brillouin spectra in two orientations. Naturally, the simplest choice of orientations is $\hat{K} = \langle 100 \rangle$ and $\hat{K} = \frac{1}{\sqrt{2}}\langle 110 \rangle$.

Table II-2 gives the phase velocities in terms of the elastic constants, and the intensity proportionalities in terms of the photoelastic constants, for all the observable modes in these two orientations.

Table II-2

$\hat{K}$	$\hat{e}$	Mode type	ρv^2	Light polarizations	Intensity proportionality
<100>	<100>	L	c_{11}	VV*	$(p_{12})^2/\rho v^2$
				HH	$((p_{11}-p_{12})/2)^2/\rho v^2$
	<010>	T_1	c_{44}	VH	$(p_{44}/\sqrt{2})^2/\rho v^2$
	<001>	T_2	c_{44}	HV	$(p_{44}/\sqrt{2})^2/\rho v^2$
$\frac{1}{\sqrt{2}}$<110>	$\frac{1}{\sqrt{2}}$<110>	L	$\frac{(c_{11}+c_{12}+2c_{44})}{2}$	VV	$(p_{12})^2/\rho v^2$
				HH	$(p_{44})^2/\rho v^2$
	<001>	T_2	c_{44}	VH	$(p_{44}/\sqrt{2})^2/\rho v^2$
				HV	$(p_{44}/\sqrt{2})^2/\rho v^2$

* The first letter refers to the polarization of the incident light, and the second letter refers to that of the scattered light. Polarizations perpendicular and parallel to the scattering plane are denoted by "V" (vertical) and "H" (horizontal), respectively.

III. EXPERIMENTAL

The work presented in this thesis represents the first formal set of results obtained from a new Brillouin spectroscopy laboratory. The present chapter describes the constituent components, their capabilities and their limitations.

The choice and design of these components were necessarily intended not only to produce reliable data for the present study, but also to offer versatility for the execution of more sophisticated experiments in the foreseeable future.

Experimental procedures which were employed throughout the work are described in this chapter. Descriptions of variations on, or additions to, these procedures for a particular sample are found in the next chapter, preceding the presentation of results for that sample.

Since one purpose of this thesis is to describe the establishment of a new laboratory, and since considerable effort was expended in trying to meet future needs, some of the topics of this chapter and all of appendix B (e.g., triple pass performance, some details of sample holder design, and some data reduction methods) will find no direct application in the present work.

(1) EQUIPMENT

The equipment which constitutes any Brillouin spectroscopy laboratory can be divided into four basic categories. They are:

(i) Monochromatic light source, generally a laser.

(ii) Sample holder.

(iii) Spectrum analyser, usually a Fabry-Perot interferometer operated in a scanning mode.

(iv) Detector and data storage facility.

These are described in the following section. Figure III-1 shows schematically the experimental arrangement employed in this work.

(i) LIGHT SOURCE

Because of its high available power and good frequency stability at two convenient wavelengths (488.0 nm and 514.5 nm), the argon ion laser is the most commonly chosen light source for Brillouin spectroscopy. In this work, an already available Coherent Radiation Model CR-3 argon ion laser was used. Since Brillouin shifts are generally in the range 3 to 30 GHz, it was necessary to isolate a single mode of the Doppler profile by the use of an intra-cavity etalon. The Coherent Radiation Model 423 oven-stabilized etalon was chosen for this purpose.

The two types of frequency instabilities which can occur in single mode laser operation are long term frequency drift, and short term "jitter". The limits given by the manufacturer on long term drift using the intra-cavity etalon are as follows:

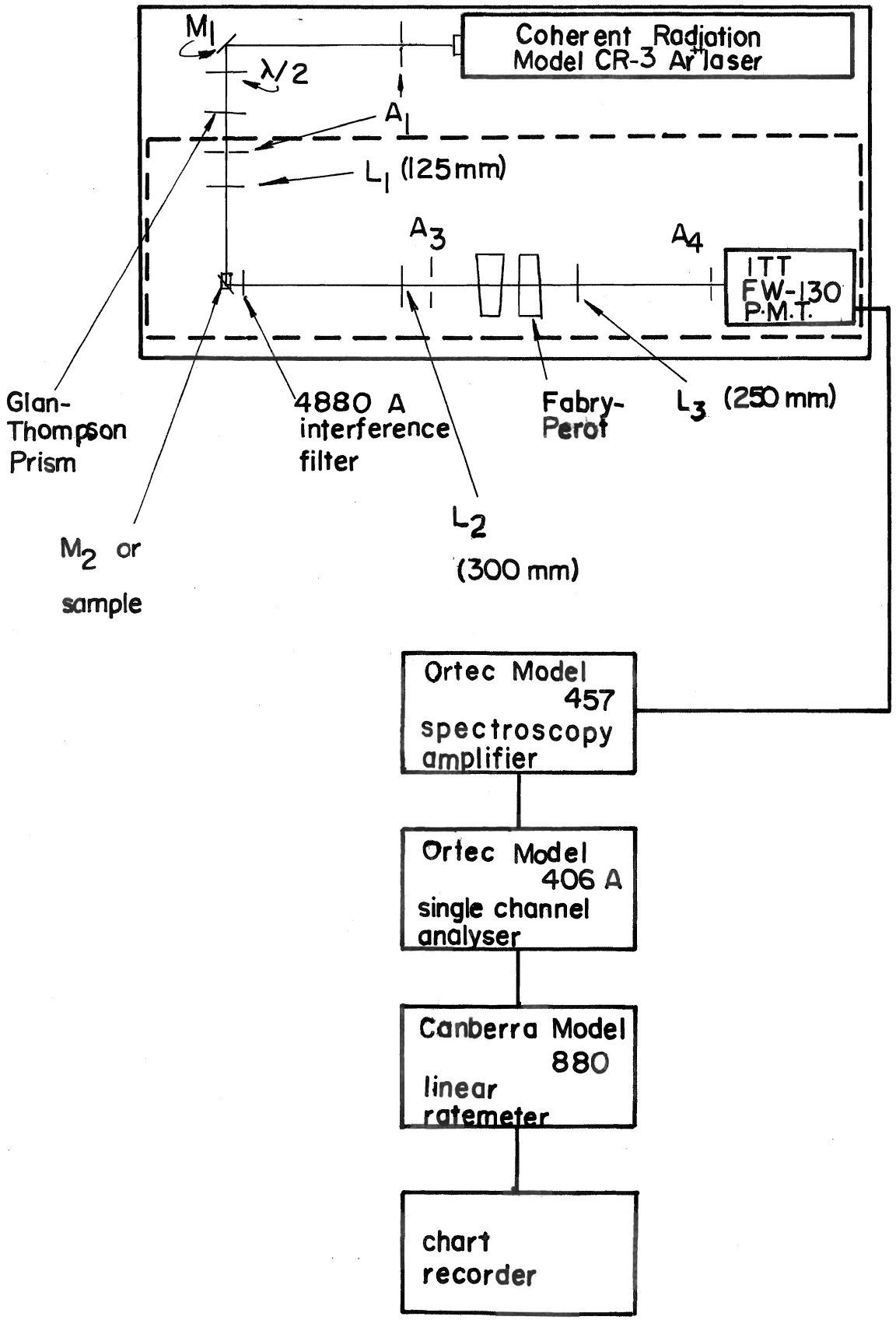

FIG·III-1 : EXPERIMENTAL ARRANGEMENT

10 h	±75 MHz
10 min	±40 MHz
10 s	±15 MHz
<1 s	±8 MHz

This drift can affect frequency as well as intensity measurements.

The longest single scan time used in these experiments was about three hours, corresponding to a possible cumulative drift in laser frequency of about 60 MHz. Thus, for example, if a Brillouin shift of 10 GHz is scanned in twenty minutes, the laser frequency may have drifted some 50 MHz, leading to a 0.5% error in frequency measurement. This is most significant for small Brillouin shifts.

During a three-hour scan of four orders, the longest time spent on a spectral component would be of the order of two minutes. The corresponding uncertainty in Brillouin linewidth is then 25 MHz. Since acoustic phonons in solids at room temperatures are relatively long-lived and have widths of about 100 MHz, considerable error in the measurement of apparent line width or intensity could result from using such a long single scan. The majority of the measurements performed were averaged over at least six orders, using fifteen minute scans. It is therefore expected that the effects of long term drift are not important in this work. It is apparent however, that the capability to superimpose many fast scans in a digital storage system is highly desirable for work on weak spectra or especially narrow lines.

Short term "jitter" contributed about 20 MHz to the instrumental width and, because of its constant nature when time-averaged, is expected to have little effect on the accuracy of linewidth or intensity data.

The laser output was often monitored either with a small confocal etalon (Spectra-Physics Model 470), or with the large plane Fabry-Perot. It was generally found that mode hopping could be essentially eliminated by proper adjustment of the laser mirrors and intra-cavity etalon.

It was found that flushing with dry nitrogen those parts of the laser cavity which were subject to suspended dust particles in the air improved the stability of the laser line profile.

(ii) SAMPLE HOLDER

The sample holder was constructed to provide ease of optical alignment and crystal orientation, as well as the capability to be used in future to control and read sample temperatures to within 0.01°C, above room temperature. A sketch of the sample holder is given in Figure III-2.

Crystals were attached with epoxy to brass inserts A, which fit into a top disc, B. The inserts could be slid up and down in B to adjust the height of the sample, and were prevented from rotating with respect to B by making both the cross-section of A and the hole in B in the shape of a "D". This assembly could be rotated within the main block C, and the

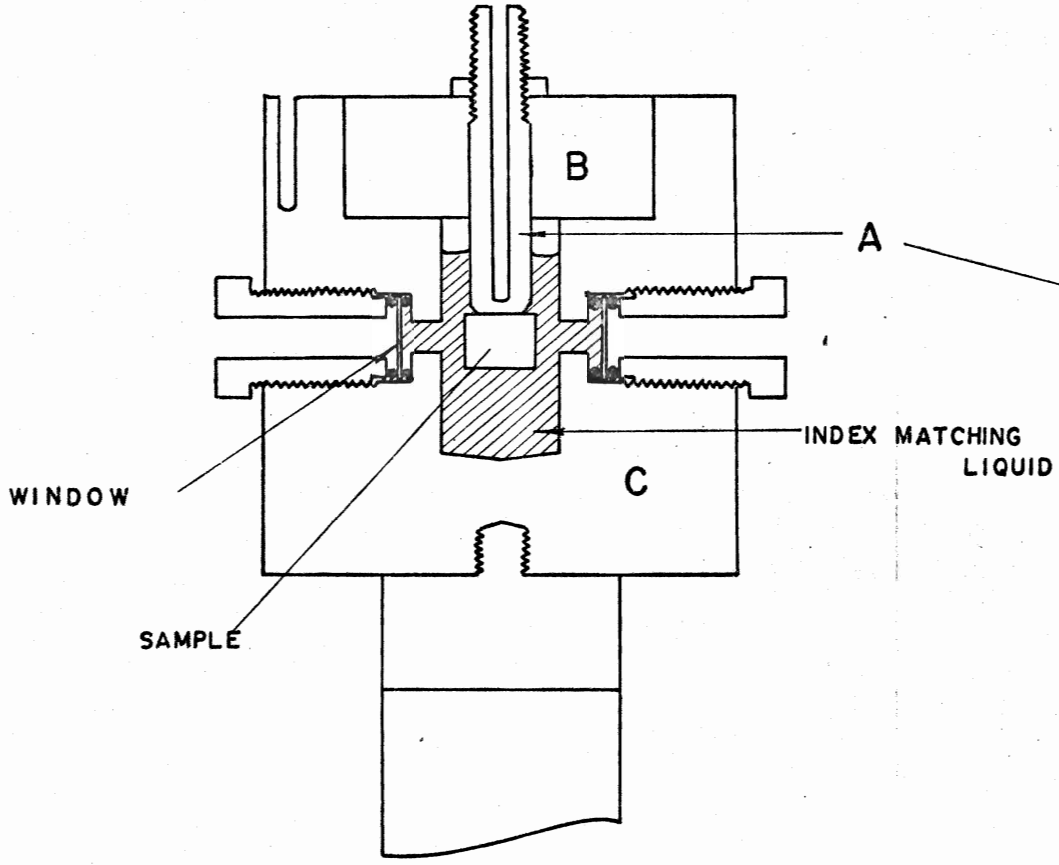

CROSS-SECTION

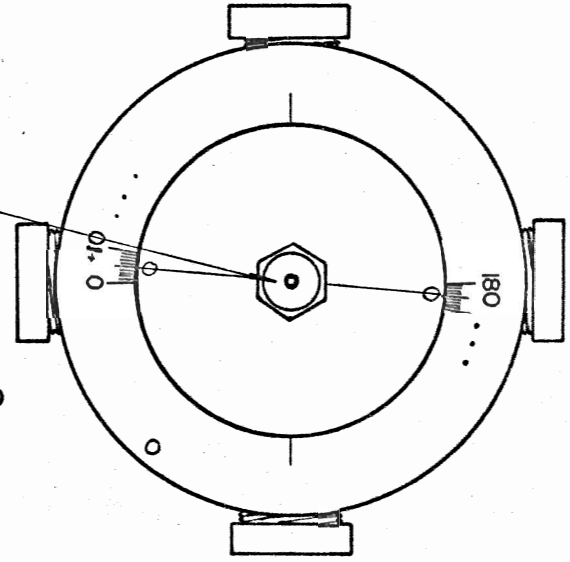

TOP VIEW

FIGURE III-2

SAMPLE HOLDER

SCALE:	APPROVED BY:	DRAWN BY
DATE:		REVISED
		DRAWING NUMBER

crystal orientation could be read from a 360° scale engraved on C. Liquids were studied by attaching a flat-sided glass vial containing the liquid to an insert A.

The orientation of the crystals with respect to a reference mark on B was determined from a back reflection X-ray photograph. The position of the sample holder was then adjusted so that the + and - 90° marks (see Fig. III-2) were along the direction of the beam. Crystal orientations could be set with a relative accuracy of ±0.1° and with an absolute error of no more than 1°. Brillouin frequencies were checked to fall symmetrically with crystal orientation about the estimated position of a high symmetry direction in the crystal.

To avoid unwanted reflections from the crystal surfaces, the sample chamber was filled with an index matching liquid. Stray light was further reduced by lining the sample chamber with "carbon black" paper.

For alignment, it was desireable to direct the laser beam along the optical axis of the Fabry-Perot system without moving the sample holder. This was accomplished by mounting a small mirror on an insert A.

For future experiments, the sample holder was designed to control the sample temperature in a range from room temperature to 300°C. The temperatures could be maintained by wrapping the holder with heating tape and insulating with glass wool. Two temperature sensing devices (thermocouples or platinum resistance thermometers) could be used. One such device,

for temperature control, is inserted near the outside of the block for maximum responsiveness. The sample temperature is read with a thermocouple or platinum-resistance thermometer in the insert, near the sample. Effort was made to minimize temperature gradients by providing an approximately symmetric thermal environment.

The entire assembly was mounted on a pedestal which provided tilt and height adjustments.

(iii) FABRY-PEROT INTERFEROMETER

A short summary of the equations governing the performance of the Fabry-Perot interferometer is given in Appendix A. The interferometer used in this project was a mechanically scanned Burleigh Model RC-110. It is constructed of "super-invar" chosen for its low coefficient of thermal expansion ($\alpha \leq 0.36 \times 10^{-6}/°C$ compared with $\alpha = 1.6 \times 10^{-6}$ for regular invar and $\alpha = 9.6 \times 10^{-6}/°C$ for stainless steel) and consequent excellent thermal stability.

The two-inch diameter etalon mirrors are flat to $\lambda/200$, and have a reflectivity of 96% over the range 580 nm to 480 nm. This gives, for example, a theoretical finesse of 51 for a plate spacing of 5 mm and a 500 μm pinhole, and 61 for 200 μm pinhole (see Appendix A). Burleigh RC-22 triple pass retro-reflector cubes were also purchased for use when higher contrast was needed to resolve lines which would otherwise be swamped by the tail of a large Rayleigh line. This option

offers an increase in contrast of six orders of magnitude and an approximate doubling of finesse (see Appendix A), but is accompanied by a 20% reduction in transmitted intensity for perfect alignment and great difficulty in keeping the instrument aligned.

Scanning of the interferometer was achieved by applying a variable voltage ramp to three piezo-electric stacks, on which one of the mirrors is mounted. The voltage ramp was produced by a Burleigh Model RC-42 ramp generator, which is capable of providing a ramp height of up to 1000 V, with duration from 20 ms to 1000 s. As will be explained later, the scan time can be extended by addition of capacitors. The low-voltage ramp was found to deviate from linearity by less than 0.5% of the total ramp amplitude. It was found, however, that the amplified high-voltage ramp developed a 60 Hz ripple of about 4%, due to improper voltage regulation. This difficulty was overcome by the installation of a high-voltage regulator, designed and built by J. Rustenburg of the Brock University Electronics Shop.

Once supplied with a truly linear ramp, it was found that the piezoelectric stacks did not in general respond linearly to applied voltage. The dominant observed effect was a weaker response at lower stack voltage, producing a roughly quadratic apparent ramp.

Ramp nonlinearity is best seen in a manner discussed by Hernandez (1978). If the position of the first order on a ramp

is labelled $x_1 = 0$ and that of the i-th order x_i, then a plot of x_{i+1} vs x_i can be made and compared with the straight line that would correspond to a linear stack response; that is,

$$x_{i+1} = x_i + x_2$$

The circular points in Figure III-3 represent measurements of inter-order distances. The amount by which the slope of the line through the measured points deviates from unity is an indication of the extent of nonlinearity of the stack response. In this case, the slope is 0.973.

To compensate for this apparent ramp curvature, a negative quadratic shape was programmed into the ramp by the use of a Burleigh Model RC-43 ramp curvature option. The improved linearity gave a slope very close to unity for the middle orders (triangular points, Fig. III-3), but significant curvature could not be avoided near the beginning and end of the scan. The central orders in the scan were generally used for measurements, and any spectrum in which two adjacent orders differed in spacing by more than about 1% was rejected.

Aside from the above general ramp curvature, random deviations from linearity occurred within each ramp on long scans. These deviations, probably a result of some hysteresis in the stacks, could result in distortions approaching 1% in a given order. It was thus necessary to average large numbers of measurements to assure reliable results.

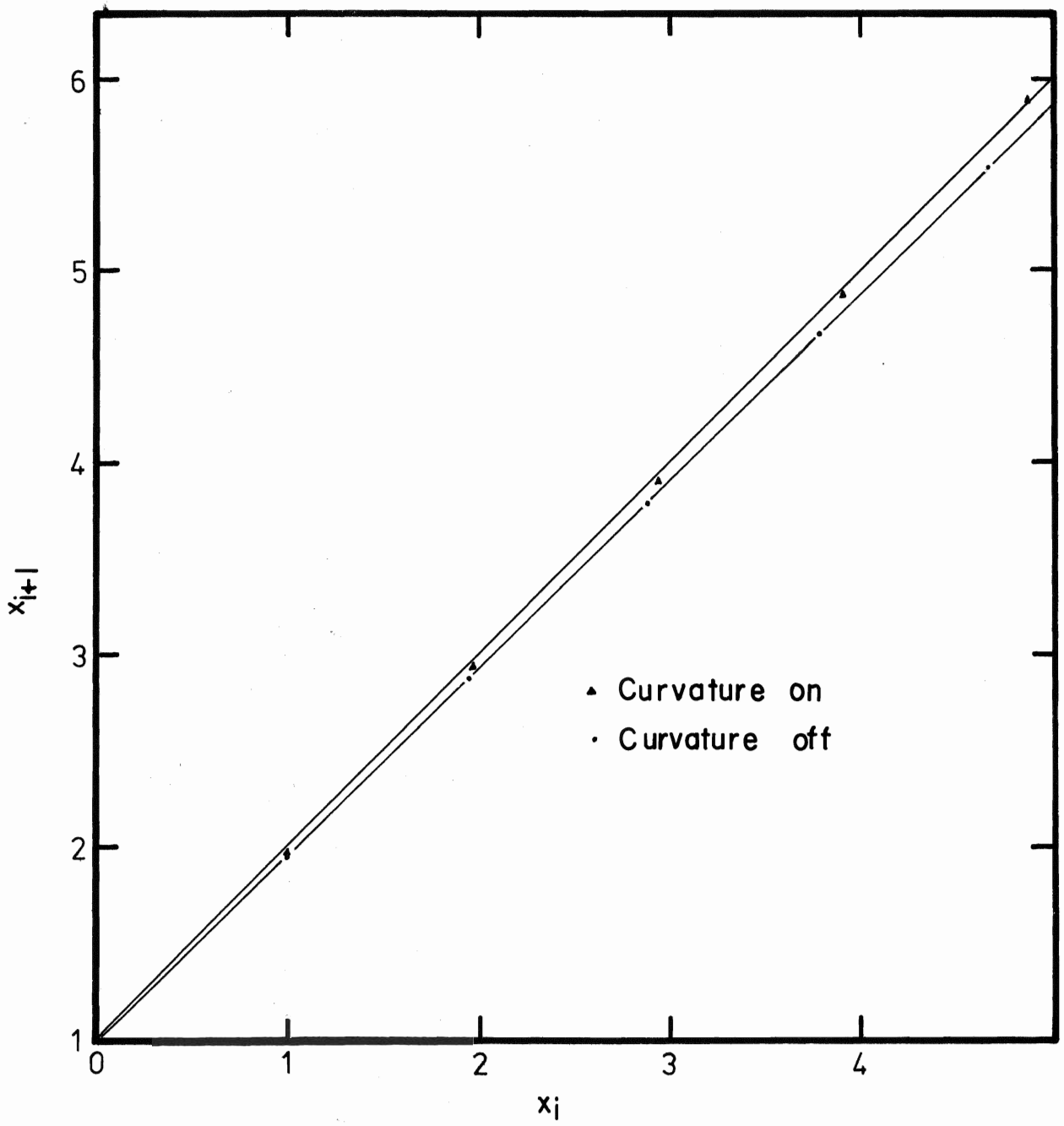

FIGURE III-3: Ramp Linearity Plot

The instrument was initially aligned by directing the laser beam along its axis with mirror M_2 (see Fig. III-1), and observing the line profile on an oscilloscope with a photodiode as a detector. The finesse thus observed was usually about 60, and remained unchanged for at least several hours.

When larger apertures were employed in taking sample spectra, however, plate parallelism became much more critical and performance sometimes degraded to an unacceptable level after only a few minutes. Operating finesse was usually around 30 to 40 using a 500 μm pinhole, and 40 to 50 using a 200 μm pinhole. The greater transmission obtained with the 500 μm pinhole generally took priority over the improvement in finesse in using a smaller pinhole. Although the stability of the system varied considerably from day to day, adequate alignment could usually be maintained for about two hours.

Triple pass operation could be achieved only when observing the laser beam directly, using a fast scan. Although the finesse observed in this case using a 200 μm pinhole clearly approached the theoretical finesse of 120, stability was very poor and consistent observations of Brillouin spectra were impossible, due to the inability to maintain plate parallelism over the duration of a longer scan. It is believed that this is a combination of individual hysteresis effects in the stacks and uneven high voltage ramp input to the three stacks. It became obvious that some of the work originally scheduled,

which requires the enhanced contrast and finesse offered by triple pass, was simply impractical until the capability of automatic stabilization and digital superposition of repetitive fast scans could be developed.

(iv) DETECTION AND DATA STORAGE

The light was detected with an ITT FW-130 photomultiplier which was thermoelectrically cooled to -20°C by a Products for Research housing.

The photomultiplier signal was processed by standard photon-counting electronics, including a spectroscopy amplifier, single channel analyser, and linear ratemeter (see Fig. III-1). The spectrum was recorded on a chart recorder.

An attempt was made to store repetitive fast scans in a 1024 channel multichannel analyzer (MCA) in order that the effects of laser drift and stack hysteresis could be minimized. A digital-to-analogue converter was built by J. Rustenburg to trigger the sweep of the MCA when the voltage level produced by some part of the usually strong Rayleigh component exceeded a set threshold value. Problems were encountered however in that the Rayleigh component was generally not strong enough to trigger the MCA reproducibly, resulting in the broadening of the spectrum as accumulation time increased.

Unknown to us at the time, Bechtle (a), (1976) has described the experiencing of essentially the same problem. In a subsequent paper (Bechtle (b) (1976)), he describes a device

which analyzes the line profile and triggers the MCA on an assigned centre point. Since this approach was successful, plans are being made for the construction of a similar device.

OTHER APPARATUS

The laser beam was focussed into the sample holder with a simple plano-convex lens L_1, of focal length of 125 mm. The light was collected from the sample and collimated with a 300 mm plano-convex lens L_2, operated at around f/20.

The light emerging from the Fabry-Perot was focussed on a pinhole A_3 by a 250 mm plano-convex lens L_3. These components were part of the Burleigh RC-41 collimator.

The entire apparatus (excluding electronics) was mounted on a granite slab, mass about one tonne, which in turn was mounted on 10 cm thick natural rubber pads. This arrangement provided adequate vibration isolation to suppress the dominant 30 Hz building vibration.

The optics were enclosed in a plywood box for thermal stability and protection from room-light.

(2) ALIGNMENT TECHNIQUE

The technique used to obtain a true 90° scattering angle, and to align the optical system is outlined below.

(i) Optical benches were placed as closely perpendicular as possible with a large carpenter's square. It

is estimated that by using extreme care, the right angle could be set to within two minutes of arc.

(ii) The Fabry-Perot was set perpendicular to the beam by back-reflection and the plates adjusted for parallelism.

(iii) The laser beam was directed along both benches by means of mirror M_2 (see Fig. III-1). Mirrors M_1 and M_2 were very carefully adjusted until the beam turned at 90° ± 3'.

(iv) Lens L_2 was placed in the beam so that the diverging beam was centred on a small aperture about 1.5 m away, through which the original beam was aimed. Lens tilt was adjusted so that the back reflection of the beam from the plane side of the lens was made to return through aperture A_1. This lens was then considered to have its axis parallel to the optical bench on which it was mounted.

(v) Lens L_1 was placed in the beam so that the parallel beam resulting from the combination of L_1 and L_2 fell on precisely the same spot as the original unfocussed beam. If lenses L_1 and L_2 were properly placed, the finesse obtained with the unfocussed beam was unaltered.

(vi) Lens L_3 of the Burleigh collimator was geometrically centred on the beam and the pinhole was positioned on-axis. The mirror M_2 was then removed,

and the eyepiece of the collimator was then used to assure good focus by observing the scattering of the laser beam in the index matching liquid, and that the Fabry-Perot fringes were sharp and centred in the field of view.

We estimate that this technique provided a scattering angle of 90° ± 5'.

After the optical axis was thus defined, the mirror was no longer used for re-alignment. A technique which was found useful for subsequent Fabry-Perot alignment was to observe fringes produced by the strong scattering from a suspension of latex particles in water, contained in a glass cell attached to an insert. The signal from the photomultiplier, operated at low voltage (1000 to 1200 V) was observed directly on the oscilloscope, and the stacks were adjusted for best alignment.

IV. RESULTS

The experimental results are presented in two sections:

(1) elastic constants, and

(2) photoelastic constants.

Sources of error are discussed and estimates of experimental accuracy are made.

(1) ELASTIC CONSTANTS

The elastic constants were obtained by measurement of the phonon group velocities for phonons travelling in the high-symmetry directions $\hat{K} = \langle 100 \rangle$ and $\hat{K} = \frac{1}{\sqrt{2}}\langle 100 \rangle$ (see Table II-1). The phonon velocity is related to the frequency shift by equation (II-9)

$$v\left(\vec{K}_j\right) = v\left(K_j\right) \frac{\lambda_0}{2n \sin(\theta/2)} \quad , \qquad \text{(IV-1)}$$

where n is the refractive index of the crystal, and λ_0 is the vacuum wavelength of the incident light. It is clear that the accuracy of the velocity measurement is determined chiefly by the accuracy to which the frequency $v\left(\vec{K}_j\right)$ can be measured, and to which the angle θ can be set.

The scattering angle was very carefully set at 90° ± 5' (see Chapter III). The free spectral range (FSR) was determined to within about 0.02% by the procedure outlined below, which is based on a method described by Grimsditch and Ramdas (1974).

DETERMINATION OF THE FREE SPECTRAL RANGE

Given that the frequency difference, $\Delta\nu$ between two lines of an atomic emission spectrum is known to a high accuracy, the FSR can be determined from the equation

$$FSR = \frac{\Delta\nu}{\Delta n + p} \qquad \text{(IV-2)}$$

where p is the measured fractional order difference for the two lines and Δn is the number of orders by which the two lines are overlapped. If lines with small frequency differences (of the order of the FSR) are chosen, a first estimate of the FSR can be made. This estimate then provides a determination of Δn for two lines of larger frequency separation, and an improvement in the estimate of the FSR. The procedure can be repeated until the desired accuracy is obtained.

In the present work, the isotopic hyperfine structure of the Hg 546 nm line was used to provide a first estimate of the FSR. The frequency differences between the various components of the line were obtained from the American Institute of Physics Handbook, 2nd ed. (1963). Sample spectra and line assignments are shown in Figure (IV-1a). By averaging over four such orders, an estimate of FSR = 29.66 ± 0.15 GHz was made. The final FSR determination was obtained from the Hg 579.0 nm and the Hg 576.9 nm lines. Based on the works of Burns et al. (1950) and Burns and Adams (1951, 1952), we expect that both lines will show isotope and hyperfine structure of the type shown in

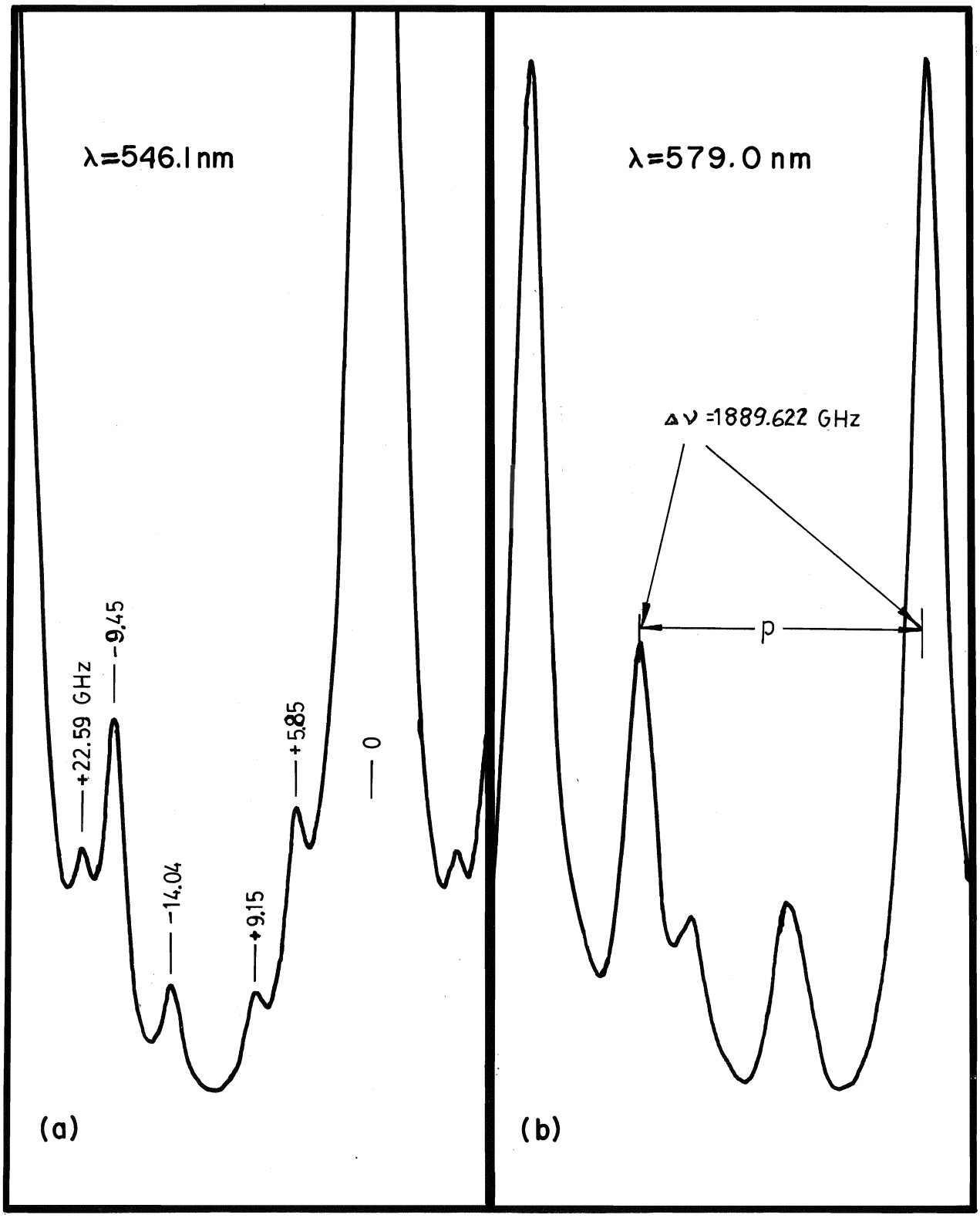

FIGURE IV-1 : Hg Spectra for Determination of FSR

Figure (IV-2), with the even isotope lines closely grouped, forming the strongest features, and Hg^{199} displaying a triplet hyperfine structure. It is thus reasoned that the strongest

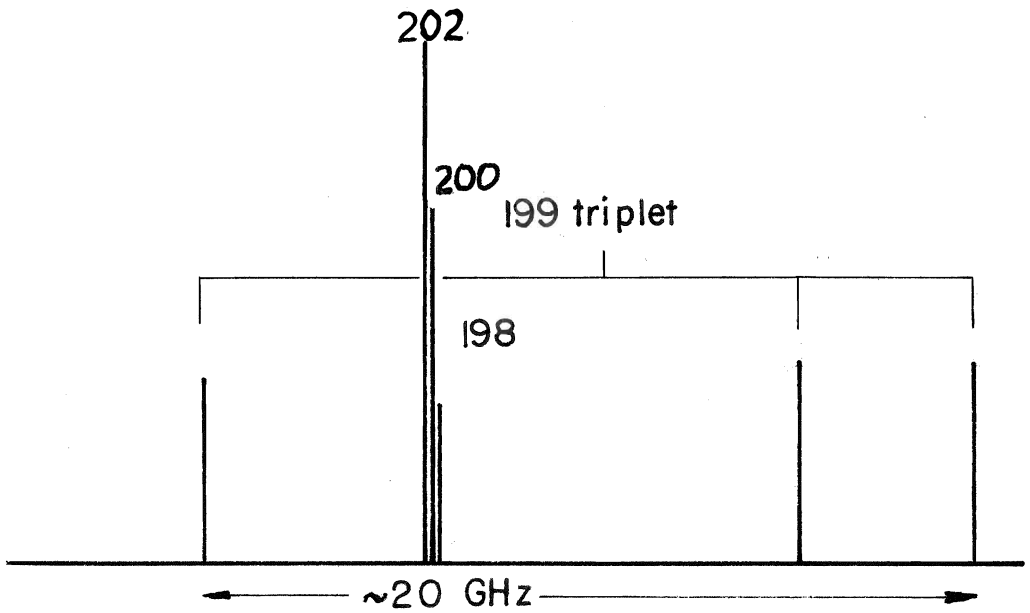

Figure IV-2: Type of structure associated with the Hg 579.0 nm and the Hg 576.9 nm lines.

lines in the spectrum observed around 579 nm will be the even isotope clusters of the 579.0 nm and the 576.9 nm lines. Assuming that the peak centres correspond to the most abundant isotope, Hg^{202}, we make the line assignments as shown in Figure (IV-1b). That is, λ = 579.06648 nm and λ = 576.9600 nm (Burns et al. (1951)). The line assignments were checked by obtaining the same intensity ratio on a Czerny-Turner double grating monochromator. Then from the previous FSR estimate, $\Delta n + p = 63.7 \pm 0.3$. The measured value of the fractional difference p is 0.720 ± 0.005, which leads to the conclusion that FSR = 29.655 ± 0.005 GHz.

This technique was employed in all frequency measurements except in some of the KBr data. These will be discussed later.

MEASUREMENT OF FREQUENCIES FROM THE CHARTS

Figure (IV-3) shows schematically a Brillouin spectrum, as it would appear on a recorder output. All frequencies were determined by measuring the ratio of distances on the chart corresponding to $2\nu/FSR$ with high quality vernier calipers. Since nonlinearities in the scan could produce variations in

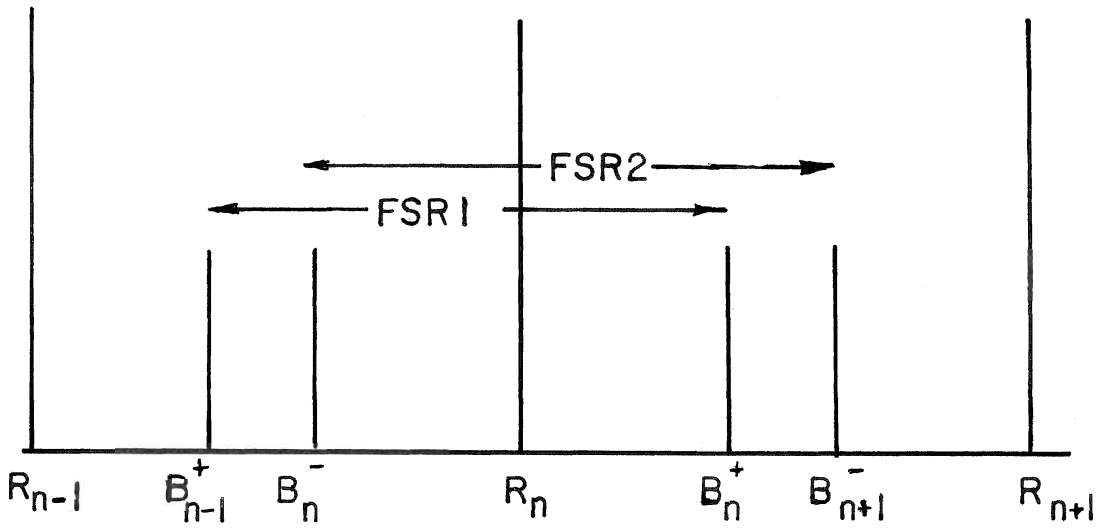

Figure (IV-3): Schematic recorder output.

the chart distance corresponding to the FSR of up to 1%, the average of FSR1 and FSR2 was used. B_n and R_n are the n-th order Brillouin and Rayleigh lines respectively.

BENZENE

Measurements of the Brillouin frequency in benzene served as a check of the FSR determination against work performed with a fixed interferometer spacing by Kato and Zdasiuk (1975) (hereafter referred to as KZ) which is believed to be of high quality.

Spectro-grade benzene was rid of dust particles by passing it through a 0.2 μm-size Millipore filter directly into a clean pyrex glass vial. The interferometer plates were set to give a free spectral range of 19.415 GHz.

Figure IV-4 shows a typical benzene spectrum taken at this FSR. Four sets of measurements were obtained at temperatures which varied between 21.0°C and 21.5°C. Since both the velocity of sound and the refractive index are temperature dependent, a suitable correction must be made to allow comparison of our results with those of Kato and Zdasiuk (1975), which were taken at 20° ± 0.5°C. Recalling equation (IV-1), we write

$$\frac{d\nu}{dT} = \frac{2\sin(\theta/2)}{\lambda_0}\left(n\frac{dv}{dT} + v\frac{dn}{dT}\right) \quad . \qquad \text{(IV-3)}$$

These temperature derivatives are given in Fabelinskii (1968) as

$$\frac{dv}{dT} = -4.6 \text{ m/sec/°C}$$

and

$$\frac{dn}{dT} = -64 \times 10^{-5}/°C,$$

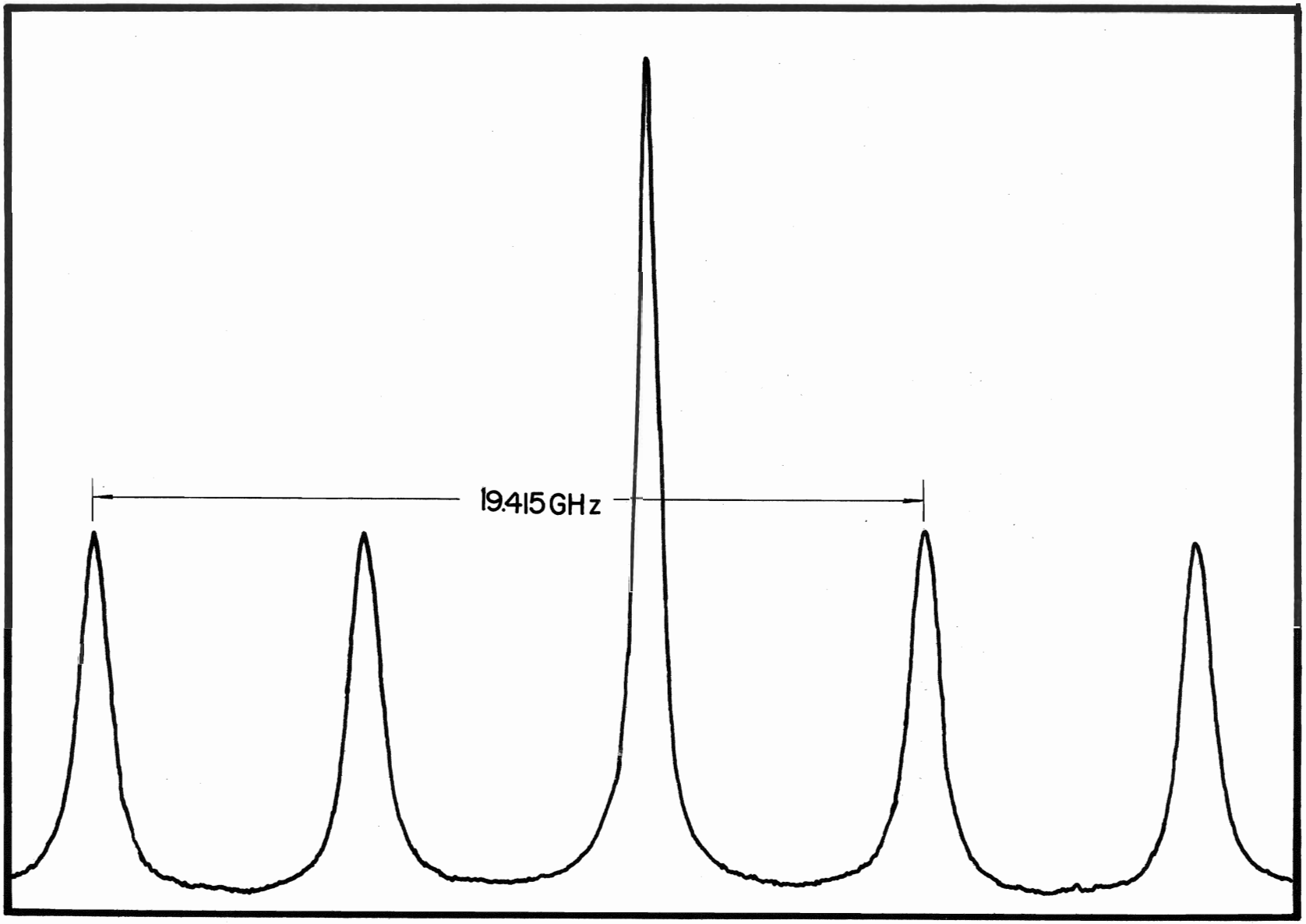

FIGURE IV-4 : Brillouin Spectrum of Benzene at 21.5° C (adjacent orders showing)

whence we get

$$\frac{d\nu}{dT} = 0.023 \text{ GHz/°C} \quad .$$

The results of the frequency measurements and the corrections to 20°C are given in Table IV-1. The number N refers to the number of spectral orders measured and serves as a weighting

Table IV-1: Brillouin frequencies in benzene

N	T(°C)	ν_T (GHz)	ν_{20} (GHz)
8	21.3	6.570 (σ = 0.013)	6.600
12	21.0	6.566 (σ = 0.008)	6.589
6	21.5	6.578 (σ = 0.033)	6.612
7	21.5	6.557 (σ = 0.003	6.592
		Weighted average = 6.60 ± 0.02	
		Kato and Zdasiuk (1975) = 6.59 ± 0.03	

factor in the final average. Standard deviations are included in the ν_T column. Temperatures were measured to within 0.1°C using a Canlab precision thermometer, the absolute accuracy of which was checked in a water and ice bath. The final error is obtained by combining the uncertainty in scattering angle, the uncertainty estimated from standard deviations at each temperature, and the spread of values around the weighted average. The optical components were removed and the scattering angle was reset between each run.

The possibility of sample heating by the ~80 mW laser beam was checked in two ways. Spectra were taken for different laser powers in a range from 10 mW to 100 mW, and showed no significant change in phonon frequency. Also, the temperature of a benzene sample was measured with a chromel-alumel thermocouple placed very close to the focussed beam. The temperatures measured by the thermocouple stayed constant throughout the above mentioned range of laser powers.

The validity of the FSR determination is shown as follows. Aside from complete misinterpretation of the Hg 579 nm spectrum (Fig. IV-1(b)), the worst miscalculation of the FSR would arise from the wrong assignment of Δn in Equation (IV-2). Changing the value of Δn by one results in a change of 1% in the frequency values, which causes disagreement with KZ which cannot be accounted for. Such a change in Δn also produces clear inconsistencies in the Hg 546.1 nm line positions. It is thus concluded that the FSR was properly determined.

NaCl

This crystal was studied to provide a check against the large volume of available ultrasonic data as well as with one Brillouin spectroscopy study by Benckert and Bäckström (1974) (hereafter referred to as BB74).

The sample was purchased from the Harshaw Chemical Company and was cleaved to approximate dimensions 15 mm x 15 mm x 5 mm. Two edges of the crystal were removed by polishing on a fine

felt pad in a water and methanol mixture to provide small, smooth, flat faces perpendicular to the incident and scattered beams. In order to minimize stray light scattered from crystal surfaces, and to assure that the intended scattering angle was not altered by refraction at the crystal surfaces, the sample was immersed in a mixture of benzene and methanol, the proportions of which were altered until no observable deflection of the beam occurred when the crystal corner was used as a prism.

The free spectral range was determined to be 29.655 ± 0.005 GHz, with adjacent orders intentionally overlapping to facilitate more precise chart distance measurements.

Sample spectra are shown in Figure IV-5(a) and (b) for incident light polarized perpendicular and parallel to the scattering plane, respectively. The latter was used in the observation of the transverse mode, due to its close proximity to the much more intense longitudinal mode. Two sets of eleven measurements each were obtained in the $\hat{K} = \langle 100 \rangle$ and the $\hat{K} = \frac{1}{\sqrt{2}}\langle 110 \rangle$ orientations, and the elastic constants are calculated from these as follows:

(i) $\hat{K} = \langle 100 \rangle$

Longitudinal: $\nu = 21.47 \pm 0.05$ GHz

$\rho v^2 = c_{11} = 49.3 \pm 0.2$ GPa.

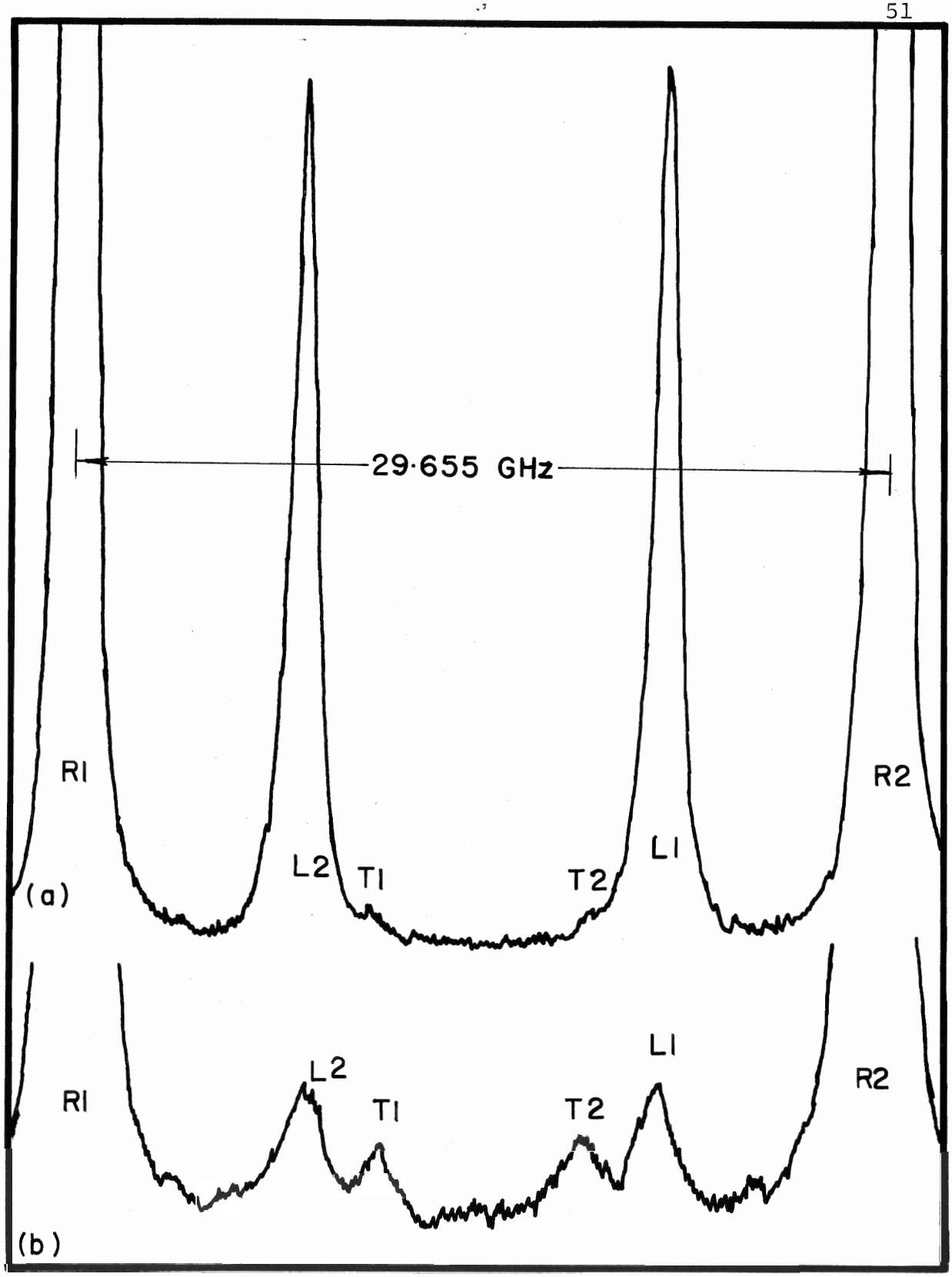

FIGURE IV-5 NaCl for (a)vertical, and (b)horizontal incident light polarizations; $K = \langle 110 \rangle / \sqrt{2}$
Adjacent orders overlapping

Transverse: $\nu = 10.90 \pm 0.08$ GHz

$\rho v^2 = c_{44} = 12.7 \pm 0.2$ GPa

(ii) $\hat{K} = \frac{1}{\sqrt{2}}\langle 110 \rangle$

Longitudinal: $\nu = 20.22$ GHz

$\rho v^2 = \frac{1}{2}(c_{11} + c_{12}) + c_{44}$

$= 43.7 \pm 0.2$ GPa

$c_{12} = 12.7 \pm 0.4$ GPa

The errors on the frequencies are the sums of the standard deviations on the eleven measurements and the uncertainty in sin ($\theta/2$) (see Eq. IV-1). Since the elastic constants depend on the squares of the frequencies, the relative errors are doubled.

The refractive indices and densities used in the calculations of the elastic constants of all three crystals are given in Table IV-2. Also given are the values of the densities found in Landolt-Bornstein (1973), vol. 7. The densities used in our calculations were chosen in the cases of NaCl and LiF to be consistent with existing Brillouin scattering work (Benckert and Bäckström (1974) and Shaham et al. (1970) respectively). It is apparent from the table that significant uncertainties (~0.2% in LiF and ~0.1% in NaCl) can arise in the elastic constants from the choice of ρ. The uncertainties in the refractive indices n do not contribute significantly to the error.

Table IV-2: Physical constants

	ρ (kg/m^3)		
	Values used*	Landolt-Bornstein (1973)	n (@ 488.0 nm)
NaCl	2165	2167.8	1.5530 ± 0.0005††
KBr	2750	2750	1.5715 ± 0.0002†
LiF	2635	2641	1.3947 ± 0.0001††

* CRC Handbook of Chemistry and Physics (1973)

† Spindler and Rodney (1952)

†† Handbook of the American Institute of Physics, 2nd ed. (1963).

The values obtained for the elastic constants are compared in Table IV-3 with the Landolt-Bornstein (1979) (hereafter referred to as LB79) values and with those obtained by BB74. The LB79 values are averaged over ten sets of data, and the errors indicated are standard deviations.

Table IV-3: Elastic constants of NaCl (T = 22°C)

	(GPa)		
	c_{11}	c_{12}	c_{44}
Present work	49.3 ± 0.2	12.7 ± 0.3	12.7 ± 0.2
Benckert and Bäckström (1974)	49.7 ± 0.2	13.1 ± 0.3	12.7 ± 0.3
Landolt-Bornstein (1979)	49.1 ± 0.5	12.8 ± 0.1	12.8 ± 0.1

KBr

Although works on the elastic constants in KBr are fairly numerous (Landolt-Börnstein (1979)), the list is considerably shorter than for NaCl, and the spread of values amongst the ultrasonic data is larger than for NaCl. The one published Brillouin study (Kaplan et al. (1970), hereafter referred to as KSL) contains values that differ from the average ultrasonic value in LB79 by 4% in c_{11} and by 20% in c_{12}. Those authors attributed the difference between ultrasonic and hypersonic values to a larger anisotropy at higher frequencies. The present study was undertaken to investigate these discrepancies.

The elastic constants were determined from frequency measurements averaged over sixteen orders for $\hat{K} = \frac{1}{\sqrt{2}}\langle 110\rangle$ and ten orders for $\hat{K} = \langle 100\rangle$. The free spectral range was determined to be 19.415 ± 0.002 GHz.

The results are as follows:

(i) $\hat{K} = \langle 100\rangle$

Longitudinal: $\nu = 16.27 \pm 0.05$ GHz

$c_{11} = 35.1 \pm 0.2$ GPa

Transverse: $\nu = 6.20 \pm 0.06$ GHz

$c_{44} = 5.1 \pm 0.1$ GPa

(ii) $\hat{K} = \frac{1}{\sqrt{2}}\langle 110\rangle$

Longitudinal: $\nu = 13.94$ GHz

$c_{12} = 6.1 \pm 0.4$ GPa

These elastic constants are compared with the results of KSL and with LB79 in Table IV-4.

Table IV-4: Elastic constants of KBr (T = 21.0°C)

	(GPa)		
	C_{11}	C_{12}	C_{44}
Present work	35.1 ± 0.2	6.1 ± 0.4	5.1 ± 0.1
Kaplan et al. (1970)	33.4 ± 0.8	3.5 ± 0.4	4.7 ± 0.4
Landolt-Bornstein (1979)	34.5 ± 0.4	5.5 ± 0.4	5.1 ± 0.2

The accuracy of our results was checked in two ways. First, the precision with which the scattering angle was set was checked by doing four scans with a complete re-setting of all optical benches, lenses and diaphragms between each scan. The maximum deviation from the average between runs was less than 0.15%, and since the standard deviation for any run is of this order, it was concluded that the scattering angle was being set reproducibly to the accuracy claimed.

As a second check, the elastic constants were used to calculate, from Equations (II-12) and (II-16), the frequencies of phonons with wavevectors lying in the [100] and [110]-

planes. The calculated frequencies are compared in Tables IV-5 and Figure IV-6 with measurements previously carried out for selected angles in these planes. Since these measurements were done before the method of FSR determination described above was known to the author, the benzene Brillouin shift given by KZ was used as a standard for FSR determination. This choice produced slightly lower (~0.4%) frequency values than those calculated from the elastic constants reported above. Such a discrepancy is not unexpected, in light of the fact that the combined error of the author and that of KZ was ~0.75%. For comparison with the calculation, the measured frequencies were scaled up to produce best agreement at $\hat{K} = \langle 100 \rangle$ and $\hat{K} = \frac{1}{\sqrt{2}}\langle 110 \rangle$. Since such a comparison serves primarily as a check on the *relative* values of the elastic constants rather than on their overall magnitude, the scaling of frequencies was felt to be justified.

Each experimental point represents the average of measurements over at least three orders. The error bars are estimated uncertainties, dependent on the spread of values in each measurements, and on the quality of the measured peak. Figure IV-8 shows a sample spectrum taken at $\phi = 26.75°$ in the [110] plane. The variation of the magnitudes of the error bars can be appreciated by inspection of the graph of scattered intensities for the three modes as a function of scattering angle.(see Fig. IV-7). The intensity curves were generated from Equations (2) and (3) of Benckert and Bäckström (1973),

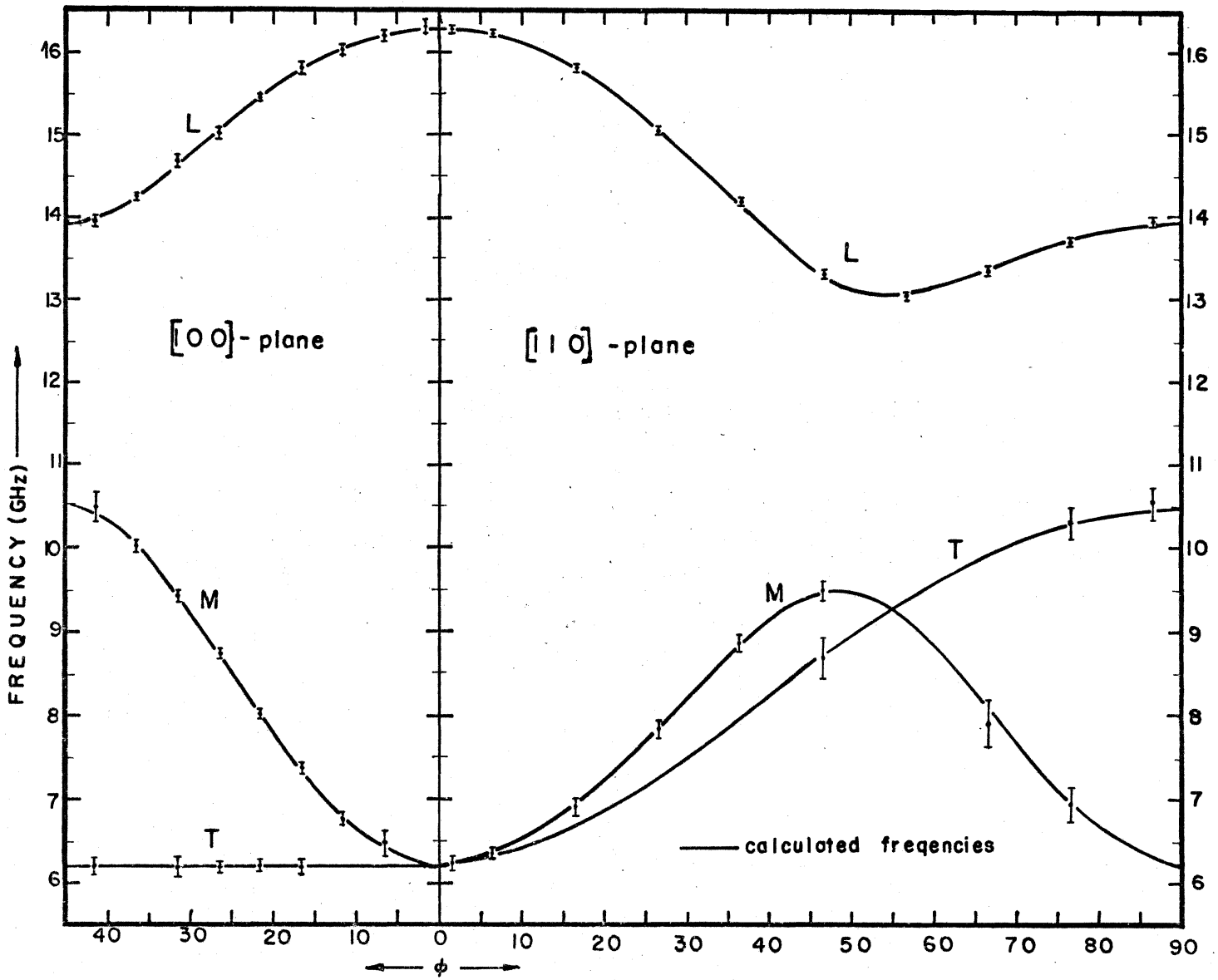

FIGURE IV-6: Brillouin frequencies for KBr in the [100] - and [110] - planes

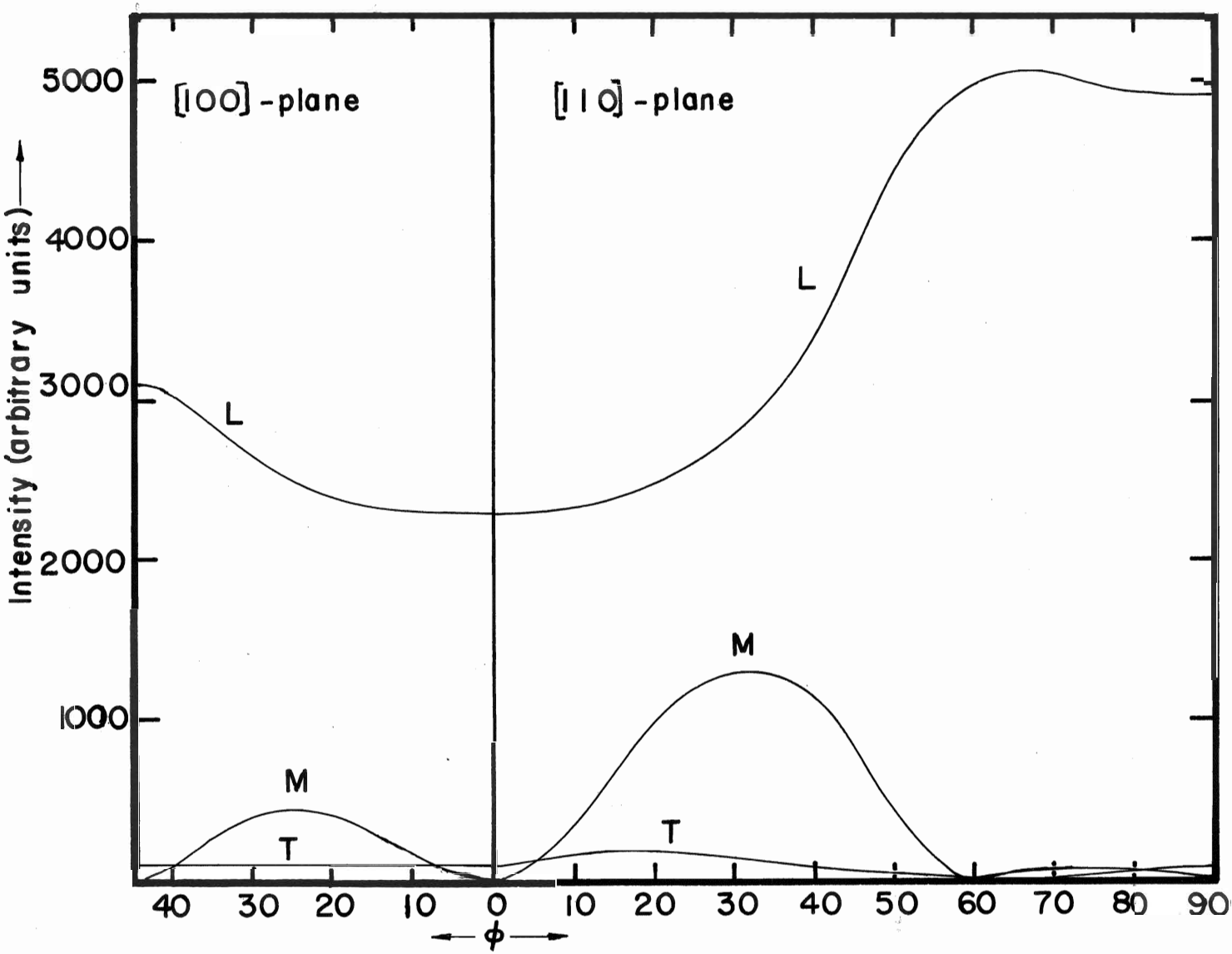

FIGURE IV-7: Scattering intensities for KBr

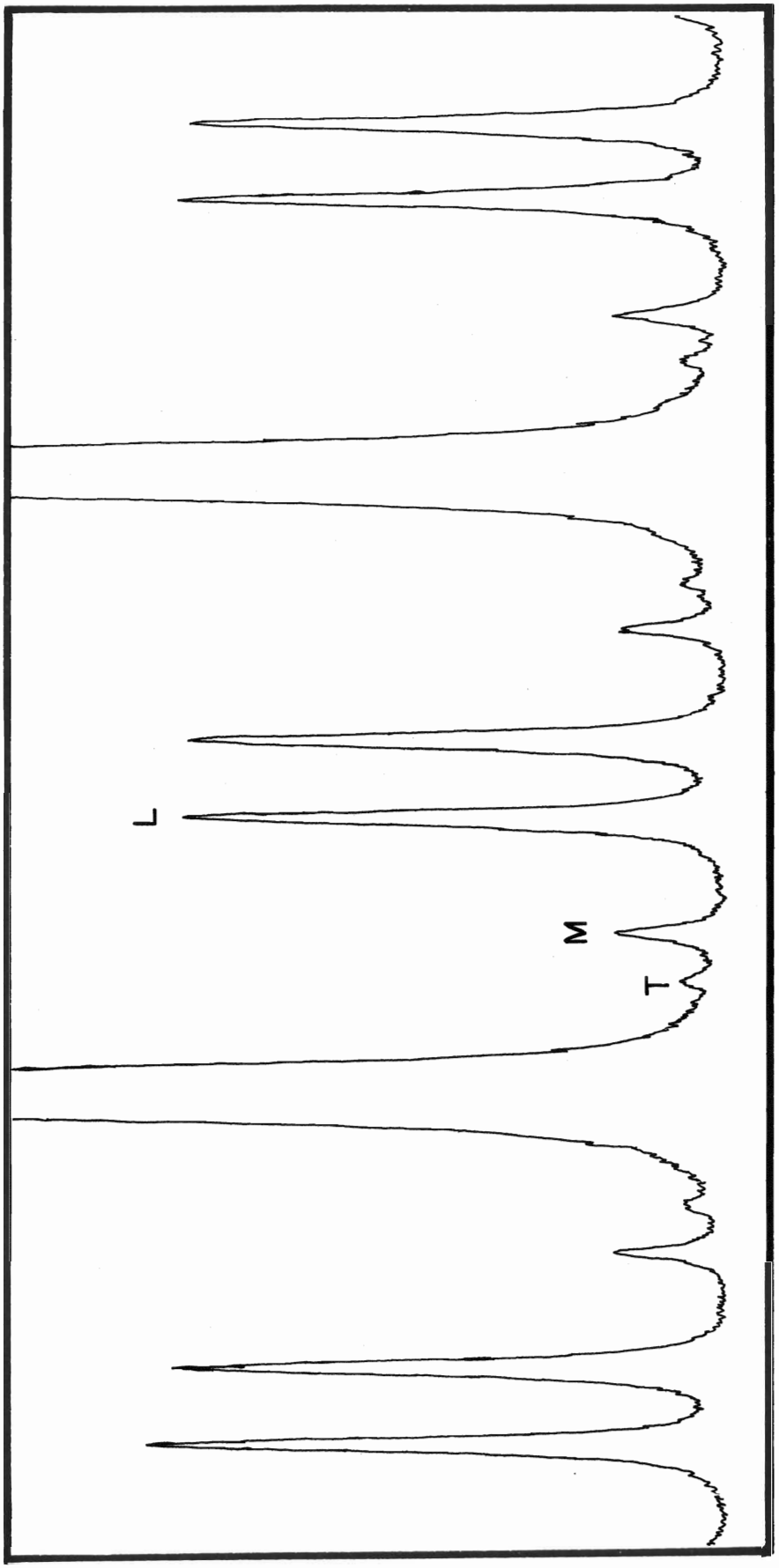

FIGURE IV-8: KBr in [100]-plane; $\phi = 26{\cdot}75°$

Tables IV-5: Measured and calculated frequencies for KBr

IV-5(a): [100]-plane

ϕ	ν_L(meas)	ν_L(calc)	ν_M(meas)	ν_M(calc)	ν_T(meas)	ν_T(calc)
1.75	16.32 ± 0.08	16.26	--	6.22	--	6.20
6.75	16.21 ± 0.08	16.19	6.46 ± 0.15	6.41	--	6.20
11.75	16.04 ± 0.07	16.02	6.77 ± 0.09	6.81	--	6.20
16.75	15.77 ± 0.08	15.77	7.38 ± 0.08	7.38	6.19 ± 0.09	6.20
21.75	15.46 ± 0.05	15.45	8.01 ± 0.08	8.03	6.20 ± 0.07	6.20
26.75	15.03 ± 0.08	15.07	8.74 ± 0.08	8.73	6.20 ± 0.07	6.20
31.75	14.68 ± 0.08	14.65	9.45 ± 0.09	9.41	6.19 ± 0.11	6.20
36.75	14.24 ± 0.05	14.26	10.00 ± 0.10	9.99	--	6.20
41.75	13.94 ± 0.07	13.98	10.49 ± 0.20	10.38	6.22 ± 0.10	6.20

IV-5(b): [110]-plane

ϕ	ν_L(meas)	ν_L(calc)	ν_M(meas)	ν_M(calc)	ν_T(meas)	ν_T(calc)
1.5	16.26 ± 0.05	16.26	6.19 ± 0.12	6.20	--	6.20
6.5	16.21 ± 0.04	16.19	6.33 ± 0.08	6.32	--	6.27
16.5	15.80 ± 0.06	15.78	6.87 ± 0.10	6.95	--	6.64
26.5	15.01 ± 0.06	15.06	7.85 ± 0.10	7.88	--	7.88
36.5	14.15 ± 0.06	14.14	8.87 ± 0.10	8.83	--	7.97
46.5	13.29 ± 0.06	13.30	9.50 ± 0.15	9.42	8.64 ± 0.50	8.70
56.5	13.03 ± 0.07	13.05		9.13		9.36
66.5	13.31 ± 0.07	13.35	7.85 ± 0.30	8.07	--	9.90
76.5	13.67 ± 0.07	13.71	6.94 ± 0.20	6.93	10.27 ± 0.18	10.27
86.5	13.92 ± 0.07	13.90	--	6.25	10.54 ± 0.18	10.44

using the values of the photoelastic constants presented in the second part of this chapter.

Equations (II-13) and (II-17) indicate that the polarizations of phonons lying in the [100]- and [110]-planes are such that one mode is almost completely longitudinal (the highest frequency mode), one mode is almost completely transverse (pure transverse in the [100]-plane) and a third is "mixed". The mode designations are shown in Figure IV-6.

The "longitudinal" mode frequencies are dominated by the value of c_{11}, whereas the transverse frequencies are strongly dependent on c_{44} in the [110]-plane, and completely determined by c_{44} in the [100]-plane. Hence, the relative positions of these curves serves as a check on the ratio c_{11}/c_{44}. The effect of c_{12} is most strongly demonstrated in the shapes of the "mixed" and "longitudinal" curves near the $K = \frac{1}{\sqrt{2}}\langle 110\rangle$ direction in both planes. Since almost all measured frequencies fall easily within experimental error of the calculated frequencies, it is felt that the elastic constants calculated from the measurements in the two high-symmetry directions are valid.

LiF

The Brillouin scattering from LiF is much weaker than from most other alkali halides (about 1/50-th the intensity of the scattering from KBr). One Brillouin study has already been

reported by Shaham et al. (1970). Figure IV-9a is a reproduction of a spectrum obtained by these authors and Figure IV-9b shows the results of their measurements at various angles in the [100]-plane.

The elastic constants obtained from their work are ~10% lower than the ultrasonic values (see Table IV-7). The difference was attributed to a dispersion between ultrasonic and hypersonic frequencies. Since this result represents to our knowledge the first report of a significant departure from ultrasonic results at room temperatures, it was decided to investigate the discrepancy.

The sample was cleaved from a one-inch cube purchased from the Harshaw Chemical Company, and had been gamma-irradiated for ease of cleavage. After cleaving, the crystal was annealed at ~600°C for 24 hours, and then brought to room temperature at a rate of 10°C/h. The laser beam appeared as a yellow column in the crystal indicating a fluorescence. Repeated annealing did not alter this condition. It was found that the fluorescence produced an unacceptable background level (~2000 counts per second, or 20 times the strongest observed Brillouin line). An interference filter the bandpass of which was centred at 488.0 nm was used to reduce the background level to about 50 counts per second.

To observe the low scattering intensity with sufficient consistency, it was necessary to use a longer scan than the 15 min maximum provided by the ramp generator. An increase to

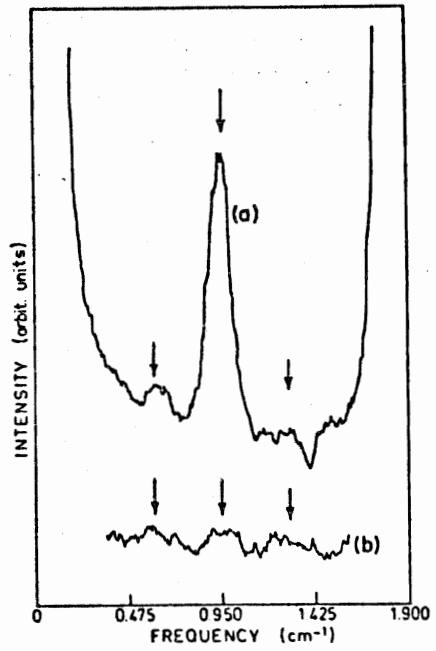

(a)

The Brillouin spectrum of LiF for phonons in the (110) direction with [100] as scattering plane: above, for $\hat{n}$ / perpendicular to that plane; below, for $\hat{n}$ / in the plane. The two longitudinal lines coincide. The laser power is not exactly the same for the two polarizations.

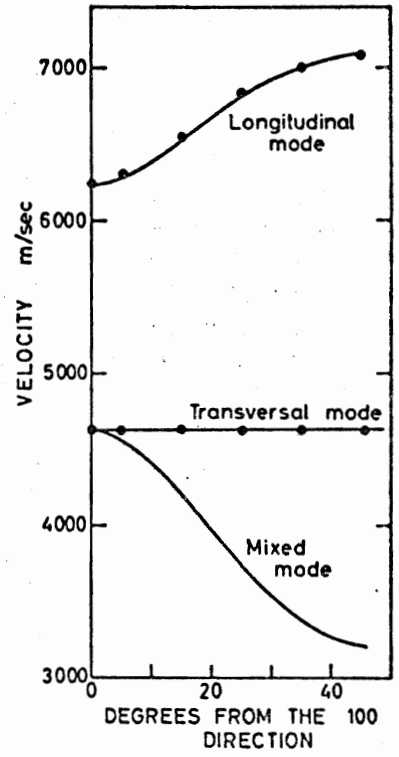

(b)

Angular variation of the phonon velocities of LiF in the [100] plane, at room temperature. The black points are the experimental points.

FIGURE IV-9: Reproduction from Shaham et al. (1970)

30 min was achieved by the addition of capacitance to the low voltage ramp control circuit.

The free spectral range was 35.770 ± 0.005 GHz. Eighteen spectra were taken for $\hat{K} = \frac{1}{\sqrt{2}}\langle 110\rangle$ and fourteen were taken for $\hat{K} = \langle 100\rangle$, with the incident light polarized perpendicular to the scattering plane and without an analyzer after the sample.

The elastic constants were calculated from these measurements as follows:

(i) $\hat{K} = \langle 100\rangle$

Longitudinal: $\nu = 26.52 \pm 0.11$ GHa

$c_{11} = 113.5 \pm 0.9$ GPa

Transverse: $\nu = 19.75 \pm 0.11$ GHz

$c_{44} = 62.9 \pm 0.6$ GPa

(ii) $\hat{K} = \frac{1}{\sqrt{2}}\langle 110\rangle$

Longitudinal: $\nu = 29.80 \pm 0.2$ GHz

$c_{12} = 47 \pm 2$ GPa

Scattering was also investigated at five degree intervals of crystal orientation (except at $\phi = 30°$). An example of one such spectrum at $\phi = 35°$ is shown in Figure IV-10. Normally, six spectra were averaged for each orientation. The results of these measurements are compared in Table IV-6 and Figure IV-12 to frequencies calculated from the elastic constants as determined above.

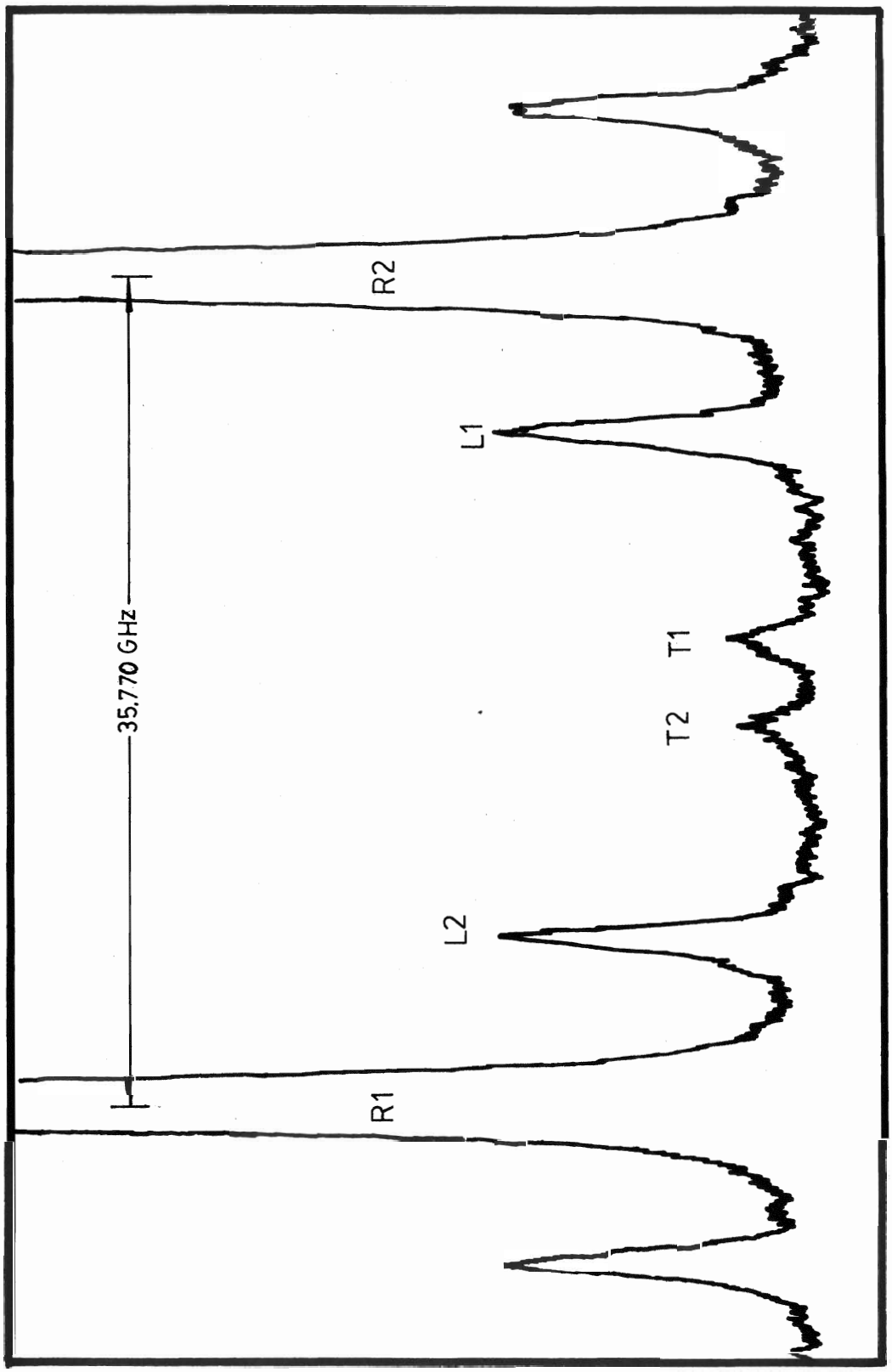

FIGURE IV-10 :LiF in [100]-plane, $\phi = 35°$

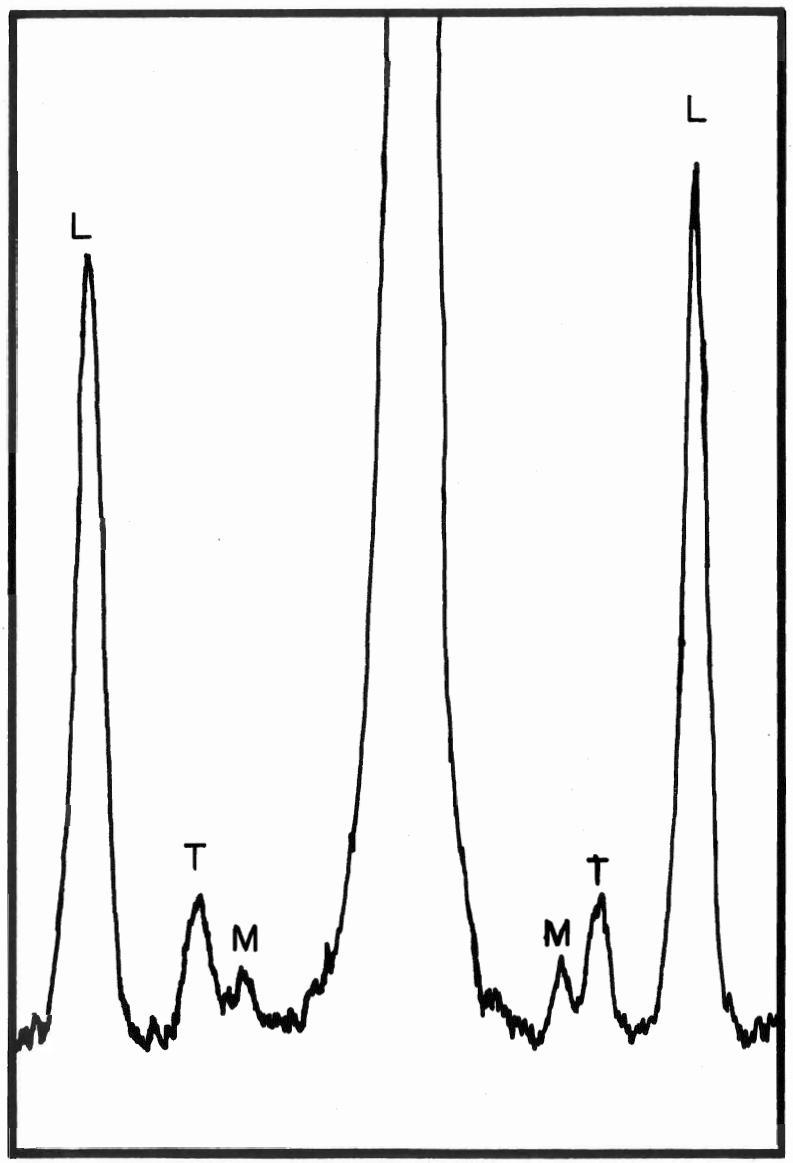

FIGURE IV-11 : LiF in [100]-plane, $\phi = 29°$
Extended (3 hour) scan

Table IV-6: Measured and calculated frequencies for LiF in the [100]-plane

ϕ	ν_L(meas)	ν_L(calc)	ν_M(meas)	ν_M(calc)	ν_T(meas)	ν_T(calc)
5	26.69 ± 0.03	26.68	--	19.53	19.74 ± 0.07	19.75
10	27.10 ± 0.04	27.10	--	19.94	19.71 ± 0.07	19.75
15	27.63 ± 0.05	27.65	--	18.13	19.71 ± 0.07	19.75
20 (19)	28.26 ± 0.04	28.23	17.5 ± 0.4	17.23	19.74 ± 0.07	19.75
25 (28)	28.75 ± 0.05	28.76	16.4 ± 0.2	16.33	--	19.75
31 (29)	29.76 ± 0.03	29.20	15.7 ± 0.2	15.52	19.81 ± 0.07	19.75
35 (34)	29.52 ± 0.03	29.53	15.1 ± 0.2	14.89	19.81 ± 0.07	19.75
40	29.68 ± 0.05	29.73	--	14.48	19.71 ± 0.07	19.75

The "mixed" mode, which was not seen by Shaham et al. (1970) has appreciable intensity, although weaker than the transverse mode, between the angles $\phi \simeq 10°$ and $\phi \simeq 35°$ (see Fig. IV-13). The free spectral range of 35.770 GHz was not ideal for the observation of this mode, because of its overlapping with the pure transverse mode. For this reason, the transverse modes observed at angles where overlapping was possible were not used for the calculation of c_{44}. To better observe the mixed mode, the free spectral range was changed to ~70 GHz, and a 3 h scan was produced by the addition of capacitance to the low-voltage ramp circuit. Because of capacitor leakage over this long ramp duration, the ramp became very non-linear, so that accurate frequency measurements were impossible.

Figure IV-11 shows the Brillouin spectrum of LiF at $\phi = 34°$ with the mixed mode clearly resolved.

The elastic constants obtained above are compared in Table IV-7 with ultrasonic data and with that of Shaham et al. (1970).

Table IV-7: Elastic constants of LiF (T = 21.0°C)

	GPa		
	c_{11}	c_{12}	c_{44}
Present work	113.5 ± 0.9	47 ± 2	62.9 ± 0.6
Shaham et al. (1970)	103 ± 3	48 ± 2	57 ± 2
Landolt-Bornstein (1979)	112 ± 2	46 ± 3	63.5 ± 0.6

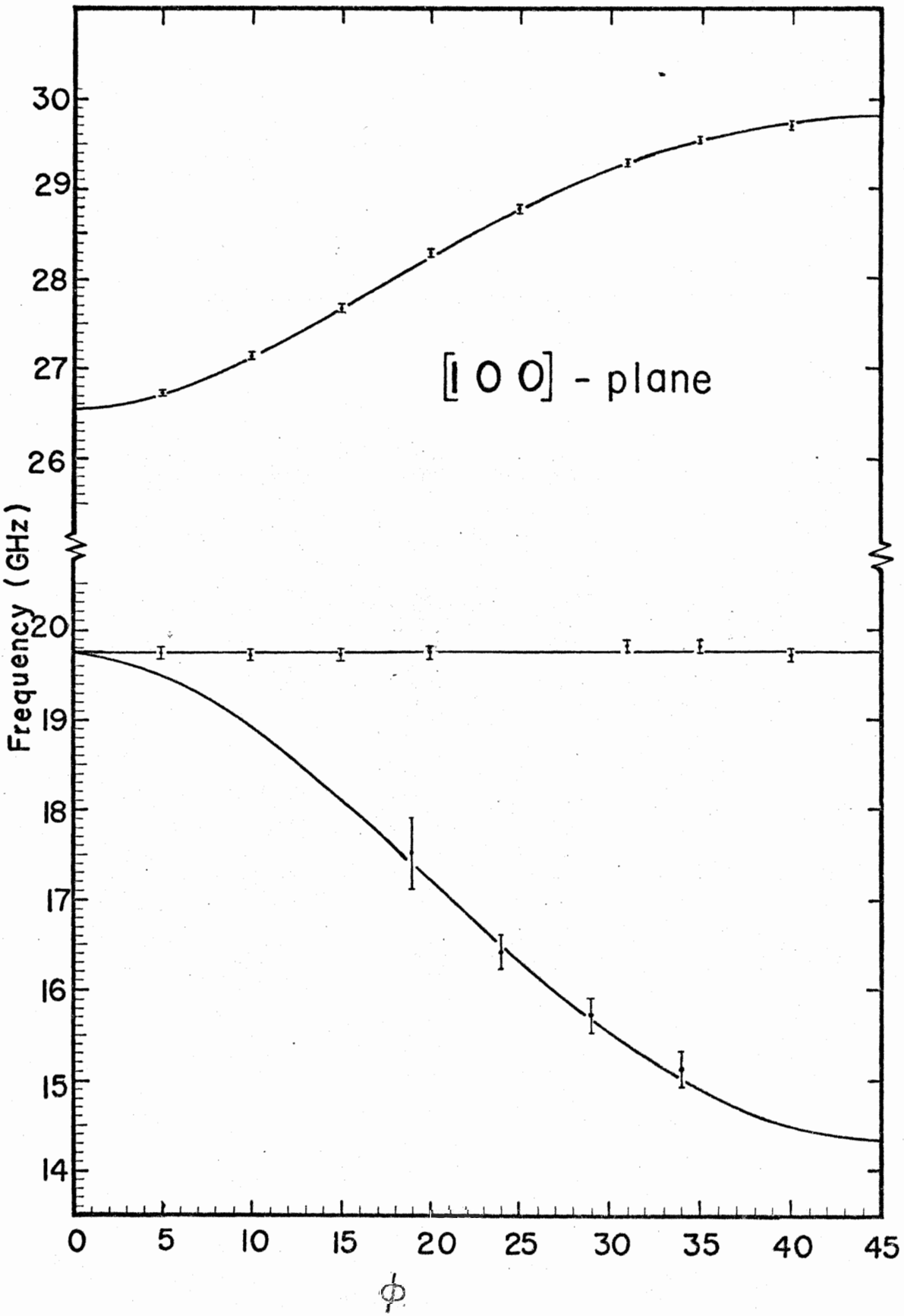

FIGURE IV-12: BRILLOUIN FREQUENCIES FOR LiF IN THE [110]-PLANE

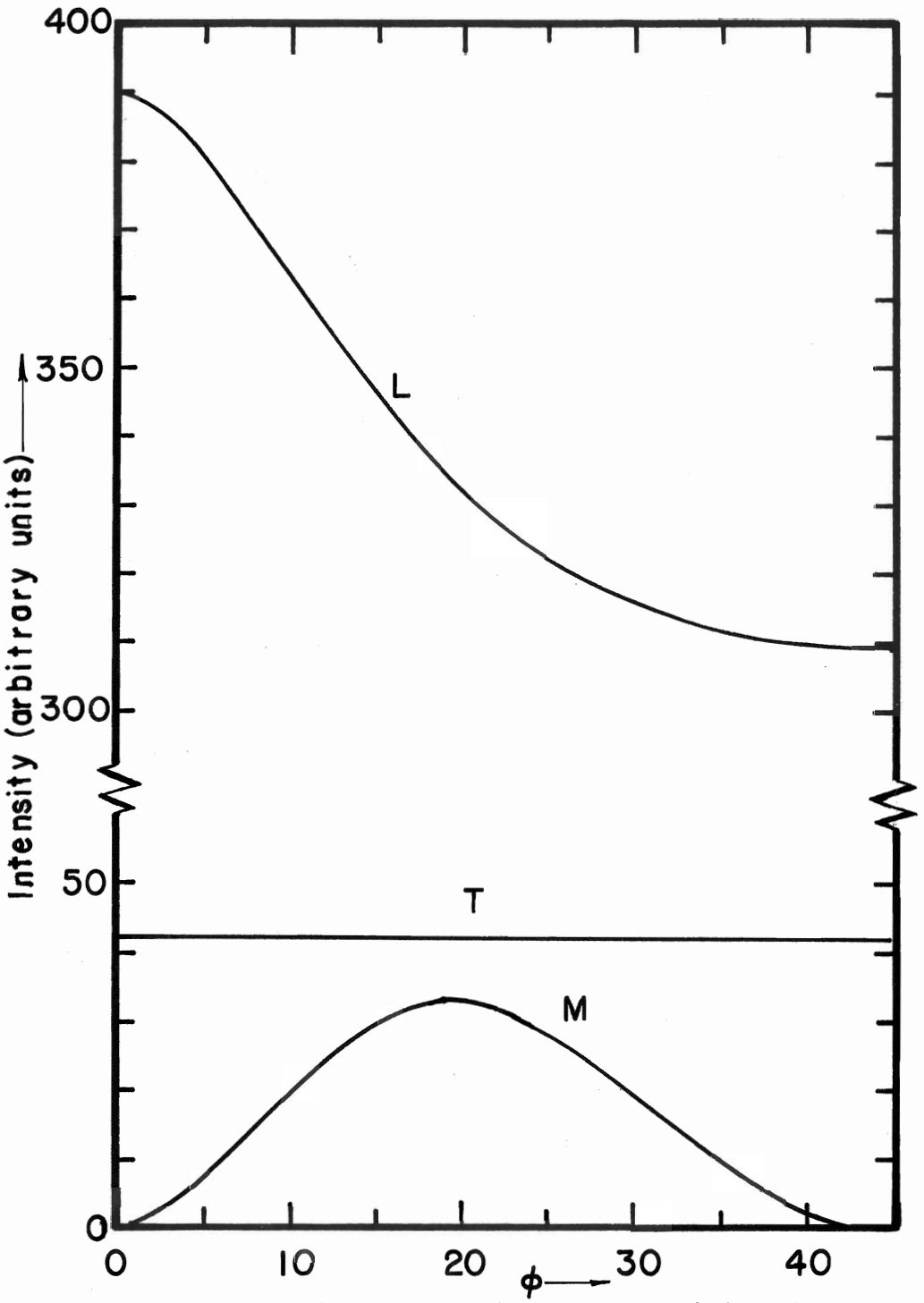

FIGURE IV-13: Scattering intensities for LiF in the [100]-plane

(2) PHOTOELASTIC CONSTANTS

The photoelastic constants of a material can be obtained either by comparing the intensity of the Brillouin scattering with the intensity of the Rayleigh scattering from an absolute standard such as Ludox SM (Kato and Zdaziuk (1975), Kato and Stoicheff (1975)), or by comparison with the Brillouin scattering from a material whose photoelastic constants are known (Benckert and Bäckström (1973); Cummins and Schoen (1968)). The direct measurement of absolute intensities is at best a difficult undertaking since anything less than ideal experimental conditions can drastically alter the apparent scattered intensity (Fabelinskii (1968)). Since careful measurements of the scattering intensity for some liquids by the absolute method are now available (Kato and Zdaziuk (1975)), the second approach was used in this work.

Liquids have only one photoelastic constant, which is related to the fluctuations of the dielectric constant due to adiabatic density fluctuations (Cummins and Schoen (1968))

$$p_\ell n_\ell^4 = \rho_\ell \left(\frac{\partial \varepsilon}{\partial \rho_\ell}\right)_S \qquad \text{(IV-4)}$$

where n_ℓ is the refractive index of the liquid, and p_ℓ is its photoelastic constant. If the value p_ℓ is known for a given liquid, then the photoelastic constants of a crystal can be obtained from the equation

$$|p_c| = \left(\frac{I_c}{I_\ell} \cdot \frac{\rho_c v_c^2}{\rho_\ell v_\ell^2}\right)^{\frac{1}{2}} p_\ell \qquad \text{(IV-5)}$$

where p_c is the appropriate photoelastic constant (or combination of photoelastic constants) of the crystal, I_c is the measured scattered intensity (relative) for a phonon whose velocity is v_c, ρ_c is the density of the crystal, ρ_ℓ is the density of the liquid and v_ℓ is the sound velocity in the liquid.

Because the index matching fluid surrounding the vial containing the liquid sample has the same refractive index as the crystal, compensation for refraction of the scattered light is made by multiplying the right hand side of Equation (IV-5) by the ratio $\frac{n_c}{n_\ell}$, where n_c and n_ℓ are the refractive indices of the crystal and the liquid respectively. Then, using (IV-4), we write

$$|p_c| = \left(\frac{I_c}{I_\ell} \cdot \frac{\rho_c v_c^2}{\rho_\ell v_\ell^2}\right)^{\frac{1}{2}} \frac{\rho\left(\frac{\partial \varepsilon}{\partial \rho}\right)_s}{n_\ell^3 n_c} \qquad \text{(IV-6)}$$

It is important to note that the quantity $\rho\left(\frac{\partial \varepsilon}{\partial \rho}\right)_s$ is, in general frequency dependent (Fabelinskii (1968)) to the extent shown for benzene and toluene in Table IV-8.

Table IV-8: Hypersonic and ultrasonic values of $\rho\left(\frac{\partial \varepsilon}{\partial \rho}\right)_s$

	Hypersonic ($\sim 10^{10}$ Hz)*	Ultrasonic ($\sim 10^{7}$ Hz)**	% Difference
Benzene	1.70 ± 0.06	1.56	9.0
Toluene	1.73 ± 0.07	1.60	8.1

* Kato and Zdasiuk (1975) ** Fabelinskii (1968)

Benzene was chosen as an intensity standard for its relatively large Brillouin frequency and relatively narrow and symmetric Brillouin line profile.

Benzene intensities were measured by a graphical determination of the area under the recorder trace of the Brillouin line. Since the Brillouin shifts of the crystals being studied are two to five times larger than the shift in benzene, it was necessary to use a large free spectral range to avoid overlapping of lines and consequent difficulty in determining intensities. Thus, some merging of the wings of the Rayleigh and Brillouin lines in the benzene spectra was unavoidable.

Separation of the components of the triplet was made difficult by the departure of the instrumental profile from the Lorentzian form, due to slight misalignment of the Fabry-Perot plates (for a discussion of this effect, see Del Piano and Quesada (1965)). Usually the profile fell more abruptly at the tail than a Lorentzian of the same width (see Fig. IV-14). Moreover, since the extent of plate misalignment often varied from order to order, approximating the Rayleigh line by an analytical function was not found to be an appropriate procedure.

An estimate of the intensity of the Brillouin component could be obtained by assuming a symmetric line profile, and then measuring the area of the outside half of the peak where the tail of the Rayleigh line is small.

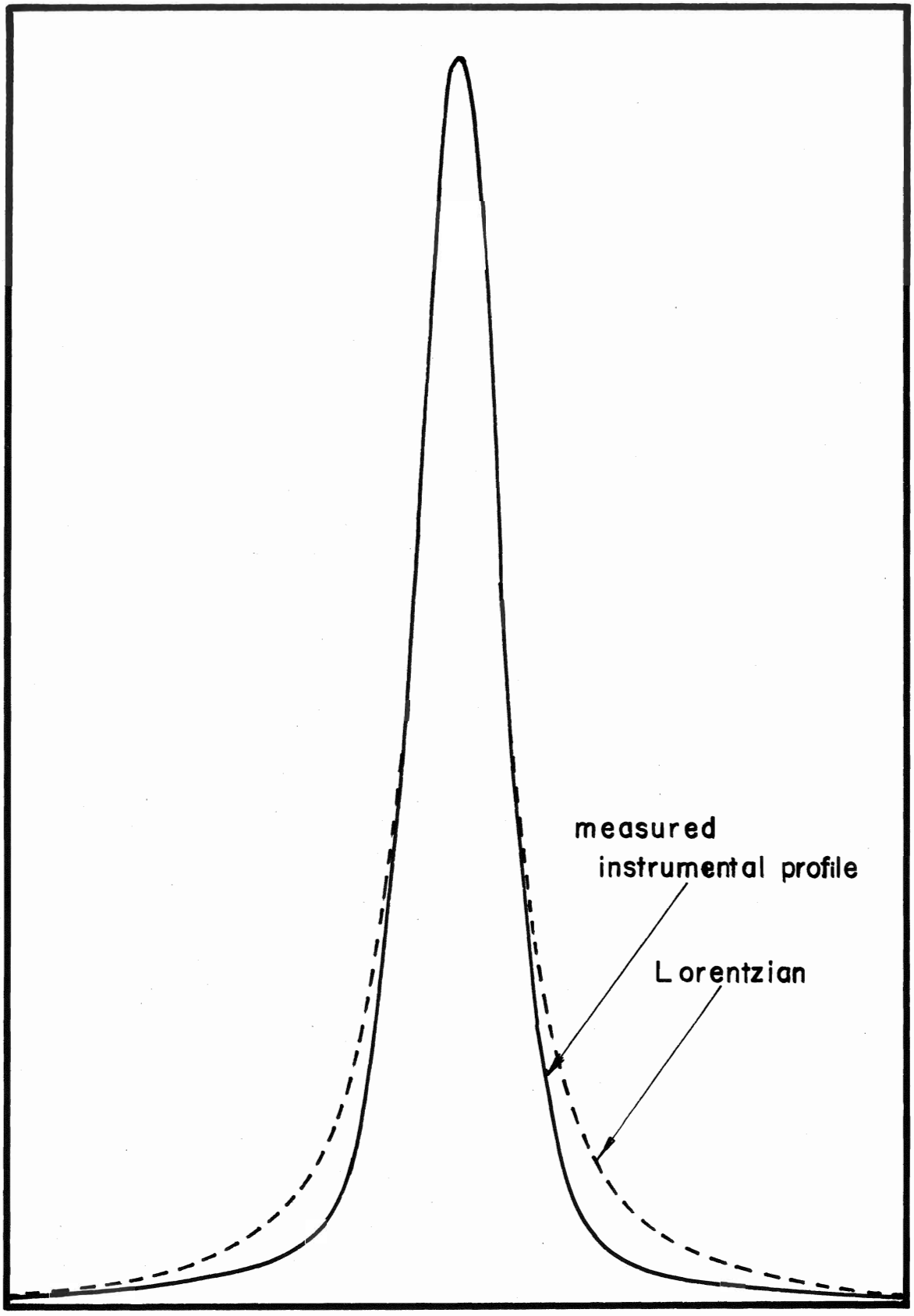

FIGURE IV-14 INSTRUMENTAL LINE PROFILE

However, it has been shown by Montrose et al. (1968) and Pinnow et al. (1968) that the Brillouin line profile in liquids is not in general symmetric due to the effects of viscosity and multiple relaxations. In fact, the dashed curve in Figure IV-15, drawn on the assumption of a symmetric Brillouin component leads to a Rayleigh line having an unrealistic "hump". On the other hand, we expect from the works of Cummins and Gammon (1965) and KZ that the extent of the asymmetry is relatively slight, since both authors found a Lorentzian to be a satisfactory approximation to the line shape in benzene.

An additional complication is the presence of a thermal relaxation peak centred at zero frequency shift, which was predicted by the theory of Mountain (1966) and observed by KZ. In the case of benzene, this component is seen as a broadening of the base of the Rayleigh component. The unavailability of data for the explicit determination of the magnitudes of the above effects, in combination with the inconsistency in the instrumental profile, leads to the adoption of the practice of visually estimating the wing of the Rayleigh line. An example of such an estimation is shown in Figure IV-15. Although this practice cannot be entirely satisfactory, it is expected that the position of the Rayleigh wing can be estimated with an accuracy leading to 5%-10% uncertainty in the intensity, depending on the separation of the lines. Uncertainties were estimated by drawing the Rayleigh wings which were felt to be

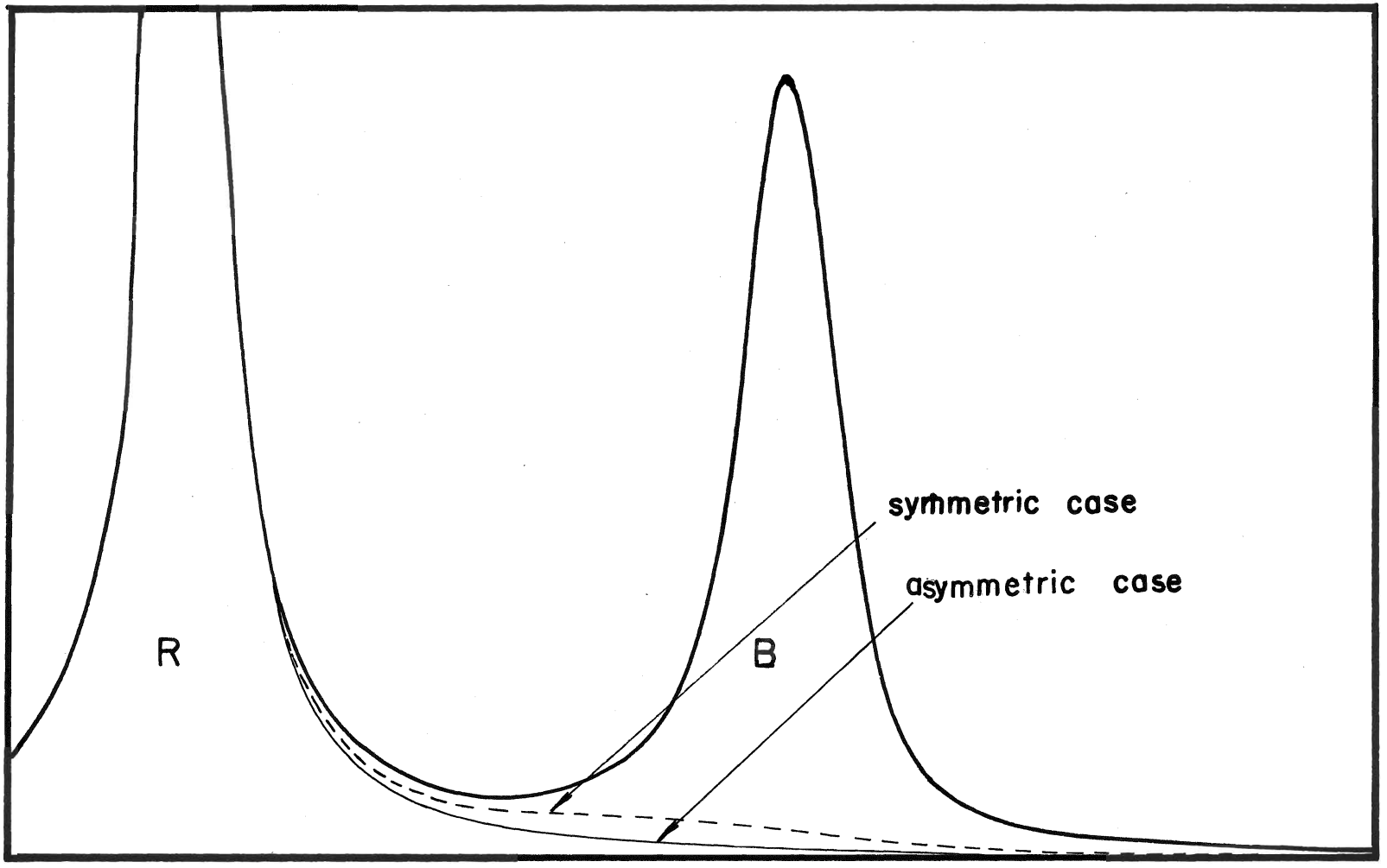

FIGURE IV-15: Visual estimate of Rayleigh wing position in the benzene intensity standard for the measurement of the photoelastic constants of KBr.

the most extreme departures from the best estimate which still conformed with the above guidelines.

The imperfect surfaces of the glass vial containing the benzene were found to cause transmission losses which depended on the refractive index of the surrounding liquid. The necessary correction was determined by measuring with a photodiode the intensity of the laser light emerging from the sample holder with and without the benzene sample in place.

NaCl

As was stated earlier, it is important that the appropriate value of $\rho\left(\frac{\partial\varepsilon}{\partial\rho}\right)_s$ be used for the liquid serving as a standard. The only other Brillouin measurements to date of the photoelastic constants of NaCl were made by Benckert and Bäckström (1973) (hereafter referred to as BB73), before the hypersonic data of Kato and Zdaziuk (1975) became available. The former authors used toluene as an intensity standard, and assumed the ultrasonic value of $\rho\left(\frac{\partial\varepsilon}{\partial\rho}\right)_s = 1.60$, quoted in Table IV-8. They arrived at photoelastic constants for NaCl, NaF, KCl and KI which are generally in good agreement with ultrasonic results. The use of the correct hypersonic value of $\rho\left(\frac{\partial\varepsilon}{\partial\rho}\right)_s$ in their calculations would have produced values which, although just within experimental error of the ultrasonic average given LB79, are generally higher by about 9%. Since the photoelastic constants are not expected to be frequency dependent, the results of BB73 are somewhat surprising.

It was therefore decided to repeat the work of Benckert and Bäckström (1973) using benzene as a standard.

The free spectral range was set to ~45 GHz, so that the longitudinal peaks of adjacent orders were overlapped. All NaCl spectra used in the determination of the photoelastic constants were taken with a 30 minute scan, and a 2.0 second time constant. To obtain an average value of the intensity over seven spectral orders in two scans, the peaks of each scan were superimposed on tracing paper, and the average line profile was drawn from these. Figure IV-16 shows the line profiles obtained with this averaging technique. To give an idea of the noise levels encountered, a sample spectrum is shown superimposed on the "average" line. Since there was no ambiguity in determining the baseline for the strong longitudinal mode (Fig. IV-16(a)), the error in the intensity for this mode is estimated to be about 3%. The spectra taken with the input polarization parallel to the scattering plane were much weaker (see Fig. IV-16(b) and (c)), and errors of 15% were assigned to those intensities. An error of 8% was assigned to the benzene intensity (Fig. IV-16(d)). The transmission loss due to the glass vial was measured to be 3.8%.

The final results are given and compared in Table IV-9 with BB73 and the ultrasonic results contained in LB79. The errors indicated for the present work include the 3.5% uncertainty in $\rho\left(\frac{\partial \varepsilon}{\partial \rho}\right)_S$ given by KZ.

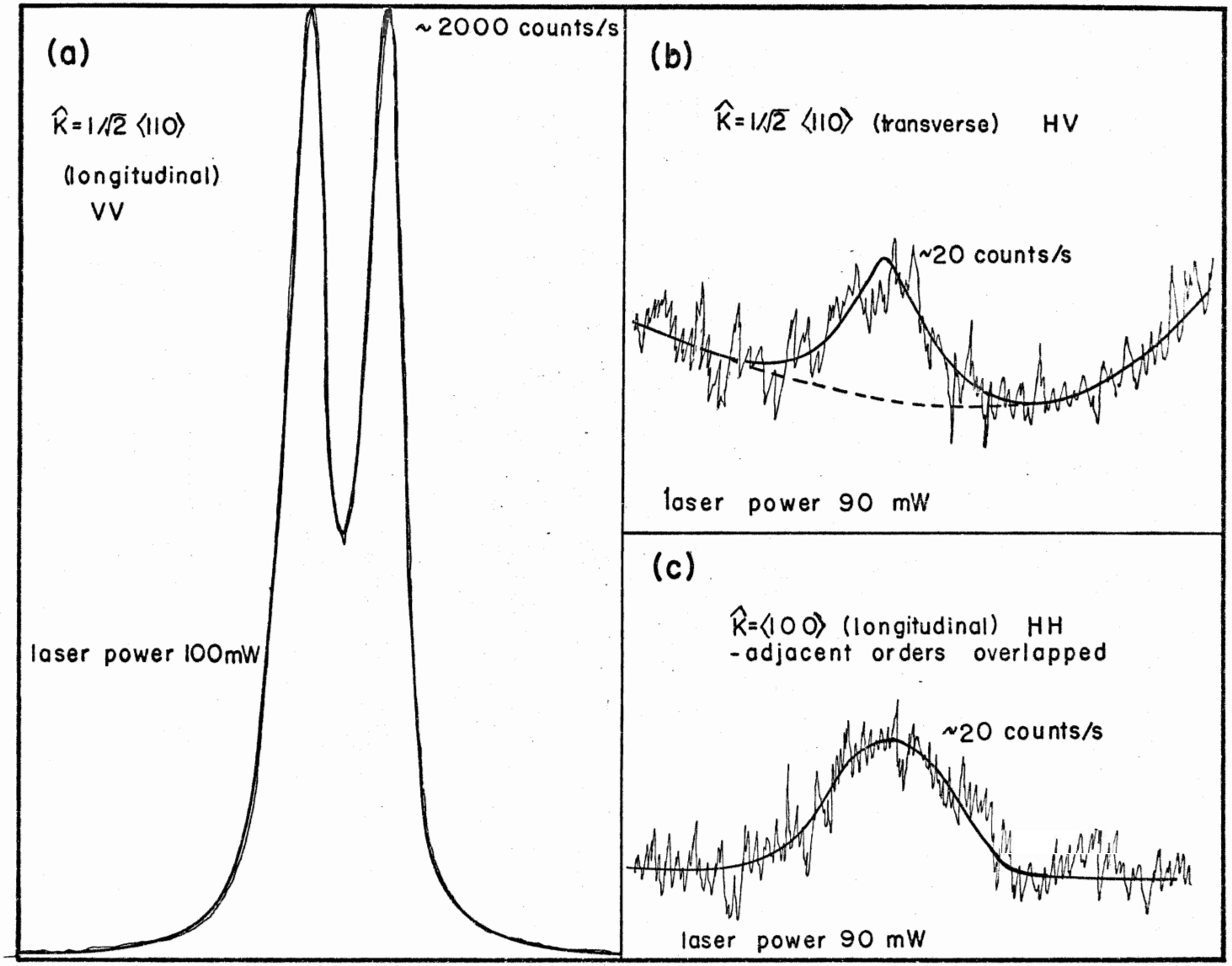

FIGURE IV-16: Typical peaks used in the determination of the photoelastic constants of NaCl

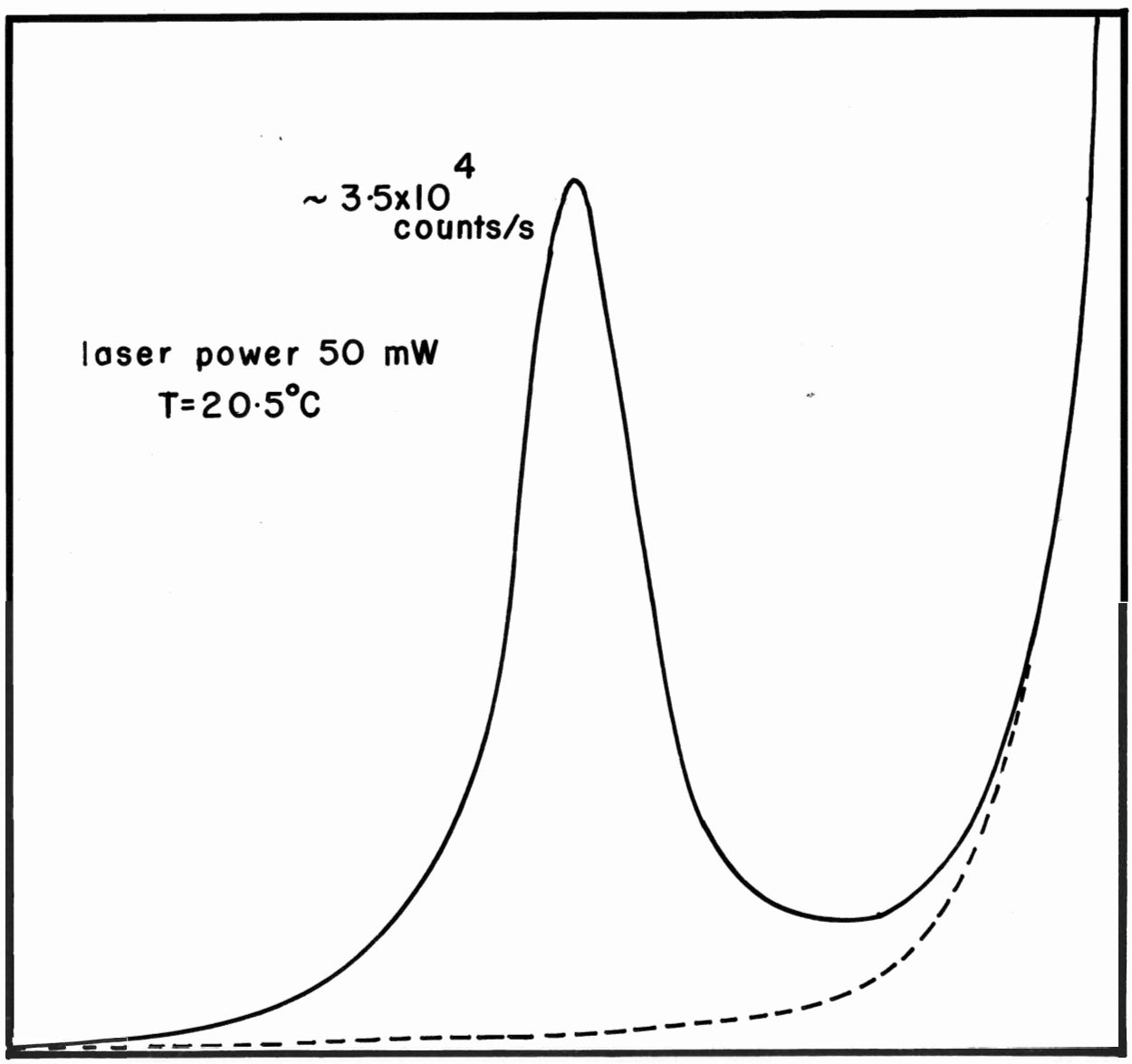

FIGURE IV-16(d) Benzene standard for NaCl

Table IV-9: Photoelastic constants of NaCl

	p_{11}	p_{12}	p_{44}	$p_{11}-p_{12}$
Present study	0.112 ± 0.019	0.158 ± 0.012	-0.013 ± 0.002	-0.046 ± 0.006
Benckert and Bäckström (1973)	0.115 ± 0.009	0.161 ± 0.008	-0.011 ± 0.001	-0.046
Landolt-Bornstein (1979)	0.115 ± 0.007	0.159 ± 0.008	-0.011 ± 0.001	-0.042 ± 0.001

KBr

The photoelastic constants of KBr have not been measured by Brillouin spectroscopy before this work.

The technique employed for KBr was the same as for NaCl, except that 15 minute scans were used with a 0.5 second time constant, because of the more favourable intensities. The free spectral range was set so that the longitudinal mode directly overlapped for $K = \frac{1}{\sqrt{2}}\langle 110\rangle$, in which orientation p_{12} was determined. Eight orders in two scans were averaged by superposition to obtain the KBr intensities and seven orders were averaged for the benzene intensities. Figure IV-17 shows the average lines drawn from the superposition of four orders of one scan. As before, the noise level is indicated for each line by the inclusion of a typical trace which contributed to the average. The use of a smaller FSR than that employed for NaCl lead to better separation of the Rayleigh and Brillouin lines, so that the estimated uncertainty in the Brillouin intensity is 6%. The intensity of the strong longitudinal mode (Fig. IV-17(a)) was determined to within an estimated 2%, and the uncertainties in the intensities of the peaks shown in Figure IV-17(b) and (c) were 15% and 8%, respectively. The results are compared in Table IV-10 with ultrasonic values.

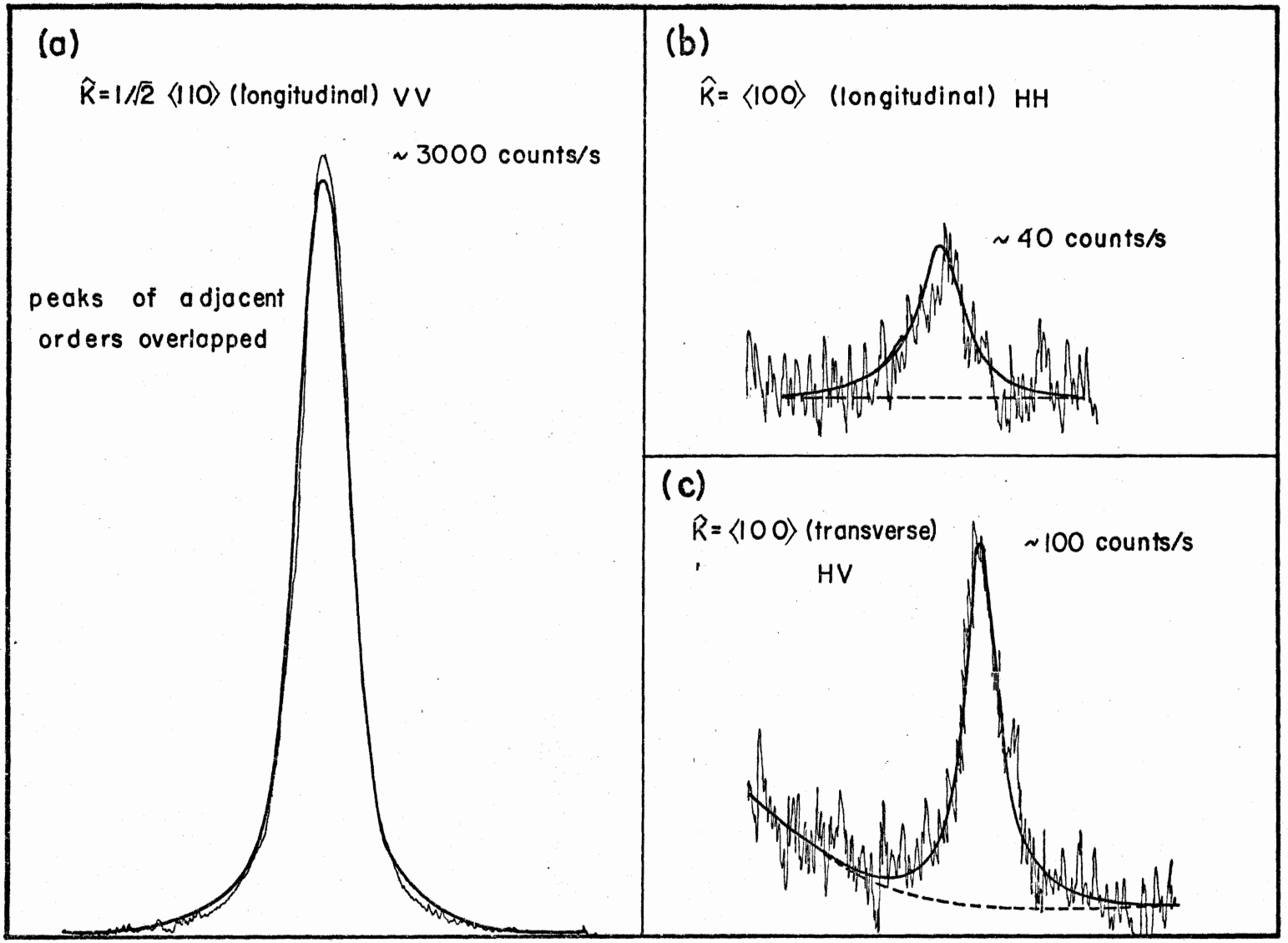

FIGURE IV-17: Typical peaks used in the deterination of the photoelastic constants of KBr (laser power 75 mW)

Table IV-10: Photoelastic constants of KBr

	p_{11}	p_{12}	p_{44}	$p_{11}-p_{12}$
Present study	0.22 ± 0.03	0.171 ± 0.013	-0.019 ± 0.002	0.048 ± 0.005
Burstein and Smith (1948)	0.22	0.171	-0.026	0.049
Iyengar (1950)	0.212	0.165	-0.022	0.047
Landolt-Börnstein (1979)*			-0.025 ± 0.003	0.047 ± 0.003

* The values of Burstein and Smith (1948) and Iyengar (1955) were given in separate rows of LB79. The values of p_{44} and $p_{11}-p_{12}$ given in this row are averages over five works. The errors indicate standard deviations.

LiF

The available photoelastic constant data on LiF are much fewer than for the other alkali halides, and the variations between the several measurements are quite large (see LB79). The low intensity of the scattering makes the measurement of the photoelastic constants by Brillouin spectroscopy more difficult than for most other alkali halides.

Long (1 h) scans were employed and individual intensity measurements for eight peaks were averaged for the p_{12} determination. The standard deviation of the eight measurements was 2.5%. A sample peak is shown in Figure IV-18(a). The lines used in the determination of p_{44} and $p_{11}-p_{12}$ were much weaker, and eight peaks were averaged by superposition. These average lines are shown in Figures IV-18(b) and (c), with the noise level for each line indicated by a sample trace. The estimated errors in the intensities of these modes is 15%.

Because a large FSR (~70 GHz) was required to avoid overlapping of orders, the measurement of the benzene Brillouin intensity was somewhat more difficult than for the previous samples. Four orders were measured individually and averaged to obtain the benzene intensity. A sample spectrum is shown in Figure IV-18(d). Although the standard deviation of the eight measured intensities was 4%, a 10% uncertainty was assigned to the intensity value, to account for a possible systematic error in estimating the Rayleigh wing. The final results are given in Table IV-11.

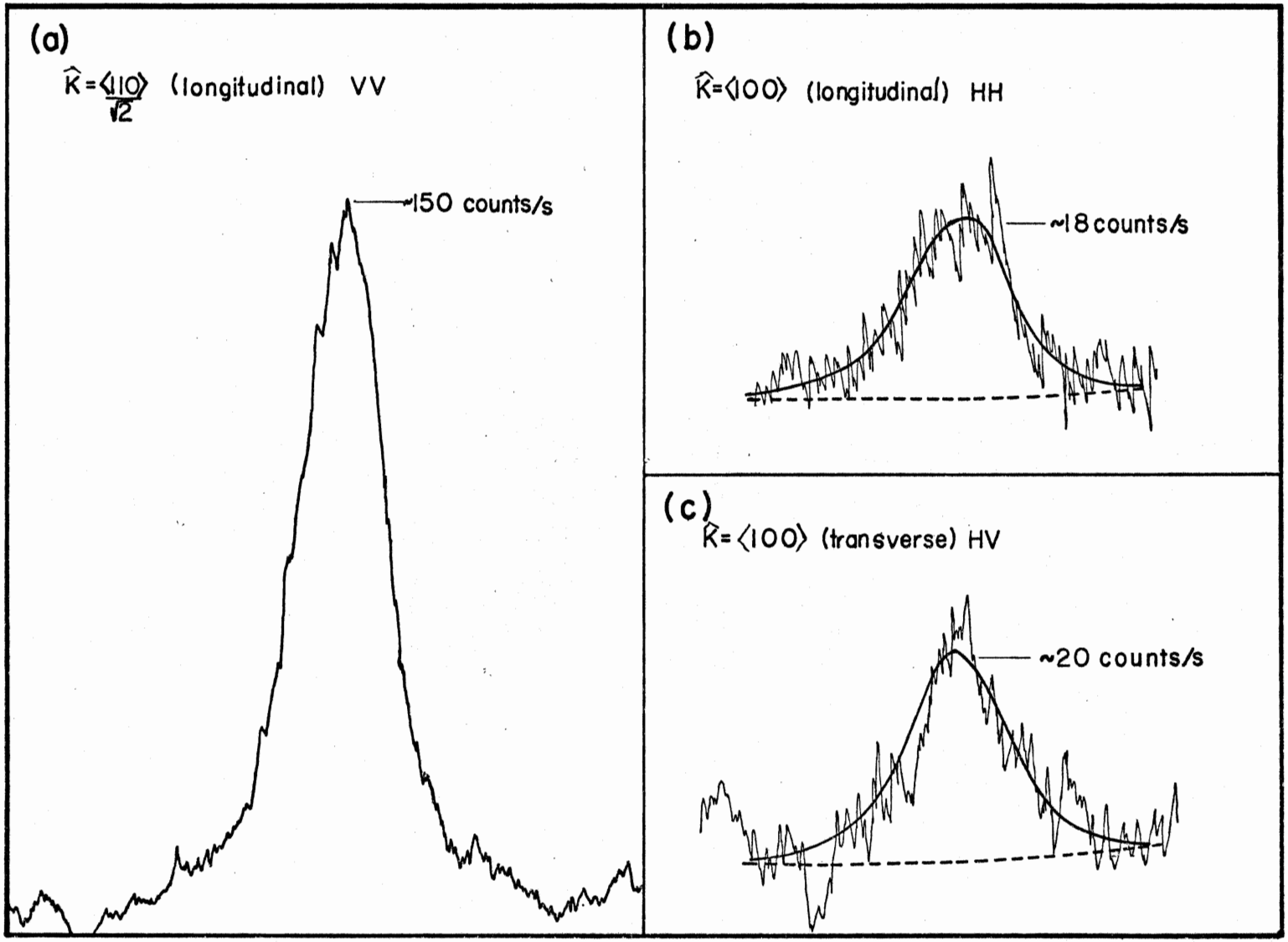

FIGURE IV-18: Typical peaks used in the determination of the photoelastic constants of LiF (laser power 100mW)

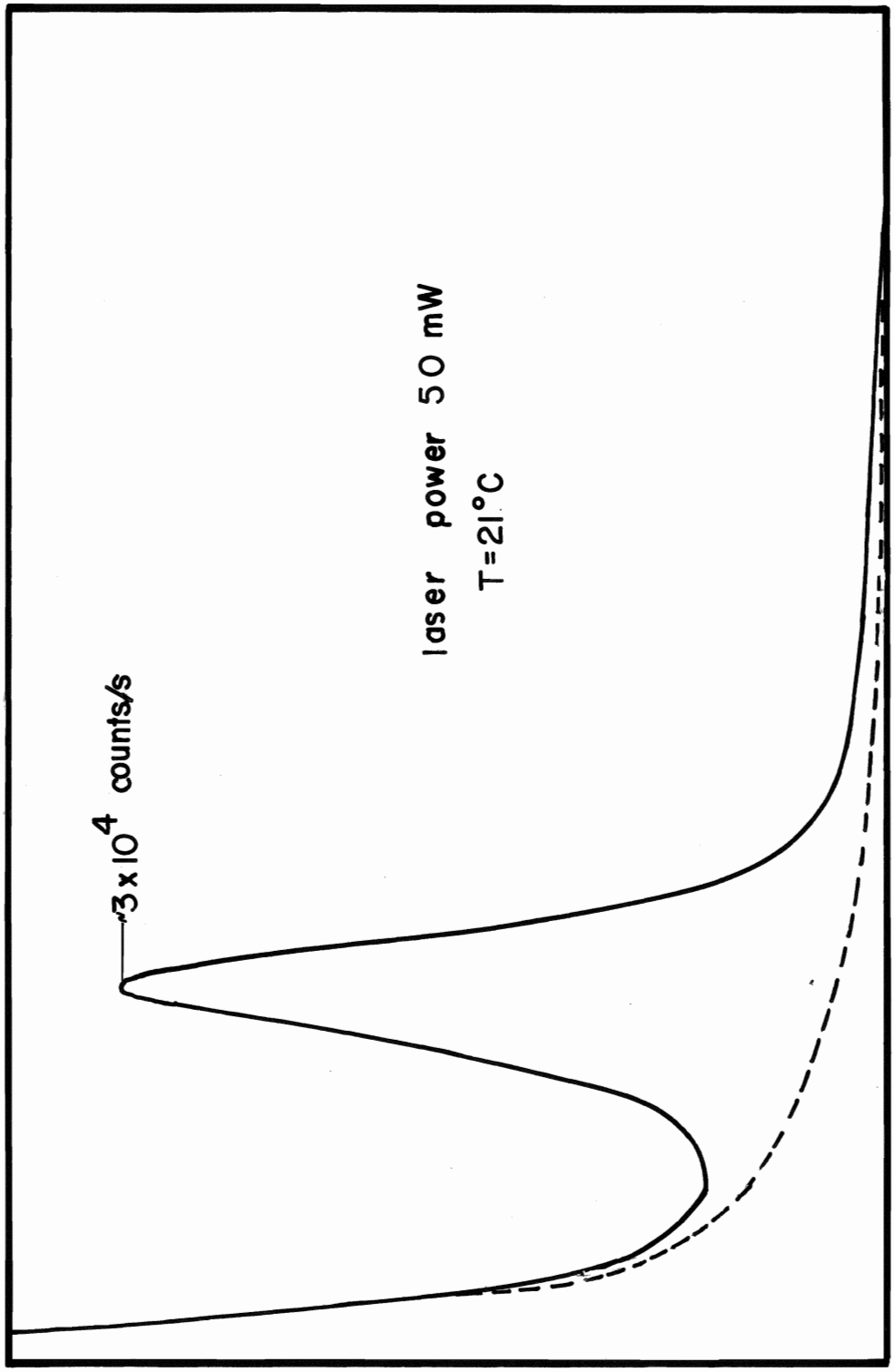

FIGURE IV-18(d): Benzene standard for LiF.

Table IV-11: Photoelastic constants of LiF

	p_{11}	p_{12}	p_{44}	$p_{11}-p_{12}$
Present study	0.032 ± 0.005	0.137 ± 0.012	-0.051 ± 0.008	-0.107 ± 0.016
Burstein and Smith (1948)	~0.02	0.13	-0.064	-0.11
Iyengar (1955)	0.02	0.13	-0.045	-0.11
Landolt-Börnstein (1979)*			-0.042 ± 0.01	-0.106 ± 0.012

* The values of Burstein and Smith (1948) and Iyengar (1955) were given in separate rows of LB79. The values of p_{44} and $p_{11}-p_{12}$ given in these rows are averages over four works in the former case and five works in the latter case. The errors indicate standard deviations.

V. DISCUSSION

Elastic constants show some temperature dependence, the most pronounced effect for the alkali halides being in the c_{11}'s. For convenience of discussion, the elastic constants of this work and that of BB74 are corrected to 20°C in Table V-1 from information contained in LB79. No specific temperatures were given by KSL and SKFL so a temperature of 20°C is assumed for convenience. The data given in LB79 are for 20°C. The photoelastic constants do not show any significant temperature dependence over the small range in which comparisons are made here (LB79, Kato (1973)).

Good agreement with ultrasonic data is obtained for NaCl in all three elastic constants and agreement with BB74 is also obtained, within the combined errors. The data of BB74 agree marginally with the LB79 data.

The elastic constants of BB74 were obtained by measuring the frequency of the longitudinal mode at 10° intervals in the [110]-plane, as well as the frequency of the very weak transverse mode at $\hat{K} = \frac{1}{\sqrt{2}}\langle 110\rangle$, which yields the value of $c_{11}-c_{12}$. With this information, the values of c_{11}, c_{12} and c_{44} were then adjusted to fit the measured longitudinal frequencies.

Such a procedure does not necessarily give unambiguous values since it was found in the case of the KBr measurements in the [110]-plane that the combination of elastic constants producing the best fit to the longitudinal mode frequencies

was not completely obvious, and deviation of ~1% from the values determined at ϕ = 0° and 90° did not worsen the fit. Also, since in the present study all three peaks necessary for the determination of the elastic constants (see Table II-2) were clearly observed, the more straightforward approach described earlier was adopted.

A possible source of error in the BB74 work is the underestimation of the effects of even a small refractive index mismatch. These authors gave 0.5° as the maximum deviation of the beam when a crystal corner was used as a prism. It is clear from the example shown in Figure V-1 that in some orientations the index mismatch could result in a 0.5° uncertainty in the scattering angle, which would produce an additional error of 0.8% to the combination of elastic constants measured at that orientation.

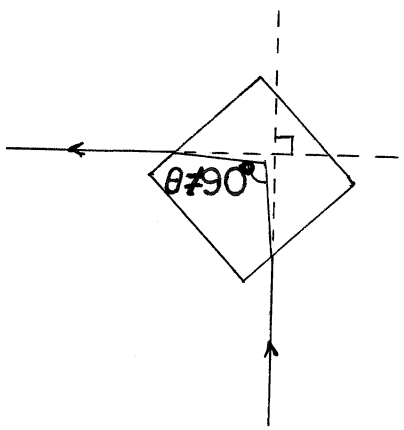

Figure V-1: Effect of slight index mixmatch.

Table V-1: Elastic constants (corrected to 20°C)

	GPa		
	c_{11}	c_{12}	c_{44}
NaCl			
Present (22°C)	49.3 ± 0.2	12.7 ± 0.3	12.7 ± 0.2
Present (20°C)	49.4 ± 0.2	12.7 ± 0.3	12.7 ± 0.2
BB74 (20°C)	49.7 ± 0.2	13.1 ± 0.3	12.7 ± 0.2
LB79 (20°C)	49.1 ± 0.5	12.8 ± 0.1	12.8 ± 0.1
KBr			
Present (21°C)	35.1 ± 0.2	6.1 ± 0.4	5.1 ± 0.1
Present (20°C)	35.1 ± 0.2	6.1 ± 0.4	5.1 ± 0.1
KSL (20°C?)	33.4 ± 0.8	3.5 ± 0.4	4.7 ± 0.4
LB79 (20°C)	34.5 ± 0.4	5.5 ± 0.4	5.1 ± 0.15
LiF			
Present (21°C)	113.5 ± 0.9	47 ± 2	62.9 ± 0.6
Present (20°C)	113.6 ± 0.9	47 ± 2	62.9 ± 0.6
SKLF (20°C?)	103 ± 3	48 ± 2	57 ± 2
LB79 (20°C)	112 ± 2	46 ± 3	63.5 ± 0.6

As was described in the previous chapter, the problem of index mismatch was avoided in this work by preparing flat faces perpendicular to the incident and scattered radiation. Also, the uncertainty of the index match is expected to be negligible, since the beam, after having traversed a corner of the crystal, was viewed on a wall some 8 m away, and the match was considered satisfactory only when the maximum deflection was <5 mm, corresponding to an angular deviation of <0.04°.

The agreement of the KBr results with the ultrasonic values is less complete than in the case of NaCl. Marginal agreement is found with LB79 for c_{11}, whereas c_{12} and c_{44} are quite close to ultrasonic values. There is less agreement with KSL for c_{11} and c_{44}, and a wide disparity is found in the two values of c_{12}.

The KSL results were obtained by a fitting procedure similar to that of BB74, with experimental points at various angles in the [110]-plane. The pure transverse mode was not observed in that work, and the only observations of a non-longitudinal mode gave three "mixed mode" frequencies around the $\phi = 40°$ orientation. Since only c_{11} could be determined independently from these measurements, and since the shapes of the longitudinal and mixed mode curves are quite insensitive to c_{12}, some ambiguity must arise in the fitting of these curves.

The estimated uncertainties for the present results, derived from measurements at only two crystal orientations,

are verified by the near ideal fit of the calculated curves in both the [100] and the [110]-planes. The index match was checked by taking equivalent spectra with the rectangular sample in the [100]-plane for which the effects of an index mixmatch would have been reversed (see Fig. V-2)

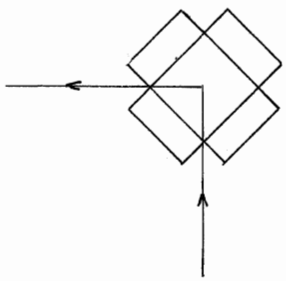

Figure V-2: Equivalent orientations used to check for refractive index mismatch.

No change in the scattered frequencies was observed. It is therefore concluded that the results obtained by KSL are in error, and that the present results represent an improvement in the accuracy of the elastic constants in KBr.

The agreement between the present LiF results and those obtained by ultrasonic techniques is excellent for all three elastic constants. The correctness of the estimated experimental errors is born out by the excellent fit of the

calculated frequency curves to the experimental points (Fig. IV-12). An additional check on consistency was provided by repeating the $\hat{K} = \frac{1}{\sqrt{2}}\langle 110\rangle$ measurement at this FSR on NaCl and obtaining the same frequency (well within experimental error) for the longitudinal mode as was obtained earlier. Once again, we find values in considerable disagreement with the Israeli group (SKLF), there being a 10% variation in c_{11}. Considering the poor quality of the spectra obtained by that group (reproduced in Fig. IV-9(a)), it is hard to imagine how the consistency shown in Figure IV-9(b) was observed, particularly in the transverse mode. It is not known if the same FSR for which the spectrum in Figure IV-9(a) was obtained was employed for the measurements shown in Figure IV-9(b), but if this is the case, perhaps difficulty in judging the true position of the longitudinal peak has led to the discrepancy.

In all three crystals, agreement with ultrasonic results is found, as expected, since the phonon wavevectors probed by Brillouin Spectroscopy lie in the first 1/1000-th of the Brillouin Zone. Thus, any contribution to the frequency from the term $0(K^4)$ in the expansion (see Kittel (1966))

$$\omega^2 = aK^2 + bK^4 + \ldots \qquad \text{(V-1)}$$

is expected to be very small. In fact, if a measurable dispersion did exist, as was suggested by SKLF, then the use of Brillouin spectroscopy to obtain the first order elastic

constants of crystals should be questioned, since this implies that the long-wavelength limit, in which these constants are defined, is not in general valid in the hypersonic frequency regime.

In all the determinations of the elastic constants, the experimental error is produced in the main by the uncertainty in setting the scattering angle, and the variation of distances between peaks on the chart due to fluctuation of stack response. It was shown by the consistency of the results for independent experiments, that the uncertainty in the scattering angle was small, and contributed less than 0.15% to the uncertainty in the elastic constants. This source of error could be almost completely eliminated by using a backscattering configuration ($\theta \sim 180°$), although stray-light problems are generally encountered using this technique (Vacher and Boyer (1972)). The use of a triple pass Fabry-Perot interferometer would be especially suitable for this configuration, since the enhanced contrast (see Appendix A) would serve to reduce the tail of the instrumental profile sufficiently to allow clear observations of relatively weak Brillouin lines close to very strong Rayleigh components.

The effects of inconsistent stack response were most noticeable on long scans. Thus, the ability to do repetitive fast scans and to store the processed photomultiplier signals in a multichannel analyser would reduce the error in frequency measurement substantially. Of course, long term changes in

stack response would still be possible, but these could be compensated by a suitable triggering device such as that described in Chapter II. It was noticed that the apparent ramp amplitude could change considerably over periods of several hours. If such changes occurred during the accumulation time of the fast-scan system, the first peak on the ramp would remain sharp, and the others would broaden with time, the broadening being most severe on the last peak. This difficulty could be avoided by the use of a feedback circuit to detect movements in the last peak, and to then adjust the ramp amplitude accordingly. Obviously, such an arrangement, together with the capability of auto-stabilization would greatly improve the accuracy of the measured elastic constants. An improvement of an order of magnitude is thus envisaged, which would provide values of the elastic constants clearly superior to those determined by ultrasonic technique to date.

A very recent development has demonstrated an improvement in the accuracy of Brillouin frequency measurements by yet another order of magnitude. The technique, developed by Sussner and Vacher (1979) involves the frequency modulation of a reference laser beam by passing it through a lithium niobate crystal set in a microwave cavity the resonance frequency of which can be determined to an accuracy of 3 parts per million. The spectrum of the modulated beam as analysed by the Fabry-Perot Interferometer contains two very sharp side-bands whose frequencies can be fixed to match the centres of

the Brillouin lines by altering the length of the cavity. The Brillouin frequency can then be determined directly from the resonance frequency of the cavity. Since this measurement is independent of stack fluctuations, Brillouin frequencies can be obtained to better than $1/10^4$ in the backscattering configuration. Hence, this elegant method makes possible the determination of the elastic constants to five significant figures.

The photoelastic constants obtained for the three crystals are given again in Table V-2 for convenience.

The photoelastic constants obtained for NaCl are in excellent agreement with both the ultrasonic data found in LB79 and with the reported values of BB73. The use by BB73 of the ultrasonic value of $\rho\left(\frac{\partial\varepsilon}{\partial\rho}\right)_S$ in their calculations leads one to question the accuracy of their work, since the corrected photoelastic constants are just within experimental error, but higher for all three constants than the LB79 values (see Table V-2).

It is clear from Figures IV-16 that the dominant error in the determination of p_{12} stems from the uncertainty in the benzene Brillouin line intensity, due to its proximity to the stronger Rayleigh component. However, the line separation is considerably more favourable for the present case than that shown in BB73 (reproduced in Fig. V-3), especially in light of the larger asymmetry and width of the toluene Brillouin line (KZ). When the benzene spectrum in Figure IV-16(d) is compared

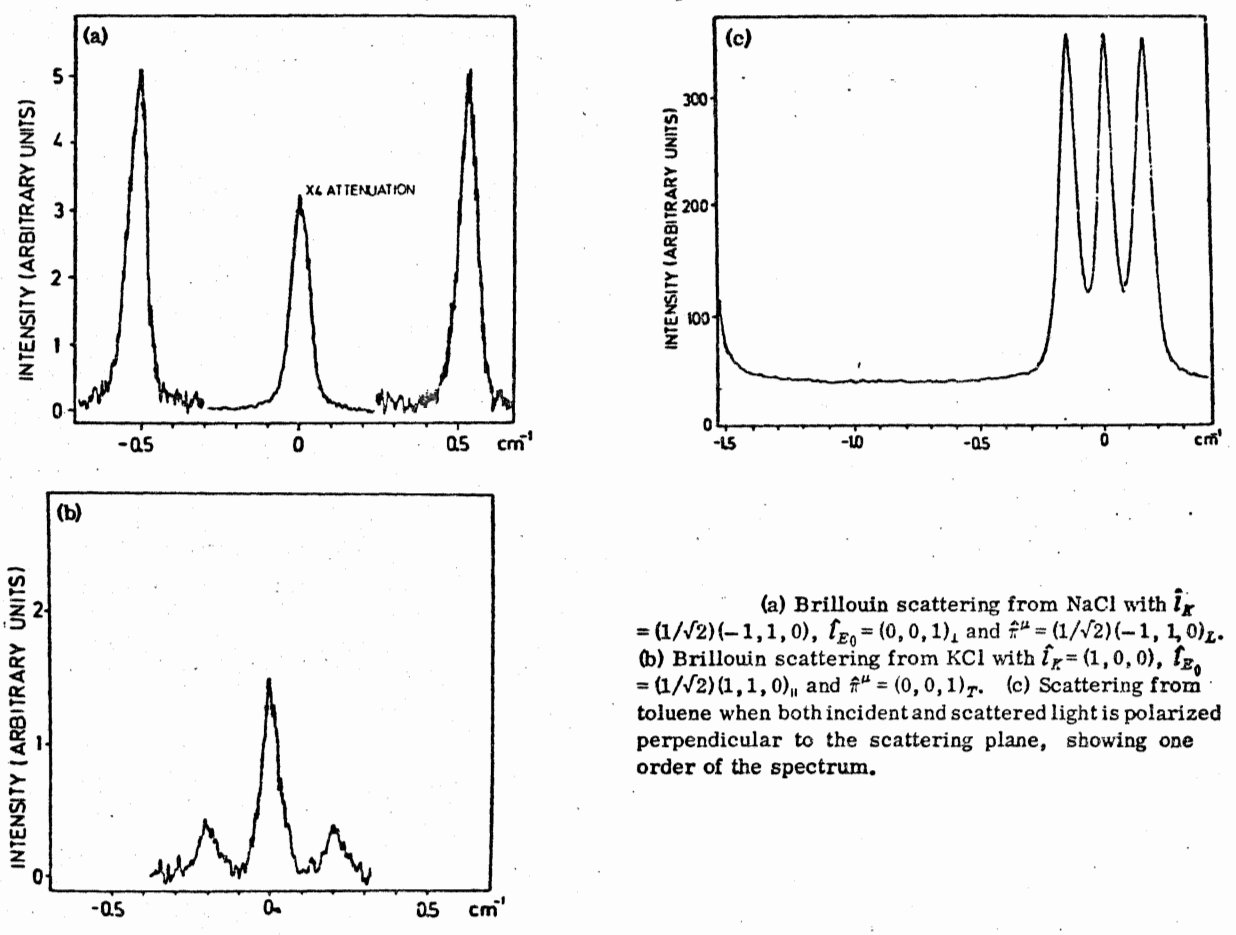

(a) Brillouin scattering from NaCl with $\hat{l}_K = (1/\sqrt{2})(-1,1,0)$, $\hat{l}_{E_0} = (0,0,1)_\perp$ and $\hat{\pi}^\mu = (1/\sqrt{2})(-1,1,0)_L$. (b) Brillouin scattering from KCl with $\hat{l}_K = (1,0,0)$, $\hat{l}_{E_0} = (1/\sqrt{2})(1,1,0)_\parallel$ and $\hat{\pi}^\mu = (0,0,1)_T$. (c) Scattering from toluene when both incident and scattered light is polarized perpendicular to the scattering plane, showing one order of the spectrum.

FIGURE V-3: Reproduction from Benckert and Bäckström (1973)

Table V-2: Photoelastic constants

	p_{11}	p_{12}	p_{44}
NaCl			
Present	0.112 ± 0.019	0.158 ± 0.012	-0.013 ± 0.002
BB73*	0.115 ± 0.009	0.161 ± 0.008	-0.011 ± 0.001
BB73**	0.124 ± 0.009	0.174 ± 0.008	-0.012 ± 0.001
LB79	0.115 ± 0.007	0.159 ± 0.008	-0.011 ± 0.001
KBr			
Present	0.22 ± 0.03	0.171 ± 0.013	-0.019 ± 0.002
Iyengar (1955)	0.212	0.165	-0.022
LiF			
Present	0.032 ± 0.005	0.137 ± 0.012	-0.051 ± 0.008
Iyengar	0.02	0.13	-0.045

* Values reported, using $\rho\left(\frac{\partial \varepsilon}{\partial \rho}\right)_s = 1.60$ (ultrasonic)

** Corrected for $\rho\left(\frac{\partial \varepsilon}{\partial \rho}\right)_s = 1.73$ (hypersonic)

with the toluene spectrum of BB73, it is apparent that the present estimate of 8% is conservative compared with the <3% error on the toluene intensity estimated by those authors. The 15% error associated with the intensities of the modes observed for light polarized parallel to the scattering plane is also conservative. Although the noise level superimposed on each individual peak was quite severe (see Fig. IV-16(b) and (c)), the average line profile of the 14 peaks was clearly defined, and the 15% estimates are felt to be the extreme deviations which could be thought reasonable.

The KBr photoelastic constants were obtained in almost identical fashion to those for NaCl. The better separation of the Brillouin triplet allowed a clearer determination of the position of the Rayleigh wing and a consequent reduction of uncertainty. The agreement with ultrasonic values is again very good.

The photoelastic constants determined for LiF are a significant improvement on available ultrasonic data, in all three constants. The three peaks used for their determination were all clearly resolved (Fig. 18), and measurement of their intensities was unambiguous. The benzene measurements, although slightly complicated by the use of a large FSR (Fig. 18(d)) were still quite easily manageable, and the errors quoted are again the maximum reasonable deviation from our "best estimate".

For all the photoelastic constants, especially the p_{12}'s, agreement with ultrasonic values is excellent and the deviations are generally less than the estimated error. A large portion of the estimated error stems from the uncertainty in $\rho\left(\frac{\partial \varepsilon}{\partial \rho}\right)_s$ of 3.5% quoted by Kato and Zdaziuk (1975). In light of the care with which their experiment was performed, 3.5% is perhaps an overly cautious estimate. Also, the consistency with ultrasonic results points to the possibility that our own estimates of error may be somewhat pessimistic, especially in the determination of the intensity of the benzene Brillouin components.

A great improvement in the accuracy of these experiments could be achieved with the use of a fast-scan feedback-stabilized triple pass interferometer since with the enhanced contrast, and the consequent essential elimination of the baseline problem, linewidth and asymmetry cease to be troublesome in the determination of the benzene Brillouin intensity. Of course, the 3.5% uncertainty in $\rho\left(\frac{\partial \varepsilon}{\partial \rho}\right)_s$ can only be eliminated by the re-measurement of this quantity by absolute methods. The capability for auto-stabilization would also allow for long term accumulation of very weak peaks and thereby reduce the experimental uncertainty in their intensities.

VI. CONCLUSIONS

A Brillouin spectroscopy laboratory has been established, and was shown to provide consistent results for the accurate determination of elastic and photoelastic constants. These constants have been measured for the alkali halide crystals, NaCl, KBr and LiF.

The accuracy of the elastic constant data is generally similar to that reported for ultrasonic measurements except on LiF where it is found that the present work represents an improvement over the ultrasonic measurements. Agreement with ultrasonic values of the elastic constants is obtained in all three crystals. It is concluded that the measurements of the elastic constants of KBr and LiF by Kaplan et al. (1970) and Shaham et al. (1970) respectively are in error. Agreement within experimental uncertainty is found with the elastic constant determination of Benckert and Bäckström(1973).

Errors in frequency measurements due to uncertainty in the scattering angle and ramp fluctuation could be avoided by employing a backscattering configuration with a triple pass Fabry-Perot interferometer and rapid-scan data handling capability.

The photoelastic constants determined from this study match those obtained by ultrasonic techniques, within experimental error. The values determined for NaCl by Benckert and Bäckström (1973) are in less satisfactory

agreement with the present values, after the appropriate value of $\rho\left(\frac{\partial \varepsilon}{\partial \rho}\right)_s$ for toluene is applied to their intensity standard, and the error estimates given in that work are questioned. The first measurements of the photoelastic constants for KBr and LiF by Brillouin spectroscopy are reported. For LiF the results are an improvement on the ultrasonic data.

Accuracy could be further improved by the use of a triple pass Fabry-Perot interferometer to avoid the problems of the determination of background intensities. Weaker scattering could be measured more accurately by the use of repetitive fast-scans and digital data storage.

APPENDIX A

In the following appendix, the essential equations governing the performance of the Fabry-Perot in single and triple pass are presented. For a detailed discussion of the theory of the Fabry-Perot, the reader is referred to Jacquinot (1960), and to Sandercock (1970) on the triple-pass Fabry-Perot. We shall restrict our attention to the plane, piezoelectrically scanned instrument of the type employed in this work.

The plane Fabry-Perot interferometer consists basically of two very flat partially reflecting mirrors which are kept parallel. If the medium between the plates is air, then the condition for transmission of light of normal incidence is

$$2d = m\lambda \ , \ m = 1, 2, 3... \qquad (A\text{-}1)$$

where d is the distance between the plates, λ is the wavelength of the light in air, and m is the interference order. The transmitted light wavelength can be scanned by altering d at a known constant rate, while maintaining plate parallelism. If perfectly monochromatic light is used, the resulting output is a series of evenly spaced maxima.

(1) FREE SPECTRAL RANGE

The wavelength separation between the m-th and the (m + 1)th orders is, from (A-1),

$$\Delta\lambda = 2d\left(\frac{1}{m} - \frac{1}{m+1}\right) \qquad \text{(A-2)}$$

But $m = \frac{2d}{\lambda}$, so

$$\Delta\lambda = \frac{\lambda^2}{2d + \lambda} \simeq \frac{\lambda^2}{2d} \qquad \text{(A-3)}$$

assuming $d >> \lambda$. This wavelength separation is called the free spectral range (FSR), and is usually expressed in terms of frequency:

$$FSR = \frac{c}{2d} \qquad \text{(A-4)}$$

where c is the speed of light in air.

(2) FINESSE

The finesse is a measure of the resolving capability of the instrument, and is defined as the ratio of the instrumental width (full width at half maximum) to the free spectral range. For most applications, there are three significant contributions to the instrumental finesse. These are:

(i) Reflectivity Finesse

$$F_R = \frac{\pi\sqrt{R}}{1 - R} \qquad \text{(A-5)}$$

where R is the reflectivity.

(ii) Figure of Flatness Finesse

$$F_F = m/2 \qquad \text{(A-6)}$$

for plates which are flat to λ/m. In our instrument, $m = 200$ for $\lambda = 546.1$ nm.

(iii) Pinhole Finesse

$$F_P = 4\frac{\lambda}{d}\left(\frac{L}{D}\right)^2 \qquad \text{(A-7)}$$

where: L = focal length of focussing lens (L_3 in Figure III-1)

D = pinhole diameter

d = interferometer plate spacing

λ = wavelength of the light

The instrumental finesse is obtained from these by the formula:

$$F_I^{-2} = F_R^{-2} + F_F^{-2} + F_P^{-2} \qquad \text{(A-8)}$$

Once the choice of plate parameters (reflectivity and flatness) is made, the finesse depends on the pinhole diameter D and plate spacing d. Figure A-1 shows the instrumental finesse as a function of d for different values of D, in the case of $R = 0.96$ and $m = 200$. Since some of the peaks observed in this work were of very low intensity, and since linewidth was of no direct concern, a 500 μm pinhole was chosen for most of the experiments.

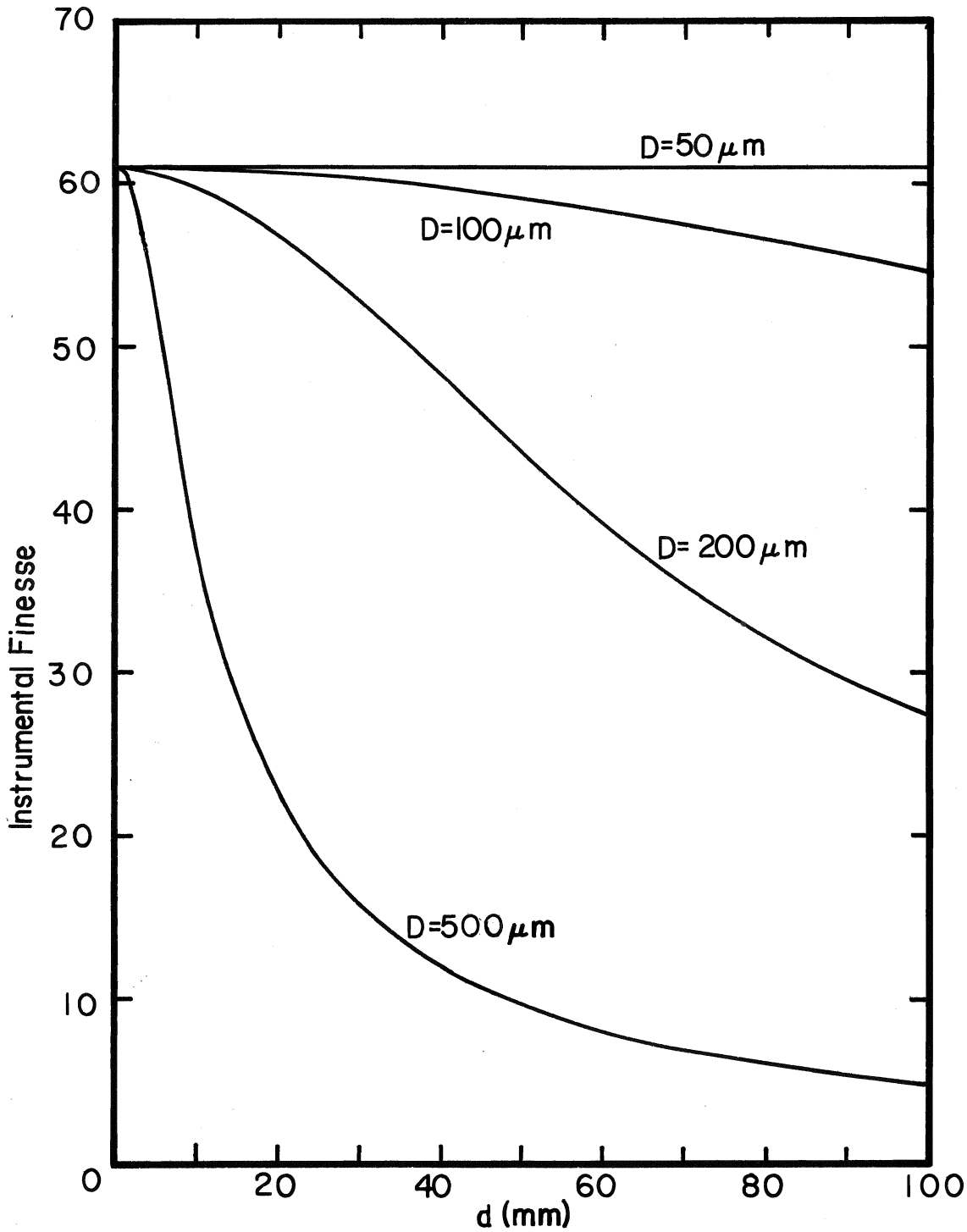

FIGURE A-I: Instrumental Finesse vs. Plate Spacing for Different Pinholes

(3) TRIPLE PASS

Passing the light through the interferometer more than once results in the enhancement of finesse and a drastic increase in the ability to resolve peaks of greatly different intensities which are in close proximity.

The plate finesse in single pass is

$$F_1^{-2} = F_R^{-2} + F_F^{-2} \quad . \tag{A-9}$$

In triple pass, this becomes

$$F_3 = \frac{F_1}{\sqrt{2^{1/3} - 1}} \quad . \tag{A-10}$$

Thus, in the case of R = 0.96 and a flatness of $\lambda/200$, $F_1 = 61$ and $F_3 = 120$. Of course, a suitable pinhole must be chosen so that this finesse is not seriously degraded.

Contrast is defined as the ratio of the maximum to the minimum intensity for monochromatic input, and is given for single pass as:

$$C_1 = \frac{4F_1^2}{\pi^2} \quad . \tag{A-11}$$

In triple pass, this becomes:

$$C_3 = C_1^3 \quad . \tag{A-12}$$

Hence in our case, $C_1 = 1.5 \times 10^3$ and $C_3 = 3.4 \times 10^9$.

One disadvantage in using triple pass is the loss of transmitted intensity. Transmission in single pass is

$$T_1 = \left(1 - \frac{A}{1 - R}\right)^2 \qquad \text{(A-13)}$$

where A is the absorption, and in triple pass,

$$T_3 = T_1{}^3 \quad . \qquad \text{(A-14)}$$

For the plates in present use, the manufacturer specifies $A < 0.002$, so the reduction of transmission in triple pass is 19%.

The above discussion is based on the condition that the plates are kept perfectly parallel. It is invariably found, however, that temperature fluctuations, mechanical vibration and non-reproducibility of the piezoelectric stack response have the effect of creating non-parallelism which in time degrades the performance to an unacceptable level. Del Piano and Quesada (1965) have considered this problem in detail and show that the general effects of plate misalignment are loss of peak transmission and serious departure of the instrumental profile from a Lorentzian form. If "adequate performance" is considered (somewhat arbitrarily) such that the peak transmission is 75% of that for perfect alignment, we infer from Figure 3 of Del Piano and Quesada (1965) that the parallelism requirement for a single pass interferometer with 96% refelctivity is $\sim\lambda/200$.

In triple pass, the parallelism requirement is much more stringent. A good indication of the dependence of performance on parallelism is obtained by calculating the instrumental response function at its maximum as a function of the fraction of a wavelength δ by which the mirrors are misaligned (see Lindsay and Shepherd (a) (1976)). This function is

$$I(\delta) = [(1 + 4F_1{}^2\delta^2)(1 + 16F_1{}^2\delta^2)]^{-1}, \qquad \text{(A-14)}$$

and is plotted in Figure A-2 for three different mirror reflectivities. As is seen from the figure, acceptable performance of our instrument (R = 0.96) can be achieved only if the plates are maintained parallel to ~λ/500.

Since it was found during our experiments that λ/200 parallelism could be maintained over ~1" plate diameter for intervals of only ~one hour, the λ/500 condition is prohibitive for work without automatic stabilization, such as is available commercially from Burleigh Instruments (Model DAC-1).

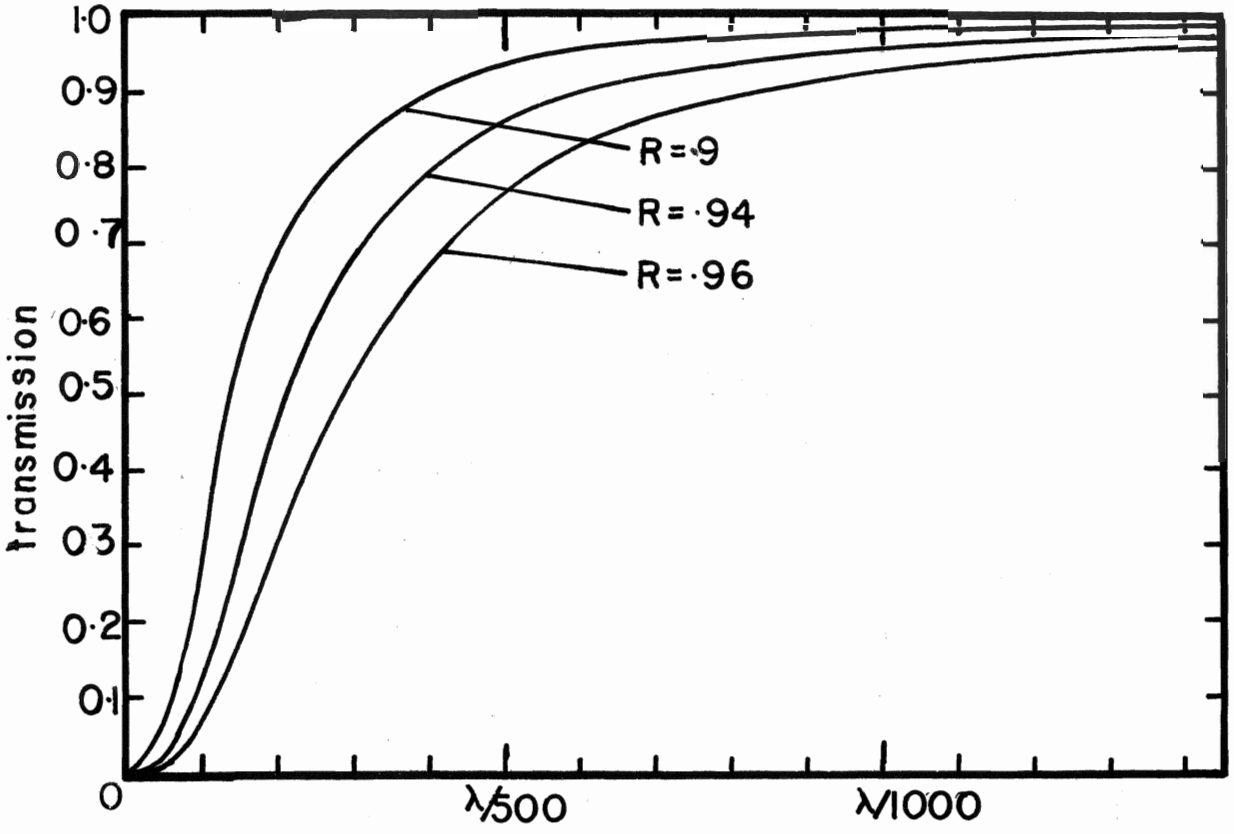

FIGURE A-2 : Transmission losses due to plate misalignment

APPENDIX B

The following appendix describes a calculation which was performed to facilitate the interpretation of linewidth data taken with a triple-pass Fabry-Perot interferometer. Although stability limitations forced the postponement of some scheduled work involving phonon linewidths near ferroelectric phase transitions, the work is presented as an interesting example of the importance of a complete and proper treatment of linewidth data.

The observed spectrum $O(\nu)$ is the convolution of three functions: $S(\nu)$, $B(\nu)$ and $I(\nu)$ representing the laser line profile, Brillouin line and instrumental profile respectively (Leidecker and La Macchia (1968)).

$$O(\nu) = S(\nu)*B(\nu)*I(\nu) \qquad \text{(B-1)}$$

Recognizing that the laser width for a stabilized single mode laser is about five times narrower than even the longest lived (narrowest) phonon lines, we assume that we can approximate (B-1) by eliminating the function $S(\nu)$ and assume that it will simply add about 20 MHz to the instrumental width. Then the observed function is

$$O(\nu) = B(\nu) * I(\nu)$$
$$= F^{-1}[F(B(\nu)) \cdot F(I(\nu))] \quad , \qquad \text{(B-2)}$$

where F and F^{-1} indicate Fourier and inverse Fourier transforms, respectively.

It is well accepted (Danielmeyer (1970)) that in the absence of heavy damping and/or mode coupling, the Brillouin lines of crystals are satisfactorily described by a Lorentzian of width 2a:

$$B(\nu) = \frac{1}{1 + (\nu/a)^2} \quad , \qquad \text{(B-3)}$$

It is also widely accepted that the Fabry-Perot interferometer, in proper alignment, has a Lorentzian instrumental profile.

$$I(\nu) = \frac{1}{1 + (\nu/b)^2} \quad . \qquad \text{(B-4)}$$

Del Piano and Quesada (1964) discuss the effect of slight misalignement on the instrumental profile, and show that large departures from the Lorentzian can result from even marginal misalignments. Hence, this discussion is necessarily limited to systems whose inherent stability is sufficient to warrant the Lorentzian lineshape approximation, or systems which are auto-stabilized so that near-perfect parallelism can be maintained for long periods (Bechtle (b) (1976)).

In the case of a Lorentzian Brillouin lineshape and Lorentzian instrumental function, Equation (B-2) readily shows that the observed function is also a Lorentzian, whose width is (a + b). It is thus commonly reasoned that the phonon linewidth can be extracted from the observed width by simple subtraction of the instrumental width.

In practice, two complications can arise. The first arises from the use of a finite accepting lens aperture, which allows a finite range of phonon wavevectors to contribute to the scattered light. This problem was first discussed by Danielmeyer in 1970 who showed that the spectrum is not described by a Lorentzian, but rather, for a circular aperture, by an equation of the form:

$$B(\nu) = \int_{-1}^{1} \frac{D(1 + NC\xi)(1 + C\xi)F(\xi)}{\left(\frac{\nu}{\nu_B} - B\xi\right)^2 + D^2(1 + NC\xi)^2} d\xi \qquad \text{(B-5)}$$

where $D = \frac{b}{\nu_B}$

b = phonon width

ν_B = backscattered ($\theta = 180°$) Brillouin frequency

$B = (\Delta\theta/2)\cos(\theta/2)$

$C = (\Delta\theta/2)\cot(\theta/2)$

$\Delta\theta$ = ½ angle of acceptance

θ = scattering angle

N = phonon attenuation number ($2 \geq N \geq 0$)

ξ = aperture integration variable

$F(\xi)$ = aperture function

ν = frequency

The shape of this curve is compared to a Lorentzian in Figure (B-1). Danielmeyer (1970) points out that aperture broadening can lead to large overestimates of phonon width, of the order of 40% in some commonly occurring experimental situations.

A second complication is introduced when a multiple-pass interferometer is used. In this case, the instrumental function is (Lindsay et al. (1977))

$$I(\nu) = \frac{1}{[1 + (\nu/b)^2]^n} \qquad \text{(B-6)}$$

where n is the number of passes. The shape of this function is compared to a Lorentzian in Figure (B-1). It was shown by Lindsay et al. (1977) that a simple subtraction of the instrumental width from the observed width could lead to overestimations of the phonon width of up to 30%. By performing analytically the convolution $I(\nu)*B(\nu)$ where $B(\nu)$ is a Lorentzian, these authors obtain a set of linewidth correction curves for 3-pass and 5-pass instruments.

To take account of both the above effects, some authors (e.g., Lindsay and Shepherd (b) (1977)) have carried out both the aperture and the multi-pass corrections, but in a successive manner. That is, taking the observed width, correcting for

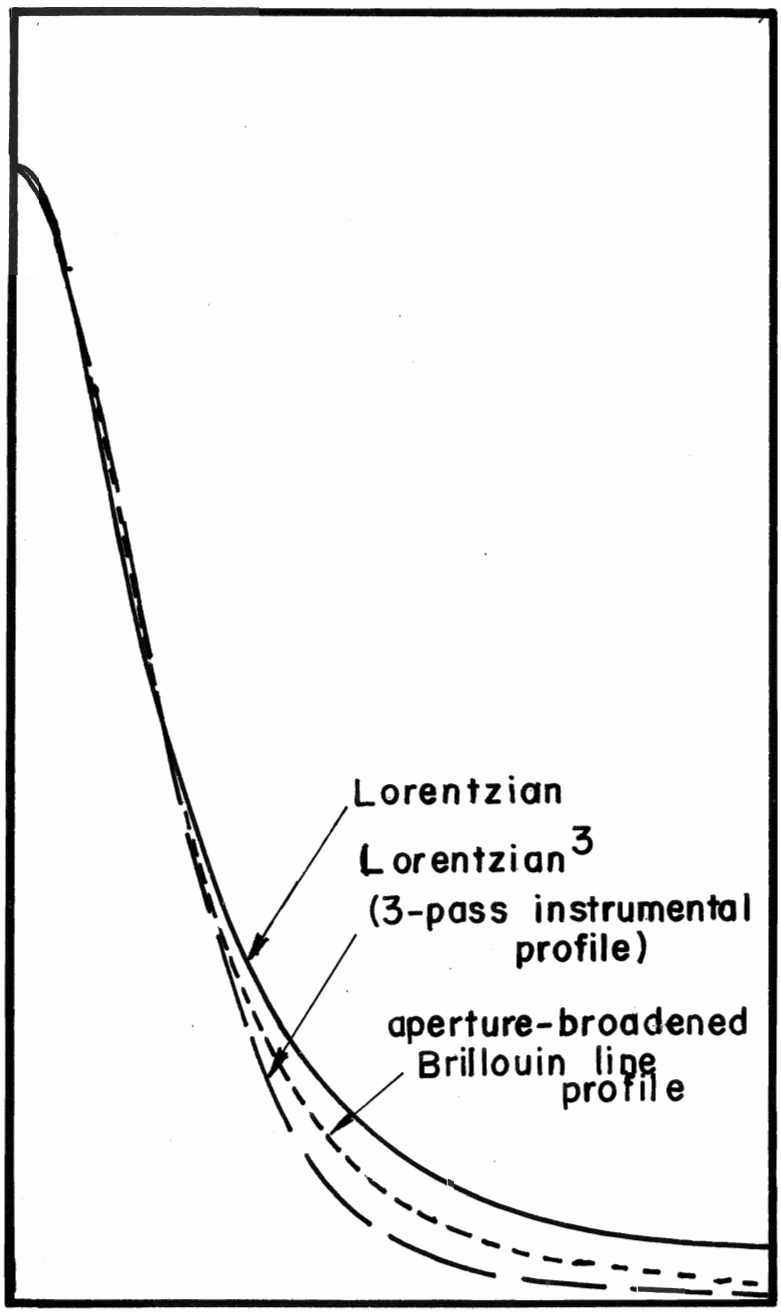

FIGURE B-1: Lineshape comparison

multi-pass, and then making the aperture correction as prescribed by Danielmeyer (1970). We have found that although this procedure is often quite adequate, it can lead to large errors in linewidth measurements.

The correct observed function is the convolution

$$O(\nu) = B(\nu) * I(\nu)$$

$$= \frac{1}{2\pi}\int_{-\infty}^{\infty}\left[\int_{-\infty}^{\infty} B(\nu')e^{i\nu' t}d\nu'\int_{-\infty}^{\infty} I(\nu'')e^{i\nu'' t}d\nu''\right]e^{-i\nu t}dt \qquad \text{(B-7)}$$

After carrying out the integrals over ν', ν'' and t analytically the remaining integral from equation (B-5) was evaluated numerically for a variety of experimental situations.

The nature of the linewidth correction is best illustrated in the form of a plot of observed linewidth vs true phonon linewidth for a given experimental situation. Consider a triple pass Fabry-Perot, with an instrumental width of 0.255 GHz, and an f/15 collecting lens, receiving the scattering from a 20 GHz phonon. The various possible corrections to the observed width are shown in Figure (B-2). The "triple pass only" curve is the correction of Lindsay et al. (1977), and the "aperture only" curve results from convolving equation (B-5) with a Lorentzian instrumental profile. The "successive corrections" curve is that obtained by correcting first for triple pass, and then for the aperature effect. The full deconvolution (Eq. (B-7)) results in the "full correction" curve.

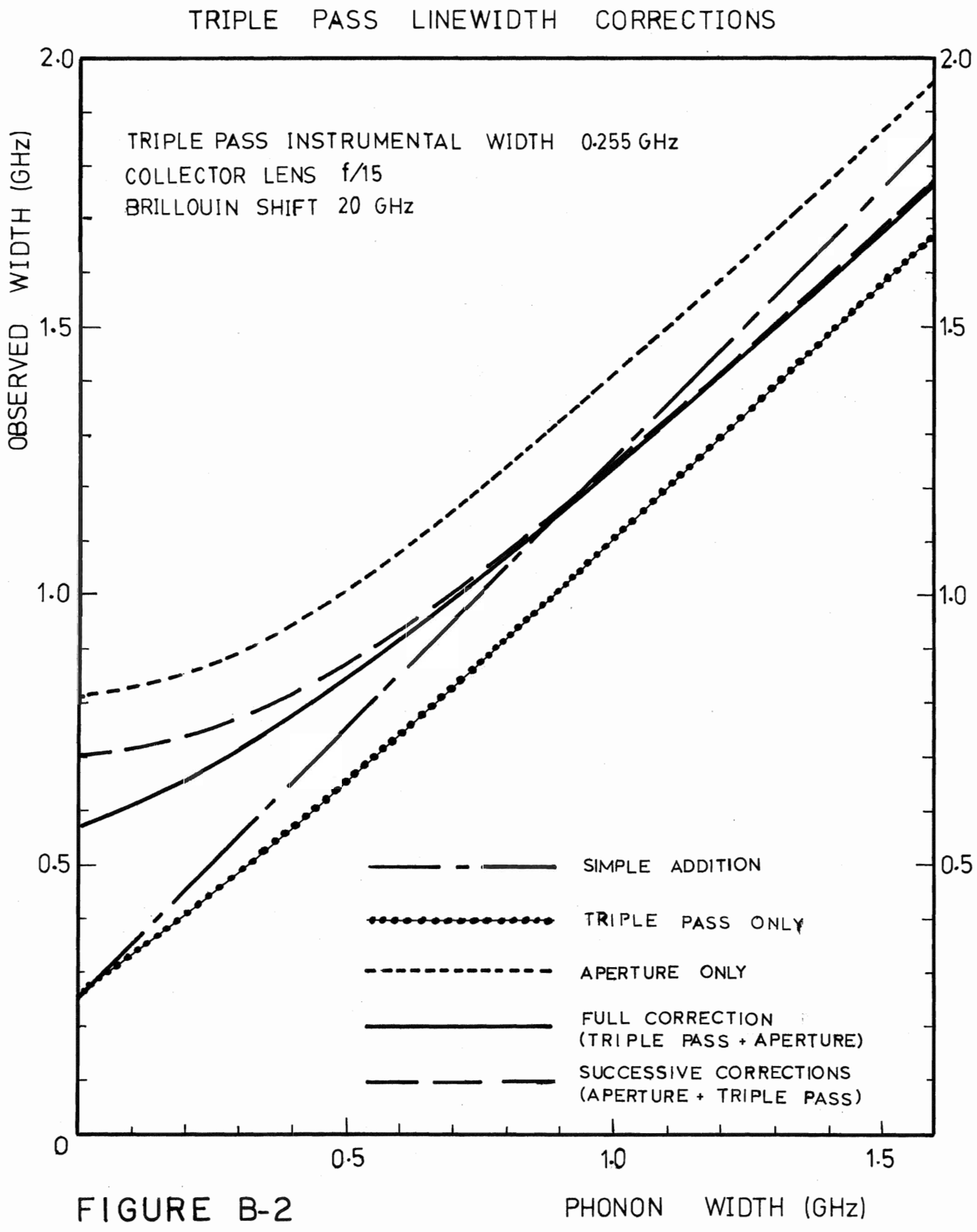
TRIPLE PASS LINEWIDTH CORRECTIONS
TRIPLE PASS INSTRUMENTAL WIDTH 0·255 GHz
COLLECTOR LENS f/15
BRILLOUIN SHIFT 20 GHz
OBSERVED WIDTH (GHz)
PHONON WIDTH (GHz)
0
0·5
1·0
1·5
2·0
SIMPLE ADDITION
TRIPLE PASS ONLY
APERTURE ONLY
FULL CORRECTION
(TRIPLE PASS + APERTURE)
SUCCESSIVE CORRECTIONS
(APERTURE + TRIPLE PASS)

FIGURE B-2

Four points should be noted.

(1) The difference between the various corrections is large, especially for small phonon widths.

(2) Unlike the "simple addition" correction, the size of the full correction depends upon the width itself. It is seen that much larger corrections are necessary for small widths than for large widths.

(3) There is a significant difference, at small widths, between the "successive" and the "full" corrections. For an observed width of 0.75 GHz for example, this difference is about 30%. It should be noted here that a similar difference arises in single pass. That is, the approach of subtracting from the observed width the instrumental width and an amount corresponding to the aperture broadening can lead to large errors, for large apertures or small phonon widths.

(4) The size of the aperture correction depends upon the phonon frequency. This dependence is illustrated in Figure (B-3) for a 0.2 GHz phonon linewidth at f/15.

The examples discussed above were to illustrate that care must be taken in analyzing Brillouin linewidth data. Since the magnitude of the necessary correction depends upon the particular experimental situation, the experimenter must

FREQUENCY DEPENDENCE OF WIDTH CORRECTION

PHONON WIDTH 0.2 GHz
TRIPLE PASS INSTRUMENTAL WIDTH 0.255 GHz
f/15

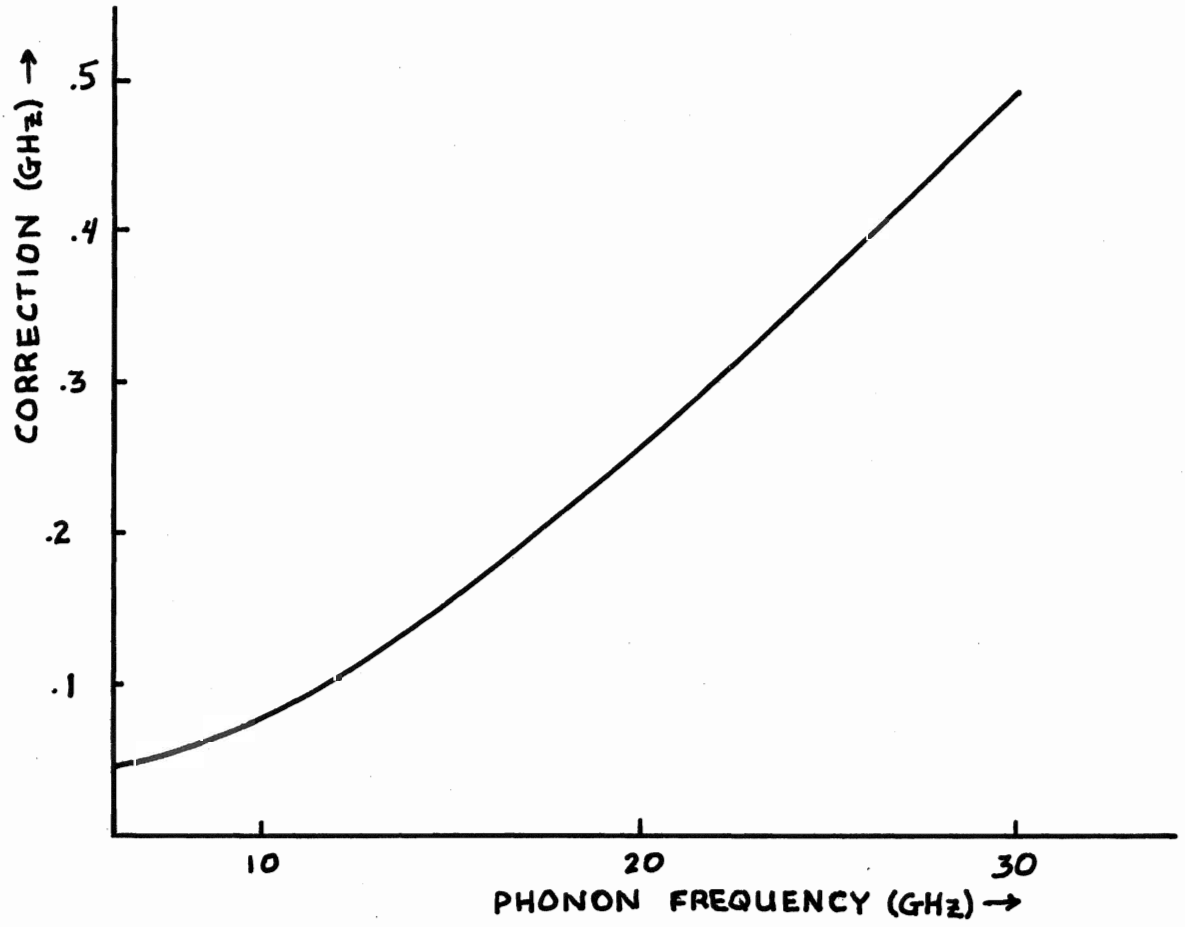

FIGURE B-3

examine each situation individually, and exercise discretion in assigning phonon linewidths.

REFERENCES

American Institute of Physics Handbook, 2nd ed., McGraw-Hill, New York (1963).

D. Bechtle, (a), Rev. Sci. Instrum. 47, 493 (1976).

D. Bechtle, (b), Rev. Sci. Instrum. 47, 1377 (1976).

G. B. Benedek, K. Fritsch, Phys. Rev. 149 647 (1966).

L. Benckert and G. Bäckström, Phys. Rev. B, 8, 5888 (1973).

L. Benckert and G. Bäckström, Physica Scripta 11, 43 (1974).

J. L. Birman, "Handbuch der Physik" 25/26 (1974).

M. Born and K. Huang, "Dynamical theory of crytal lattices", Oxford University Press, London (1954).

L. Brillouin, Ann. Physique (Paris) 17, 88 (1922).

K. Burns and K. B. Adams, J. Opt. Soc. Am. 42, 56 (1951).

K. Burns and K. B. Adams, J. Opt. Soc. Am. 42, 716 (1952).

K. Burns, K. B. Adams and J. Longwell, J. Opt. Soc. Am. 40, 339 (1950).

E. Burstein and P. L. Smith, Phys. Rev. 74, 229 (1948).

R. A. Cowley, Proc. Phys. Soc. 84, 281 (1964).

CRC Handbook of Chemistry and Physics, 53rd ed., The Chemical Rubber Company, Cleveland (1972-73).

H. Z. Cummins and R. W. Gammon, J. Chem. Phys. 44, 2785 (1966).

H. Z. Cummins and P. E. Schoen, in "Laser Handbook", Vol. 2, F. T. Arecchi and E. O. Schultz-Dubois, eds., North-Holland, Amsterdam (1972).

H. G. Danielmeyer, J. Acoust. Soc. Am. 47, 151 (1970).

J. DeLaunay, in "Solid State Physics", Vol. 2, F. Seitz and D. Turnbull, eds.

V. N. Del Piano and A. F. Quesada, Appl. Opt. 4, 1386 (1965).

A. Einstein, Ann. Physik 33, 1275 (1910).

I. L. Fabelinskii, "Molecular Scattering of Light", Plenum Press, New York (1968).

W. S. Gornall and B. P. Stoicheff, Phys. Rev. B, 4, 4518 (1971).

M. H. Grimsditch and A. K. Ramdas, Phys. Rev. B, 11, 3139 (1975).

E. Gross, Z. Phys. 63, 685 (1930).

K. S. Iyengar, Nature 176, 1119 (1955).

P. Jacquinot, Report on Progress in Physics 23, 268 (1960).

H. Kaplan, J. Shaham and W. Low, Phys. Lett. 31A, 201 (1970).

E. Kato, Phys. Lett. 43A, 51 (1973).

Y. Kato and B. P. Stoicheff, Phys. Rev. B 11, 3984 (1975).

Y. Kato and G. A. Zdasiuk, J. Opt. Soc. Am. 65, 995 (1975).

C. Kittel, "Solid state physics", 3rd ed., John Wiley and Sons, New York (1966).

R. S. Krishnan, Proc. Indian Acad. Sci. A26, 339 (1947).

Landolt-Börnstein, New Series, Vol. 7, K.-H. Hellwege and A. M. Hellwege, eds. Springer-Verlag, Berlin (1973).

Landolt-Börnstein, New Series, Vol. 11, K.-H. Hellwege and A. M. Hellwege, eds. Springer-Verlag, Berlin (1979).

H. W. Leidecker Jr. and J. T. LaMacchia, J. Acoust. Soc. Am. 43, 143 (1968).

S. M. Lindsay, S. Burgess and I. W. Shepherd, Appl. Opt. 16, 1404 (1977).

S. M. Lindsay and I. W. Shepherd, (a), J. Polymer Science: Polymer Symposium 58, 85 (1977).

S. M. Lindsay and I. W. Shepherd, (b), J. Phys. E: Scientific Instruments 10, 150 (1977).

R. A. McLaren, H. Kiefte, D. Landheer and B. P. Stoicheff, Phys. Rev. B 11, 1705 (1975).

C. J. Montrose, V. A. Solovyev and T. A. Litovitz, J. Acoust. Soc. Am. 43, 117 (1968).

R. D. Mountain, J. Res. Natl. Bur. Stand. 70A, 207 (1966).

D. A. Pinnow, S. J. Candau, J. T. LaMacchia and T. A. Litovitz, J. Acoust. Soc. Am. 43, 131 (1968).

J. R. Sandercock, Opt. Commun. 2, 73 (1970).

L. I. Schiff, "Quantum Mechanics", 3rd ed., McGraw-Hill (1968).

J. Shaham, H. Kaplan, W. Low and M. Foguel, Phys. Rev. Lett. 24, 827 (1970).

R. J. Spindler and W. S. Rodney, J. Res. Natl. Bur. Stand. 49, 253 (1952).

H. Sussner and R. Vacher, Appl. Opt. 18, 3815 (1979).

R. Vacher and L. Boyer, Phys. Rev. B 6, 639 (1972).